Doctoral Thesis

Study on Glyme-Based Lithium Solvate Ionic Liquids: Fundamental Properties and Application to Rechargeable Lithium Batteries

（溶媒和リチウムイオン液体に関する研究：基礎物性およびリチウム系二次電池への適用）

Graduate School of Engineering
Yokohama National University
(国立大学法人　横浜国立大学大学院　工学府)

Ce　Zhang
(策　　張)

September 2014

Study on Glyme-Based Lithium Solvate Ionic Liquids: Fundamental Properties and Application to Rechargeable Lithium Batteries

A Dissertation Submitted to Yokohama National University for the Partial Fulfillment of the Requirements for the Degree of Doctor of Philosophy in Chemistry

Submitted by
Ce Zhang
D11SA591

September 2014

Department of Chemistry and Biotechnology
Yokohama National University
Yokohama, Japan

Contents:

Acknowledgement

I would like to express my deepest gratitude and sincere appreciation to my supervisor **Professor Masayoshi Watanabe**, and **Associate Professor Kaoru Dokko**, Department of Chemistry and Biotechnology, Yokohama National University, Japan, for their extraordinary patience, consistent encouragement, scholastic supervision and invaluable guidance throughout the course of the present work. I appreciate a lot for giving me an opportunity to study here and supporting the good working conditions.

I am grateful to **Dr. Hisashi Kokubo**, Department of Chemistry and Biotechnology, Yokohama National University, Japan and **Dr. Tomohiro Yasuda**, Cooperative Research and Development Center, Yokohama National University, Japan for their encouraging suggestion and inspiration during this work.

I would like to express my gratitude to Professor Masayoshi Watanabe, Professor Kazuyoshi Ueda, Professor Mahito Atobe, Associate Professor Kaoru Dokko and Associate Professor Satoshi Inagaki for their constructive suggestions as members of the examining committee.

I am thankful to **Professor Yasuhiro Umebayashi**, Graduate School of Science and Technology, Niigata University, Japan for his kind cooperation and suggestions during this study.

I am indebted to **Dr. Kazuhide Ueno**, **Dr. Toshihiko Mandai**, **Dr. Kazuki Yoshida**, **Dr. Jun-Woo Park**, **Mr. Heejoon Moon**, **Ms. Azusa Yamazaki** and **Mr. Junichi Murai** for their cooperation and guidance throughout this work.

I am pleased to acknowledge **Dr. Kazuhide Ueno**, **Dr. Naoki Tachikawa**, **Dr. Toshihiko Mandai**, **Dr. Shiguo Zhang**, **Dr. Zhengjian Chen**, **Dr. Yutaro Kamei** and **Dr. Muhammed Shah Miran**, Assistant Professor, Department of Chemistry, University of Dhaka, Bangladesh for their enlightening instructions, encouraging suggestions and fruitful discussions during the course of the present work.

I am happy to express my gratitude to the secretaries and all the students of the laboratory, including my Japanese tutor Mr. Yuzo Kitazawa and Mr. Shusuke Yanaka since my enrollment in this university for their earnest help and friendship not only in my research but also to the every aspects of my daily life.

I would like to thank the China Scholarship Council (CSC) for their financial support for three years Ph.D. studentship at Yokohama National University.

I am also grateful to all of my friends in Japan and China for their support and encouragement during all these years.

At last but not least I wish to express my heartfelt thanks to my family members for their patient, consistent support and encouragement all the time.

Synopsis

Solvate ionic liquids are a new class of room-temperature ionic liquids (ILs) in which ligand molecules, as a third component of the liquids, strongly solvate the cations and/or anions of salts to form solvate complex ions. The lithium solvate ILs as lithium-conducting electrolytes exhibit many desirable properties. However, their compositions are considered to be very similar to common concentrated electrolyte solutions, thus it is quite required to establish a substantial criterion to distinguish these two mixtures. The studies were pursued with a view to getting a fundamental understanding of the lithium solvate ILs based on coordination chemistry and solution chemistry. The physicochemical properties of glyme-based non-aqueous solvents and Li salt mixtures were investigated by certain parameters such as the ratio of diffusion coefficient (D_{sol}/D_{Li}) and ionicity. In addition, those mixtures were applied as electrolytes for rechargeable lithium batteries.

First, a series of binary systems, which consist of lithium bis(trifluoromethanesulfonyl)amide (Li[TFSA]) and different kinds of ether solvents with a continuous range of Li[TFSA] concentrations were prepared and characterized by multiple-techniques. Transport properties of the electrolytes indicated that the physicochemical properties of the binary systems strongly depend on the employed solvent. The concentration dependency of self-diffusion coefficient (D) of each chemical species in the electrolyte solutions revealed the diffusivity increases with decreasing of the concentration. D_{sol} in solvate ILs was equal to D_{Li}, however, the D_{sol}/D_{Li} is greater than unity in the mixtures with some kinds of solvent even in extreme concentrated solutions. The result suggested that stable solvate complex cations could not form in some mixtures, which thus cannot be classified as solvate ILs. Evaluation of the ionicity based on both the Walden plot and the pulsed-field gradient spin-echo (PGSE) NMR method revealed that the maximum ionicity appears at an $[O]/[Li^+]$ ratio of 4 or 5 in the mixtures. Two solvent effects in the glyme-based non-aqueous electrolyte, i.e., the solvating effect of the ligand and the dipolar effect, were considered to realize this intriguing behavior.

Then, a comparative study of the electrolytes with an $[O]/[Li^+]$ ratio equal to 4 or 5 in order to gain an insight into the relationship between the physicochemical properties and structural chemistry was carried out. The chelate effect of the ligands is verified to be effective for obtaining a stable complex cation in the concentrated liquid regime. The solvent with high complex formation capability is able to form long-live solvate cations, and the properties of the electrolyte is close to typical ILs, whereas other solvents are poor one and can be cataloged as concentrated solutions. Finally, the thermal stability evaluated by thermogravimetric analyses (TGA) and electrochemical stability measured by linear sweep voltammograms (LSV) indicated that solvate ILs are promising electrolytes in terms of thermal and oxidative stabilities, superior to the concentrated solution, even if the latter one possesses the same $[O]/[Li^+]$ ratio with that of solvate ILs.

Further, the aforementioned mixtures were used as electrolytes for Li-ion and Li-S batteries. The capacity of Li-$LiCoO_2$ cell with concentrated solution electrolyte was observed to dramatically decrease upon charge/discharge cycling, whereas solvate IL electrolyte showed a stable charge-discharge cycle with a high Coulombic efficiency (> 99% over 100 cycles). Corrosion on Al current collector of the cathode was also affected by the composition of electrolytes. The persistent Al corrosion indeed took place in the concentrated solution electrolytes, as expected; while it was significantly suppressed in solvate IL electrolytes. Furthermore, the solubility of lithium polysulfides, which is formed as reaction intermediate of the sulfur cathode, was found to be greatly depressed in the solvate IL electrolytes as compared to concentrated solutions. Therefore, a higher Coulombic efficiency and much more stable cycle ability were achieved in Li-S cells with solvate IL electrolyte. Based on the above discussions, it was concluded that the electrochemical properties in the batteries are dominated by the presence or absence of uncoordinating solvents in the electrolytes. In other words, the structural stability of the solvate cations in electrolytes played an important role in the performances of the rechargeable lithium batteries.

Chapter One

General Introduction

1.1. Lithium Secondary Batteries

1.1.1 Rechargeable Li-ion batteries

Nowadays the demand of portable electronic devices such as smart phones and tablet computers exponentially grows; consequently enormous interest has been focused in compact and lightweight batteries with high energy density. Also, the scientific world faces multiple challenges such as environmental concerns and swift depletion of fossil fuels around the globe. The looming energy crisis has shifted the bias from conventional fuels and heat engine technology to high efficiency energy storage devices and drove the development of advance batteries for vehicles and on-site-use electricity/heat cogeneration system in urban environment. The next generation secondary batteries are considered as an alternative option to power automotive transportation and limit the release of greenhouse gas from consumption of the fossil petroleum.[1]

Lithium is appealing for use in batteries because it is the most electropositive element, generating a large potential difference when paired with a positive electrode material. In addition to being the lightest electrical conductor, lithium is considered as a low-density electrode material. As a result, lithium batteries have higher gravimetric and volumetric energy densities compared to the other secondary battery systems such as lead-acid, nickel-cadmium (Ni-Cd), and nickel-metal hydride (Ni-MH) shown in **Figure 1-1**.[2] The increase in gravimetric energy density (horizontal axis) in lithium battery systems can be close to an order of magnitude larger than that of lead-acid systems, while volumetric energy density (vertical axis) can be around eight times greater. This means that lithium batteries can store more energy in smaller volumes with less mass.

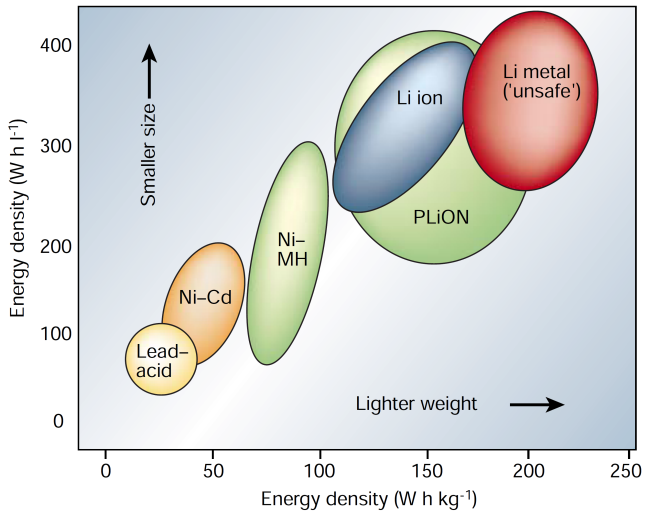

Figure 1-1. Comparison of different battery technologies in terms of volumetric and gravimetric energy density [2]

The rechargeable lithium ion batteries have become to commercialize by SONY in the early 1990s. A single cell consists of a positive electrode (cathode), a negative electrode (anode) and non-aqueous electrolyte. **Figure 1-2** shows a schematic representation and operating principles of secondary Li-ion batteries and the reaction mechanism of Li-ion batteries.[3] The lithium insertion/extraction process occurs with a flow of lithium ions through the electrolyte, which accompanied by a reduction/oxidation reaction of the host matrix assisted with electron transfer through the external circuit. To fulfill this strategy, the selection of cathode and anode with the highest and lowest voltage respectively in order to maximize the cell voltage, as well as high ion-conductive electrolytes with good chemical stability is critically required. Typical electrode reactions of a Li-ion cell with $LiCoO_2$ as the cathode and graphite as the anode is as:

$$\text{Cathode: } LiCoO_2 \rightleftarrows Li_xCoO_2 + xLi^+ + e^-$$

$$\text{Anode: } C + xe^- + xLi^+ \rightleftarrows Li_xC$$

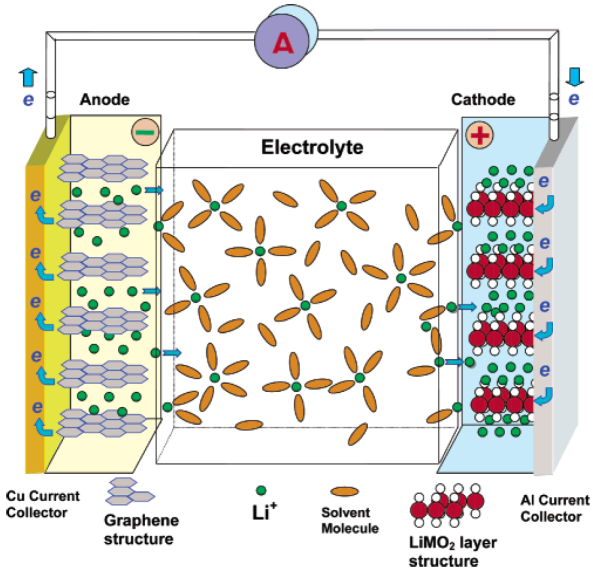

Figure 1-2. Schematic representation and operating principles of rechargeable Li-ion batteries [3]

1.1.2.Cathode of Li-ion batteries

The layered oxides materials ($LiMO_2$, M = Co, Mn, Ni) have been the most widely used and commercialized cathode materials.[4-8] $LiCoO_2$ was first recognized as a cathode material by Goodenough in 1980.[9] It exhibits the α-$NaFeO_2$ type structure, which has space group *R*3*m* with lithium and cobalt ions located in octahedral 3*a* and 3*b* sites respectively, separated by layers of cubic close-packed oxygen ions (**Figure 1-3a**). The theoretical capacity of the cathode is ~270 mAh/g ($LiCoO_2 \leftrightarrow CoO_2$), and the average voltage is ~4 V (vs. Li/Li^+). However, the commercialized cell has only a half of the theoretical capacity because only ~0.5 Li can be reversibly cycled. After 50% extraction of the lithium from the structure, the

oxygen layers rearranged and structure transformed from hexagonal to monoclinic phase.[10, 11] Consequently the structural change slowed down the insertion/extraction rate of Li and leads to cathode instability. In recent years, various attempts have been made to improve the capacity of the $LiCoO_2$-based electrodes, by modifying the surface with other oxides such as Al_2O_3 or ZrO_2, improvement of reversible capacity and cyclability was achieved.[12-16]

Another approach to prepare binary or ternary materials was also extensively investigated in addition to the single transition metal element compounds, such as $LiCo_xNi_{1-x}O_2$,[17,18] $LiCo_xMn_{1-x}O_2$[19-21] and $LiCo_xNi_{1-x-y}Mn_yO_2$.[22-24] The composition with equal amounts of ternary metal ions, $LiCo_{1/3}Ni_{1/3}Mn_{1/3}O_2$, showed the best electrochemical performance with high operating voltages (~4.7 V). It shows high reversible capacity, ~160 mAh/g in the voltage range 2.5–4.4 V and 200 mAh/g in 2.8–4.6 V, which makes this material a very promising cathode for high power and high energy lithium ion battery.[25] However, the presence of Li in the transition metal layer could not be avoided, and in fact short-range ordering between Li and Mn in the $LiMn_6$ pattern was observed, during charging, Li extraction was preceded by the change in oxidation states of Ni^{+2}/Ni^{+4} via Ni^{+2}/Ni^{+3} and Co^{+3}/Co^{+4}, whereas Mn remained +4 during charge/discharge cycles.

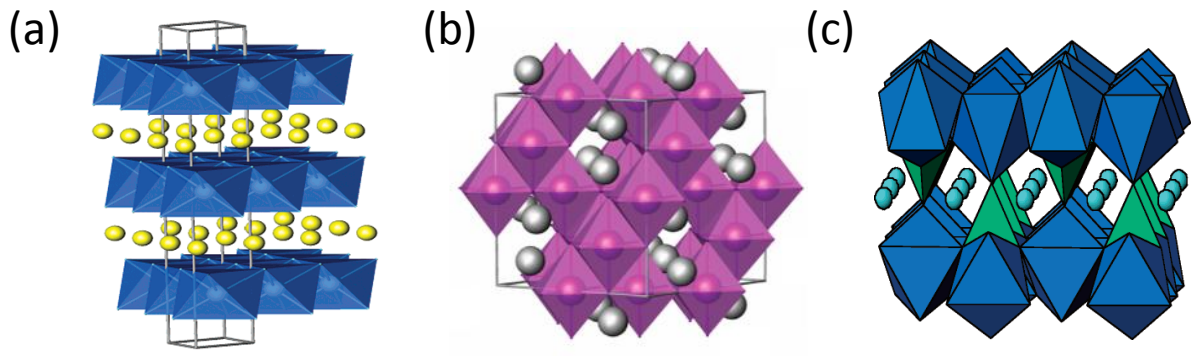

Figure 1-3. Crystal structures of (a) $LiCoO_2$, (b) $LiMn_2O_4$ and (c) $LiFePO_4$ [6, 7]

Spinel oxides with the chemical formula $LiMn_2O_4$ were first proposed in the 1983 and developed in 1990s.[26-28] Typical structure of $LiMn_2O_4$ is shown in **Figure 1-3b**. In the lattice the manganese cations occupy a quarter of the octahedral sites in the lithium layer and lithium cations occupy the tetrahedral sites. The unique framework in this structure provides a three dimensional pathway for lithium diffusion. However, capacity fade of this cathode material around 4 V (vs. Li/Li^+) could be observed due to the dissolution of manganese and impact of the *Jahn-Teller* distortion associated with the Mn^{3+} ions.[29, 30] Various dopants were used to suppress the formation of distorted Mn^{3+} ions and the Ni-doped material with composition $LiNi_{0.5}Mn_{1.5}O_4$ exhibited the best electrochemical performance.[31] In $LiNi_{0.5}Mn_{1.5}O_4$ the redox couple $Ni^{2+}/Ni^{4+}$and Mn^{3+}/Mn^{4+} broadened the operating voltage

window to 4.7 V during the charge/discharge cycles and obtained experimental capacity is ~140 mAh/g.[32, 33]

Olivine phase material $LiFePO_4$ was first reported in 1997 and has been has been considered a promising cathode.[34] This cathode material with low cost and plentiful also has many other merits, such as environmentally benign, low volume expansion and high safety. $LiFePO_4$ demonstrated a flat discharge plateau at 3.4 V (vs. Li/Li^+) and no obvious capacity fading was observed even after several hundred cycles. The structure of $LiFePO_4$ is shown in **Figure 1-3c**, in which Li, Fe, and P atoms occupying octahedral 4a, 4c, and tetrahedral 4c sites respectively. In the lattice, an octahedral FeO_6 shares edges with two octahedral LiO_6 and one tetrahedral PO_4. Because of low Li diffusion at the interface, this material has very low conductivity at room temperature, and it could achieve the theoretical capacity (~170 mAh/g) at very low current density or under heating condition.[35, 36] $LiFePO_4$ particles can be synthesized by hydrothermal or sol-gel method and deliver high electrochemical activity.[37, 38]

Except for the aforementioned cathode materials, new classes of intercalation compounds were profusely investigated. The silicate with the molecule formula Li_2MSiO_4 (M = Fe, Mn) was reported in 2005.[39] In this compound, silicates andtetrahedral transition metal layer shared edges and Li cations was able to diffuse through a 2D zigzag pathway. The theoretical capacity of the Li_2FeSiO_4 was predicted as 166 mAh/g with one Li extraction and 333 mAh/g for two. However, the experimental capacity was stabilized ~140 mAh/g. The borate $LiMBO_3$ (M = Fe, Co, Mn) was another cathode material that showed high theoretical capacity of 220 mAh/g.[40] It has been reported that $LiFeBO_3$ had a practical capacity as 200 mAh/g and the moisture on the surface was expected as the main reason for depleting capacity.[41]

1.1.2. Anode of Li-ion batteries

Although metallic lithium has one of the highest capacity among anode materials, the formation of dendrites upon continuous cycling can cause short-circuit and other safety concerns, whereas prevents the use of lithium as anode in the lithium battery.[42] The state-of-art for anode is represented definitely by graphite owing to its low working potential (vs. Li/Li^+), low cost and high cyclability.[43, 44] Graphite allows an interaction reaction with the product stoichiometry of LiC_6 and has a theoretical capacity of 372 mAh/g. In recent years many investigation of novel anode materials has been done to improve the capacity and realize the fast diffusion of Li ions into the anode. Carbon-based materials have been recognized as appropriate anode, such as carbon nanotubes (CNTs), carbon nanofibers, mesoporous carbons and graphenes have been revealed improved capacity as well as great retard of surface degradation during charge/discharge cycles.[45-49]

Lithium alloy belongs to another promising class of anode materials, including Si, Ge, SiO, TiO_2 and so on, which reacts with lithium according to an alloy/de-alloy electrochemical mechanism and shows satisfied theoretical capacity.[45] The most interesting example is silicon, which has the highest gravimetric capacity (~4200 mAh/g) and the discharge potential of Si is similar to graphite. However, high volumetric expansion of the Si anode was detected during lithiation, resulting in the electrode pulverization and substantial capacity loss.[50, 51] It has been proposed to overcome this issue and improve the electrode performance by preparing nanostructured Si and modifying its morphology with alternative fabrication methods.[52-54] Transition metal compounds such as oxides, phosphides or sulfphides have been considered as another class of anode materials by reacting with lithium in an electrochemical conversion reaction, nevertheless these materials are still far away from practical application due to poor capacity retention and large potential hysteresis.[45, 55-58]

1.1.3. Electrolytes of Li-ion batteries

Electrolyte is another important factor in a Li-ion cell that can offer high performance and long cycle life. Several criteria are crucial in designing a good electrolyte for Li-ion cells, for instant, high ionic conductivity is essential to achieve good rate capability, high Li ion diffusivity to minimize the polarizations of the electrode, and high chemical or electrochemical stability to avoid undergoing unfavorable side reaction with the electrodes. Nowadays, most compositions of electrolytes for Li-ion batteries are compounded of one lithium salt and mixtures of two or more solvents.[3] The solvents with very different physical and chemical natures are often mixed together to obtain diverse functions simultaneously because the important features desired for battery application such as high fluidity and high dielectric constant could hardly meet in a single solvent. The ingredients of electrolyte for the overwhelming majority of commercialized Li-ion cells are apparently based on two indispensable components: ethylene carbonate (EC) as the solvent and lithium hexafluorophosphate ($LiPF_6$) as the solute. In the vast majority of cases, one or several solvents are selected as the co-solvents to increase the fluidity and reduce the melting point of the electrolyte. The linear carbonates such as dimethyl carbonate (DMC), diethyl carbonate (DEC), or ethyl methyl carbonate (EMC) are often used as the additive reagent.

However, it remains some severe problems. (1) The cell using these electrolytes can only be operated in a narrow temperature range (from −20 to 50 °C). At the temperature lower than −20 °C both the capacity and the charge-discharge rate are decimated due to the high melting point of cyclic carbonate solvent and the high liquid temperature it confers on the mixture electrolytes. Besides that, when the temperature over than 60 °C, the electrolytes is rather fragile because the irreversible reaction occurs between the lithium salts and solvents, thus the

cell performance deterioration is permanent. (2) The poor stability of the electrolytes under a wide variety of circumstances, which leads to the failure of the cell and relevant devices. For example, high rate charge-discharge, overcharge or short circuit will heat up the cell and improve the reactivity of the electrolyte components. Furthermore, the internal chemical reaction is accompanied by gas generation, results in hazardous pressure build-up and escalating failure within the cells.

1.2. Next Generation Electrolytes

Development of new lithium battery systems, such as Li-S and Li-O_2 battery require for update of the conventional electrolytes. Additionally improvement of the electrolyte in order to meet current and future needs, for example, large-scale lithium cell, is rather important. Nonflammable, thermally stable electrolytes have been desired to improve the needed safety and reliability of Li batteries effectively. Polymer based electrolytes are expected to be effective in preventing the growth of lithium dendrite during cycling with several other advantages. On the other hand, ionic liquid electrolytes are promising for its outstanding properties such as high thermal or chemical stability.[3] Recently, these two kinds of electrolyte have been wildly investigated and applied to the latest electrochemical devices.[59-62]

1.2.1 Polymer Electrolytes

Polymer electrolytes were proposed for batteries in 1970s after the discovery of ionic conductivity in alkali metal salt complexes of poly(ethylene oxide) (PEO).[63, 64] Solid polymer electrolytes (SPEs) is solid state solutions of lithium salts in polymers with supramolecular architectures and has been considered that combine the advantages of excellent processability and flexibility with high thermal and dimensional stability, on the other hand, low ionic conductivity was an insurmountable barrier. **Figure 1-4** shows the illustration of lithium ion transport in the PEO based polymer electrolytes. The mobility of the Li cations is decreased by the complexation with the ether oxygens of the PEO chain and the cation transport is described as the motion of the Li^+ species between complexation sites assisted by the segmental motion of the PEO matrix.[3, 65] Until now most reported SPEs have been shown an upper limit ionic conductivity ~0.1 mS cm^{-1} in ambient temperature.[66-68] Although this electrolytes has acceptable mechanical strength, poor transport properties lead to them far from application and thus utilization at elevated-temperature environments may be feasible.

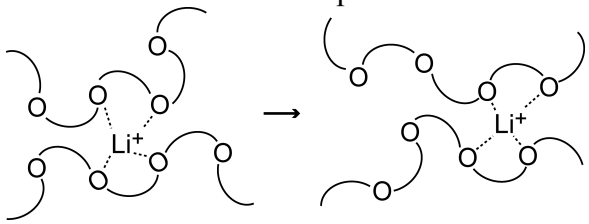

Figure 1-4. Illustration of lithium ion transport in poly(ethylene oxide) [7]

The second category of polymer electrolyte is gel polymer electrolyte (GPEs). GPEs possess both cohesive properties of solid and transport properties of liquid, and exhibits excellent ionic conductivity.[69, 70] In the gels only a small portion of polymer is employed and forms networks by the cross-linking of mobile chains, which are then swollen by lithium salt solutions and thus the matrix in which the ion transport occurs is liquid-like. Other than PEO based GPEs, poly(acrylonitrile) (PAN), poly(methyl methacrylate) (PMMA), poly(vinyl chloride) (PVC) and poly(vinylidene fluoride) (PVDF) based polymer electrolytes have been wildly studied. Although GPEs technology has been used by several major manufactures of Li-ion batteries and known as so-called "PLion cells" (plastic lithium ion cells), the improvement of electrochemical stability and mechanical strength was necessarily required.[71,72]

1.2.2 Ionic Liquid Electrolytes

Room temperature ionic liquids (RTILs) are salts consisting of entirely ions with weak inter-ionic interactions, which allow them to be liquid at room temperature (typically below 100°C). **Figure 1-5** shows the various combinations of cations and anions following the order of Lewis acidity and basicity. It was found that four groups can be cataloged: a strongly Lewis-acidic cation and a strongly Lewis-basic anion, a weakly Lewis-acidic cation and a strongly Lewis-basic anion, a strongly Lewis-acidic cation and a weakly Lewis-basic anion, and a weakly Lewis-acidic cation and a weakly Lewis-basic anion, which are represented as type I~IV respectively. However, ILs can only be classified as type IV, which indicates the ions in these mixtures behave like "solvated ions" and no solvent molecules participate to dissociate the ions by a strong coordination around them.[73] Owing to their unique physicochemical properties, such as thermal and chemical stability, low melting point, negligible volatility, nonflammability, high ionic conductivity, moderate viscosity, high polarity, and solubility with many compounds, RTILs currently have offered a wide range of applications like energy generation, storage and so on.[74-76] In particular, it is worth emphasizing that most of the success in their application, especially in the green chemistry area in which RTILs may replace volatile solvents of environmentally hostile features. In addition, the unlimited structural variations of RTILs as a "designable" material is an advantage for the development of multi-purpose materials for organic synthesis, extraction, dissolution and so on.[77, 78] Electrochemical processes have been another important application area for RTILs because of their remarkable electrochemical stability such as wide electrochemical window.[79, 80] Recently, IL research have extended for designing task-specific ILs with special functionalities, and ILs have been classified into four categories such as protic, aprotic, inorganic and solvate ILs.[81] Some of those ILs are ideal candidates of the next generation electrolytes for the electrochemical devices.[82-85]

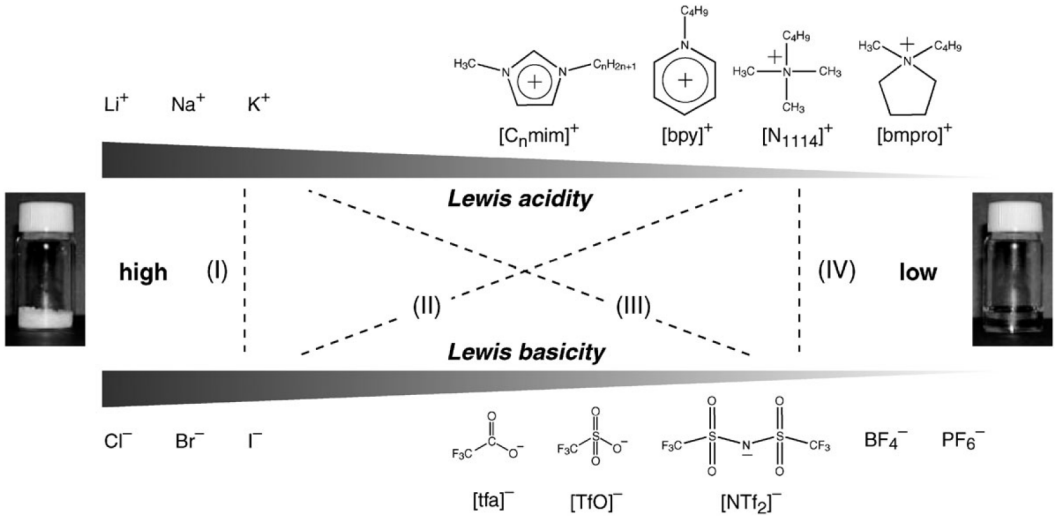

Figure 1-5. Schematic representation of ionic liquids [73]

1.3. Fundamentals of Chemistry in Electrolytes

1.3.1 Solvation

Ion solvation is a phenomenon of fundamental interest in many aspects of chemistry and of importance in the process of dissolution. A dissolution process can be described as **Figure 1-6**.[86] In Process I, M^+ and X^- ions, which are bound by electrostatic force strongly in the crystal, are dissociated and converted to a gaseous state. In Process II, the M^+ and X^- ions in the gas phase dissolve into the solvent by solvation. In Process III, the crystal of MX directly dissolves into the solvent, forming the M^+ and X^- ions. If the Gibbs energy of crystal lattice MX is denoted by ΔG_{lat}, ΔG_I is equal to $-\Delta G_{lat}$. When MX is completely dissociated into free ions in the solution, ΔG_{II} could be obtained as the sum of the solvation energies of M^+ and X^- ions ΔG_{SV}. ΔG_{III} corresponds to the Gibbs energy of dissolution of MX, which is defined as ΔG_S. The equation can be achieved as follow:

$$\Delta G_S = \Delta G_{SV} - \Delta G_{lat}$$

If the solubility constant of solute MX is expressed by K_{sp}(MX), the relation between ΔG_S and K_{sp}(MX) is shown as:

$$\Delta G_S = -RT \ln K_{sp}(MX)$$

In general, the solvated ions also play a key role in electrochemical applications, where for instance the conductivity and degree of dissociation in non-aqueous electrolytes.Some fundamental aspects, such as ion-solvent (solute-solvent) interactions or ion-ion (solute-solute) interactions, also affect ion solvation crucially.

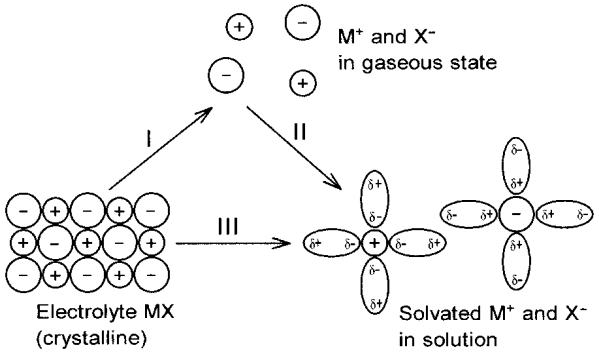

Figure 1-6. Dissolution of crystalline MX into a solvent [86]

1.3.2 Ion-Solvent Interactions

Ion-solvent interaction has been considered as an important aspect because it participates solvation process and further affects the properties of the solution. In principle, ion-solvent interactions can be split into electrostatic interactions, non-electrostatic interactions and chemical contributions. Based on modern conception of electrochemistry and reliable equations the electrostatic interactions gave major contributions of the ion-solvation in the conventional dilute electrolytes. Electron pair donor-acceptor interaction is another common ion-solvent interaction in the ionic electrolytes, in which the solvent molecules interact with the solute cations by their negative charge or with the solute anions by their positive charge. Therefore, the stability of the solvate cation is closely correlated with the electron pair donor capability (or Lewis basicity) of the solvents and tends to become higher with increasing donor ability. Moreover, it was revealed that the ion-solvent interaction related with the properties of solvent, and caused orientation of the neighboring inner solvent molecules and extended with greater or less attenuation into the bulk solution. In most cases solvation shells are chosen as the basis of models and solvent mixtures introduce the possibility of preferential ion solvation.[86-90]

The study of complexes formed between organic or inorganic ligands and transition metal has been well established by coordination chemistry. In addition, the alkali cation complexes were obtained through forming strong and selective solvate complex cations with some special classis of organic ligands such as crown ethers or cryptands, thus a rich expertise of alkali complexes has been established, displaying a whole range of complexes with varied structural, thermodynamic and kinetic properties. The chelate effect of organic ligands was extended to the strong and selective complexation of complex alkali cation such as Li^+, Na^+, and K^+ with various cyclic or acyclic ligands by characteristic features, i.e. substrate inclusion, high stability, high selectivity and slow exchange rates.[91] However, most of the study was performed with models in crystalline states or high dilute solutions.

1.3.3 Ion-Ion Interactions

In ideal infinite dilute solution the dissociation of solute was assumed completely and only ion-solvent interaction was considered. However, the real situation of most non-aqueous electrolytes is more complex and the mutual interactions between ions exist. Indeed in high-permittivity solvents ($\varepsilon > 40$), the solute dissociate almost completely into ions in dilute solutions. Moreover, with the decrease in permittivity the complete dissociation becomes difficult and part of the dissolved electrolyte remains undissociated. In low-permittivity solvents, most of the ionic species exist as ion-pairs and ion-pairs is expected contribute neither ionic strength nor electric conductivity to the electrolyte. The formation process of ion-pairs and the present of ion-association constants K_A for common solute MX are shown as follow:

$$M^+ + X^- \rightleftarrows M^+X^- \text{ (ion-pair)}$$

$$K_A = [M^+X^-] / ([M^+][X^-])$$

Indeed, the real ion association may have several different types of ion-pairs, i.e. solvent-separated ion-pairs (SSIP), contact ion-pairs (CIP) and aggregate solvate (AGG) types, in which the ions are coordinated to 0, 1, or more than one counterion depending on the strength of ion-solvent interactions.[86-90, 92] In low-permittivity solvents, ions of opposite charges are inclined to form ion-pairs even in dilute solutions. With the increase of concentration, ions form triple ions and quadrupoles, and the positive and negative triple ions can remain without being associated due to the large size of aggregate solvates. Because the aggregate ions are conductive, highly concentrated electrolyte solutions in low-permittivity solvents are possibly used as electrolyte solutions for lithium batteries. The formation of aggregate ions was also observed in high-permittivity aprotic solvents; for example, triple ions of lithium are formed in the solutions of acetonitrile (AN) and lithium salt such as lithium chloride (LiCl) or lithium acetate (LiAc).[86] In such case, single ions is highly reactive due to the week ion solvation with the solvent molecules and thus prone to stabilize by the formation of triple ions. For an alkali salt such as LiX, the negative charge delocalization, size, and steric effects of the anion X^- determine its ionic association strength. Generally, the salt with different anions could be classified as dissociated salts, intermediate salts, and associated salts. For instant, such as bis(trifluoromethanesulfonyl)amide ($[TFSA]^-$) and bis(pentafluoroethenesulfonyl)amide ($[BETI]^-$) regard as dissociated type, tetrafluoroborate (BF_4^-) and perchlorate (ClO_4^-) belong to intermediate type, and nitrate (NO_3^-) and trifluoromethanesulfonate ($[OTf]^-$) belong to associated type.[92] It has been reported that the physicochemical properties of the solutions with low-permittivity solvent and different salt are directly affected by the ionic association strength of the anion.[93]

1.3.4 Transport Properties

The conductivity of an electrolyte solution is a result of the transport of ions, and generally between two plane electrodes it is expressed by $\kappa=L/AR$, where L is the distance between the two electrodes, A is the electrode area, and R is the electrical resistance of the solution. For dilute electrolyte solutions, the conductivity κ is proportional to the concentrations of the constituent ions,

$$\kappa = \sum |z| Fuc = \sum \lambda c$$

Herein u is the electric mobility of the ions, c is the molar concentration of the carrier ions, and λ is the molar conductivity of the ions. If a strong electrolyte consisting of ν_+ species of cation and ν_- species of anion is dissolved to obtain an infinite dilute solution, the molar conductivity can be expressed as:

$$\Lambda^\infty = \varkappa/c = \nu_+\lambda^\infty_+ + \nu_-\lambda^\infty_-$$

The molar conductivity decreases with increasing electrolyte concentration due to the influence of ion-ion interactions. In a solution of strong electrolytes Λ is related to concentration and could be presented as empirical Kohlrausch law:

$$\Lambda = \Lambda^\infty - kc^{1/2}$$

where k is a constant. According to Debye-Hückel-Onsager limiting law similar relation has been obtained theoretically:

$$\Lambda = \Lambda^\infty - (A\Lambda^\infty + B)\, c^{1/2}$$

where A and B are parameters that depend on ionic charges, viscosity and relative permittivity of solvent, and temperature. In a solution of weak electrolytes the ion association is extensive and the concentration of free ions is low, the influence of interactions between free ions can be ignored and Λ is equal to $\alpha\Lambda^\infty$ (α is the degree of dissociation of the ion-pair). In such case Arrhenius-Ostwald relation is valid:

$$\frac{1}{\Lambda} = \frac{1}{\Lambda^\infty} + \frac{c\Lambda K_A}{(\Lambda^\infty)^2}$$

where K_A is the association constant and other semi-empirical equation is also available. For highly concentrated electrolyte solutions, it has been lack of theoretically well-founded equations for transport data. Such as molten salt approaches, empirical extensions of equations for dilute solutions, and empirical equations for fitting measured data could be found from literature to evaluate the transport properties with less accurate.[90, 94] The temperature-dependence of molar conductivity of glass forming liquids and of fused salts can be interpreted by the modified Vogel-Fulcher-Tammann (VFT) equation:

$$\Lambda = \Lambda_0 \exp[-B/(T-T_0)]$$

where Λ_0 and B are given transport properties and T_0 ideal glass transition temperature. Investigations on various solutes in non-aqueous solvents showed that competition between ion-ion and ion-solvent interactions with increasing salt concentration leads to comparable states of the different solutions at their respective maximum conductance, i.e. the maximum specific conductance for every solution is obtained when the conductance-determining effects have established a critical energy barrier which depends almost exclusively on solvent or temperature and not on the solute. However, in extreme concentrated solutions the conductance is probably relation to the role of dynamical solvent properties and confused ion-solvent interactions in despite of large ion association constant.[88-90] Further study in details is also necessary to understand the features of concentrated electrolytes.

1.4. High Energy Storage Lithium Batteries

1.4.1 Brief Introduction

After 20-year development of Li-ion batteries, lithium intercalation-based cathode materials have approached the theoretical energy density limit, and breakthroughs will probably come from the redox conversion reaction-based materials, similar to the evolution of anode materials from graphite to metal oxides and lithium alloys. Currently, two types of redox conversion cathodes, Li-S and Li-O_2, have drawn much attention and are considered to be the most promising cathodes for future-generation rechargeable lithium batteries. They both have much higher theoretical capacities and energy densities than Li-ion batteries; however, both of them face significant challenges in order to realize practical devices.[95]

1.4.2 Lithium-Sulfur Batteries

The typical rechargeable Li–S cell is shown in **Figure 1-7a**, consisting of a sulfur cathode, a lithium anode and non-aqueous electrolyte, and operates by reduction of S at the cathode on discharge to form intermediate lithium polysulfide that combine with Li to produce Li_2S. **Figure 1-7c** displays a typical discharge/charge profile of a Li–S cell: two discharge plateaus are identified at ~2.3 V and 2.0 V, and the first one is relevant to the gradual reduction of molecular S_8 to polysulfide S_8^{4-} ions in which exists a complicated equilibrium among several soluble intermediates such as S_8^{2-}, S_6^{2-} and S_4^{2-}. Further reduction of these long-chain polysulfide species produces non-soluble Li_2S_2, corresponding to the lower plateau at ~2.0 V. Finally Li_2S_2 is converted into Li_2S and this step is the most difficult due to the block impeded by sluggishness of solid-state diffusion.[96] During charge, two plateaus are present in the curve, indicating the formation of Li_2S_m (m>2) and elemental sulfur, respectively. It is worthy to note that the two charge plateaus usually merge into a continuous one especially when the cells are run at high current rates.

Li–S batteries have many attractive features, including: (1) the natural abundance and low cost of S; (2) non toxic and environmentally benign; and (3) high theoretical energy density (1672 mAh/g). However, several challenges must be faced and overcome before reaching mass commercialization, which are: (1) poor electrode recharge ability and limited rate capability owing to the insulating nature of sulfur and the its reduction products Li_2S and Li_2S_2; (2) fast capacity fading owing to the generation of various soluble lithium polysulfide intermediates, which gives rise to an undesirable shuttle effect.[97-100] **Figure 1-7b** shows the discharge capacity curves of a common Li–S cell, the poor retention of capacity in several ten cycles due to the redox shuttle effect, which arises by the soluble lithium polysulfides that are formed at the cathode are transported to the anode where they are reduced to lower polysulfides, then transported to the cathode and became to re-oxidize and then return to the anode. On the anode, reduction proceeds to form insoluble Li_2S_2 or Li_2S and deposit on the surface. To resolve the above problems the most common strategy is preparing sulfur and carbon mixtures to improve the conductivity of the cathode. Various attempts have been made to fabricate C/S composites by introducing carbon materials, such as mesoporous carbon, carbon nanotubes, graphene or graphene oxide and so on.[101-106] Designing and optimizing electrolytes is also important because the electrolytes play a crucial role in the performance of Li–S cell and are required to suppress the dissolution of the lithium polysulfides during charge/discharge cycling. Addition of $LiNO_3$ in the electrolyte was proved as an effective method to prevent the corrosion of anodes by forming a protective layer on the lithium metal.[107] Moreover, ionic liquid electrolyte, extreme concentrated electrolyte and gel polymer electrolyte has been invited to improve the cell performance that are capable of delivering electrons efficiently as well as restraining the lithium polysulfides disolve.[108-112]

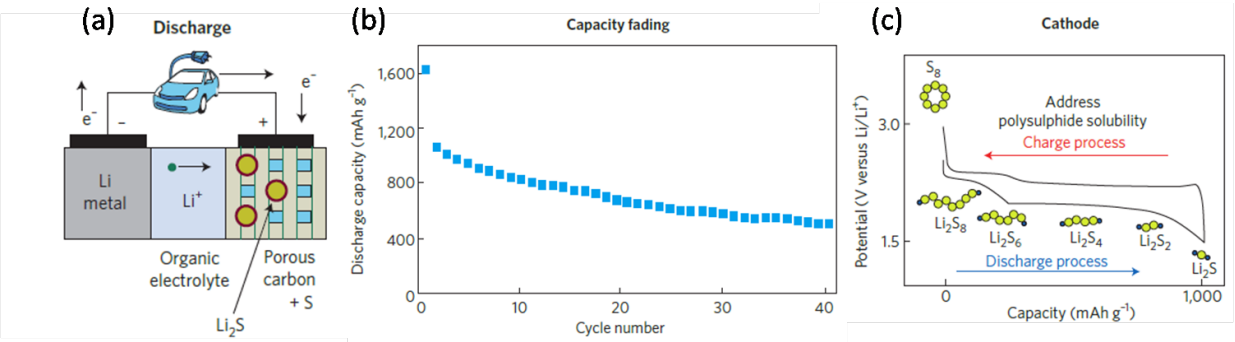

Figure 1-7. Schematic representation and operating principles of rechargeable Li-S batteries [95]

1.4.3 Lithium-Oxygen Batteries

$Li–O_2$ cell is especially attractive because it has the highest theoretical specific energy among all of the metal air type cells. The first $Li–O_2$ cell based on nonaqueous electrolytes was

reported in 1996 and **Figure 1-8a** shows the schematic representation of this system.[113] On discharge, the Li-metal anode is oxidized to release Li^+ into the electrolyte, and the process is reversed on charge. At the positive electrode, O_2 enters the porous cathode and dissolves into the electrolyte, then is reduced at the electrode surface on discharge. O_2^{2-} is formed along with Li^+ from the electrolyte, and Li_2O_2 as the final discharge product in a suitable non-aqueous electrolyte. On charging the peroxide is then decomposed and the reversible reaction is as $2Li^+ + O_2 + 2e^- \leftrightarrow Li_2O_2$. Although some important progress was achieved recently, formidable challenges have been remained such as the fast capacity fading in the cycling shown in **Figure 1-8b**, and large voltage difference between the charge and discharge cycles illustrated in **Figure 1-8c**.

The electrolyte is considered as a key component and one of the bottlenecks at present. The electrolyte is required to be stable both to O_2 and its reduced species, and also need to meet sufficient Li^+ conductivity, O_2 solubility and diffusion to ensure satisfactory rate capability. Moreover, the electrolyte must possess low volatility to avoid evaporation at the cathode due to the safety concern.[95] Conventional organic carbonate electrolytes have demonstrated degradation occurred on discharging process and the reaction at the cathode involves some by-products.[114-117] This rules out that the remarkable capacity of Li–O_2 cells with organic carbonate electrolytes to sustain cycling could be explained by reversible Li_2O_2 formation, whereas the ubiquitous capacity fading is due to the simultaneous electrolyte degradation as shown in **Figure 1-8b**. Despite reversible Li_2O_2 formation can occur in a cell by using appropriate electrolytes, the cell performance has not been satisfied and far from practical utilization up to now.[118-120] Novel electrolytes with high electrochemical and thermal stability or new strategy is urgent require to reach the high capacity and cycling stability of Li–O_2 battery.

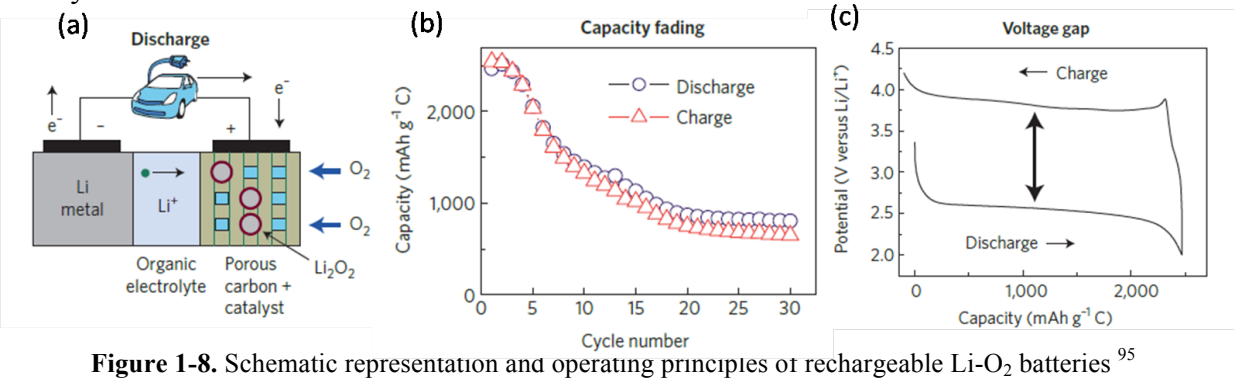

Figure 1-8. Schematic representation and operating principles of rechargeable Li-O_2 batteries [95]

1.5. Aim of this study

Attempt has been made in this study to achieve the following goals:

- To establish a correlation between transport properties of solvents and Li[TFSA] mixtures with certain parameters such as ratio of diffusion coefficient and ionicity for obtaining the electrolytes with desirable chemistry.
- To realize the unique behavior of ionicity in solvents and Li[TFSA] mixtures and maximum of ionicity in a large concentration range.
- To unveil the effect of various factors for the solvents and diverse properties of solvents and Li[TFSA] mixtures.
- To elucidate the relation between ion-solvent interactions and stability of the complex cations to find out the criteria of solvent ionic liquids.
- To demonstrate a suitable electrolytes with promising properties for lithium battery applications.

1.6. Current Work

The studies were pursued with a view to getting a fundamental understanding of the lithium solvate ILs based on coordination chemistry and solution chemistry. The physicochemical properties of glyme-based non-aqueous solvents and Li salt mixtures were investigated by certain parameters such as the ratio of diffusion coefficient (D_{sol}/D_{Li}) and ionicity. In addition, those mixtures were applied as electrolytes for rechargeable lithium batteries.

a) A series of binary systems, which consist of lithium bis(trifluoromethanesulfonyl)amide (Li[TFSA]) and different kinds of ether solvents with a continuous range of Li[TFSA] concentrations were prepared and characterized by multiple-techniques.

b) Evaluation of the ionicity based on both the Walden plot and the pulsed-field gradient spin-echo (PGSE) NMR method revealed that the maximum iconicity occurs at an $[O]/[Li^+]$ ratio of 4 or 5 in the mixtures. Two solvent effects in the glyme-based non-aqueous electrolyte, i.e., the solvating effect of the ligand and the dipolar effect, were considered to realize this intriguing behaviour.

c) The chelate effect of the ligands is verified to be effective for obtaining a stable complex cation in the concentrated liquid regime. The solvent with high complex formation capability is able to form long-live solvate cations, and the properties of the electrolyte is close to typical ILs, whereas other solvents are poor one and can be catalogued as concentrated solutions.

d) Further, the aforementioned mixtures were used as electrolytes for Li-ion and Li-S batteries. Corrosion on Al current collector of the cathode was also studied to explain the deterioration of the Li-ion cells with the concentrated solution electrolytes.

e) Finally it was concluded that the electrochemical properties in the batteries are dominated by the presence or absence of uncoordinating solvents in the electrolytes. In other words, the structural stability of the solvate cations in electrolytes played an important role in the performances of the rechargeable lithium batteries.

1.7. References

1 Dresselhaus, M. S.; Thomas, I. L., *Nature*, **2001**, *414*, 332.
2 Armand, M.; Tarascon, J. M., *Nature*, **2008**, *451*, 652.
3 Xu, K., *Chem. Rev*., **2004**, *104*, 4303.
4 Wakihara, M.; Yamamoto, O., *In Lithium Ion Batteries*, Kodansha, Tokyo, **1998**.
5 Nazri, G. A.; Pistoia, G., *Lithium Batteries: Science and Technology*, Springer Press, New York, **2008**.
6 Whittingham, M. S., *Chem. Rev*., **2004**, *104*, 4271.
7 Yoshida, K., Fundamental Properties and Applications of Glyme-Alkali Metal Salt Complexes as Electrolytes for Batteries. *Ph. D. Thesis*, Yokohama National University **2013**.
8 Goodenough, J. B.; Park, K. –S., *J. Am. Chem. Soc.* **2013**, *135*, 1167.
9 Mitzushima, K.; Jones, P. C.; Wiseman, P. J.; Goodenough, J. B., *Mater. Res. Bull.* **1980**, *15*, 783.
10 Amatucci, G. G.; Tarascon, J. M.; Klein, L. C., *J. Electrochem. Soc.*, **1996**, *143*, 1114.
11 Rossen, E.; Reimers, J. N.; Dahn, J. R., *Solid State Ionics* **1993**, *62*, 53.
12 Cho, J.; Kim, G., *Electrochem. Solid State Lett.* **1999**, *2*, 253.
13 Cho, J.; Kim, C.; Yoo, S. I., *Electrochem. Solid State Lett.* **2000**, *3*, 362.
14 Cho, J.; Kim, Y. J.; Kim, J. T.; Park, B., *Angew. Chem. Int. Ed.* **2001**, *40*, 3367.
15 Wang, Z.; Wu, C.; Liu, L.; Chen, L.; Huang, X., *Solid State Ionics* **2002**, *148*, 335.
16 Wang, Z.; Wu, C.; Liu, L.; Wu, F.; Chen, L.; Huang, X., *J. Electrochem. Soc.* **2002**, *149*, A466.
17 Niewa, R.; Zherebtsov, D.; Hu, Z., *Inorg. Chem.* **2003**, *42*, 2538.
18 Herbst, J. F.; Meyer, M. S., *J. Alloys. Compd.* **2010**, *492*, 65.
19 Kushida, K.; Ichihashi, Y.; Suzuki,Y.; Kuriyama, K., *Physica B* **2010**, *405*, 2305.
20 Juza, R.; Anschütz, E.; Puff, H., *Angew. Chem. Int. Ed.***1959**, *71*, 161.
21 Niewa, R.; Wagner, F. R.; Schnelle, W.; Hochrein, O.; Kniep, R., *Inorg. Chem.* **2001**, *40*, 5215.
22 Juza, R.; Langer, K.; Benda, K. V., *Angew. Chem. Int. Ed.***1968**, *7*, 360.
23 Niewa,R.; Disalvo, F. J., *Chem. Mater.* **1998**, *10*, 2733.
24 Niewa, R.; Zherebtsov, D.; Leoni, S., *Chem. Eur. J.* **2003**, *9*, 4255.
25 Ohzuku, T.; Makimura, Y., *Chem. Lett.* **2001**, *30*, 642.
26 Thackeray, M. M.; David, W. I. F.; Bruce, P. G.; Goodenough, J. B., *Mater. Res. Bull.* **1983**, *18*, 461.
27 Tarascon, J. M.; McKinnon, W. R.; Coowar, F.; Bowmer, T. N.; Amatucci, G.; Guyomard, D., *J. Electrochem. Soc.* **1994**, *141*, 1421.
28 Yonemura, M.; Yamada, A.; Kobayashi, H.; Tabuchi, M.; Kamiyama, T.; Kawamoto, Y.; Kanno, R., *J. Mater. Chem.* **2004**, *14*, 1948.
29 Aurbach, D.; Levi, M. D.; Gamulski, K.; Markovsky, B.; Salitra, G.; Levi, E.; Heider, U.; Heider, L.; Oesten, R., *J. Power Sources* **1999**, *81*, 472.
30 Shin; Y. J., Manthiram, A., *J. Electrochem. Soc.* **2004**, *151*, A204.

31 Ohzuku, T.; Takeda, S.; Iwanaga, M., *J. Power Sources* **1999**, *81*, 90.
32 Takahashi, K.; Saitoh, M.; Sano, M.; Fujita, M.; Kifune, K., *J. Electrochem. Soc.* **2004**, *151*, A173.
33 Kim, J. H.; Myung, S. T.; Sun, Y. K., *Electrochim Acta* **2004**, *49*, 219.
34 Padhi, A. K.; Nanjundaswamy, K. S.; Goodenough, J. B., *J. Electrochem. Soc.* **1997**, *144*, 1188.
35 Andersson, A. S.; Thomas, J. O.; Kalska, B.; Haggstrom, L., *Electrochem. Solid-State Lett.* **2000**, *3*, 66.
36 Ravet, N.; Goodenough, J. B.; Besner, S.; Simoneau, M.; Hovington, P.; Armand, M., *Electrochem. Soc. Abstr.* **1999**, *99-2*, 127.
37 Dokko, K.; Koizumi, S.; Nakano, H.; Kanamura, K., *J. Mater. Chem.*, **2007**, 17, 4803.
38 Choi, D.; Kumta, P. N., *J. Power Sources* **2007**, *163*, 1064.
39 Nyten, A.; Abouimrane, A.; Armand, M.; Gustafsson, T.; Thomas, J. O., *Electrochem. Commun*, **2006**, *16*, 2266.
40 Legagneur, V.; An, Y.; Mosbah, A.; Portal, R.; Le Gal La Salle, A.; Verbaere, A.; Guyomard, D.; Piffard, Y., *Solid State Ionics* **2001**, *139*, 37.
41 Yamada, A.; Iwane, N.; Harada, Y.; Nishimura, S. I.; Koyama, Y.; Tanaka, I., *Adv. Mater.* **2010**, *22*, 3583.
42 Orsini, F.; duPasquier, A.; Beaudouin, B.; Tarascon, J. M.; Trentin, M.; Langenhuizen, N.; de Beer, E.; Notten, P., *J. Power Sources* **1999**, *81*, 918.
43 Girishkumar, G.; McCloskey, B.; Luntz, A. C.; Swanson, S.; Wilcke, W., *J. Phys. Chem. Lett.* **2010**, *1*, 2193.
44 Scrosati, B.; Garche, J., *J. Power Sources* **2010**, *195*, 2419.
45 Goriparti, S.; Miele, E.; De Angelis, F.; Fabrizio, E. D.; Zaccaria, R. P.; Capiglia, C., *J. Power Sources* **2014**, *257*, 421.
46 Landi, B. J.; Ganter, M. J.; Cress, C. D.; DiLeo, R. A.; Raffaelle, R. P., *Energy Environ. Sci.* **2009**, *2*, 638.
47 Kim, C.; Yang, K. S.; Kojima, M.; Yoshida, K.; Kim, Y. J.; Kim, Y. A.; Endo, M., *Adv. Funct. Mater.* **2006**, *16*, 2393.
48 Hou, J.; Shao, Y.; Ellis, M. W.; Moore, R. B.; Yi, B., *Phys. Chem. Chem. Phys.* **2011**, *13*, 15384.
49 Zhou, H.; Zhu, S.; Hibino, M.; Honma, I.; Ichihara, M., *Adv. Mater.* **2003**, *15*, 2107.
50 Misra, S.; Liu, N.; Nelson, J.; Hong, S. S.; Cui, Y.; Toney, M. F., *ACS Nano* **2012**, *6*, 5465.
51 McDowell, M. T.; Lee, S. W.; Harris, J. T.; Korgel, B. A.; Wang, C.; Nix, W. D.; Cui, Y., *Nano Lett.* **2013**, *13*, 758.
52 Wu, H.; Chan, G.; Choi, J. W.; Ryu, I.; Yao, Y.; McDowell, M. T.; Lee, S. W.; Jackson, A.; Yang, Y.; Hu, L.; Cui, Y., *Nat. Nano* **2012**, *7*, 310.
53 Song, T.; Xia, J.; Lee, J. –H.; Lee, D. H.; Kwon, M. –S.; Choi, J. –M.; Wu, J.; Doo, S. K.; Chang, H.; Park, W. I.; Zang, D. S.; Kim, H.; Huang, Y.; Hwang, K. –C.; Rogers, J. A.; Paik, U., *Nano Lett.* **2010**, *10*, 1710.
54 Wen, Z.; Lu, G.; Mao, S.; Kim, H.; Cui, S.; Yu, K.; Huang, X.; Hurley, P. T.; Mao, O.; Chen, J., *Electrochem. Commun.* **2013**, *29*, 67.
55 Xu, J.; Zhu, Y., *ACS Appl. Mater. Interfaces* **2012**, *4*, 4752.
56 Ji, L.; Lin, Z.; Alcoutlabi, M.; Zhang, X., *Energy Environ. Sci.* **2011**, *4*, 2682.
57 Chen, J.; Xia, X.; Tu, J.; Xiong, Q.; Yu, Y.; Wang, X.; Gu, C., *J. Mater. Chem.* **2012**, *22*, 15056.

58 Li, X.; Wang, C., *J. Mater. Chem. A* **2013**, *1*, 165.
59 Page, K. A.; Soles, C. L.; Runt, J., *Polymers for Energy Storage and Delivery: Polyelectrolytes for Batteries and Fuel Cells*, American Chemical Society, Washington DC, **2012**.
60 Stephan, A. M., *Eur. Polym. J.* **2006**, *42*, 21.
61 Galinski, M; Lewandowski, A; Stepniak, I, *Electrochim. Acta.* **2006**, *51*, 5567.
62 Visse, A. E.; Bridges, N. J.; Rogers, R. D., *Ionic Liquids: Science and Applications*, American Chemical Society, Washington DC, **2012**.
63 Fenton, D. E.; Parker, J. M.; Wright, P. V., *Polymer* **1973**, *14*, 589.
64 Armand, M.; Duclot, M., *French Patent* **1978**, 78 329 76.
65 Ratner, M. A.; Shriver, D. F. *Chem. Rev*. **1988**, *88*, 109.
66 Armand, M. *Solid State Ionics* **1994**, *69*, 309.
67 Song, J. Y.; Wang, Y. Y.; Wan, C. C. *J. Power Sources* **1999**, *77***,**183.
68 Nishimoto, A.; Agehara, K.; Furuya, N.; Watanabe, T.; Watanabe, M., *Macromolecules*, **1999**, *32*, 1541.
69 Dias, F. B.; Plomp, L.; Veldhuis, J. B. J. *J. Power Sources* **2000**, *88*, 169.
70 Wang, H.; Huang, H.; Wunder, S. L. *J. Electrochem. Soc.* **2000**, *147*, 2853.
71 Han, K. N.; Seo, H. M.; Kim, J. K.; Kim, Y. S.; Shin, D. Y.; Jung, B. H.; Lim, H. S.; Eom, S. W.; Moon, S. I. *J. Power Sources* **2001**, *101*, 196.
72 http://www.sony.net/Products/SC-HP/cx_news/vol18/pdf/cxeye.pdf
73 Ueno, K.; Tokuda, H.; Watanabe, M., *Phys. Chem. Chem. Phys.* **2010**, *12*, 1649.
74 Noda, A.; Susan, M. A. B. H.; Mitsushima, S.; Hayamizu, K.; Watanabe, M., *J. Phys. Chem. B* **2003**, *107*, 4024.
75 Belieres, J. –P.; Gervasio, D.; Angell, C. A. *Chem. Commun.* **2006**, 4799.
76 Miran, M. S.; Kinoshita, H.; Yasuda, T.; Susan, M. A. B. H.; Watanabe, M. *Phys. Chem. Chem. Phys.* **2012**, *14*, 5178.
77 Visser, A. E.; Swatloski, R. P.; Reichert, W. M.; Mayton, R.; Sheff, S.; Wierzbicki, A.; Davis, Jr. J. H.; Rogers, R. D., *Chem. Commun*. **2001**, 135.
78 Huddleston, J. G.; Willauer, H. D.; Swatloski, R. P.; Reichert, W. M.; Mayton, R.; Sheff, S.; Wierzbicki, A.; Davis, Jr. J. H.; Rogers, R. D., *Chem. Commun*. **1998**, 1765.
79 Matsumoto, K.; Hagiwara, R.; Ito, Y., *Electrochem. Solid State Lett.* **2004**, *7*, E41.
80 Zein El Abedin, S.; Endres, F., *Chem. Phys. Chem.* **2006**, *7*, 58.
81 Angell, C. A.; Ansari Y.; Zhao, Z. *Faraday Discuss*. **2012**, *154*, 25.
82 Lee, S. –Y.; Ogawa, A.; Kanno, M.; Nakamoto, H.; Yasuda T.; Watanabe, M. *J. Am. Chem. Soc*. **2010**, *132*, 9767.
83 Seki, S.; Ohno, Y.; Miyashiro, H.; Kobayashi, Y.; Usami, A.; Mita, Y.; Terada, N.; Hayamizu, K.; Tsuzuki, S.; Watanabe, M., *J. Electrochem. Soc*. **2008**, *155*, A421.
84 Park, J. –W.; Ueno, K.; Tachikawa, N.; Dokko, K.; Watanabe, M. *J. Phys. Chem. C* **2013**, *117*, 20531.
85 Tatara, R.; Tachikawa, N.; Kwon, H. –M.; Ueno, K.; Dokko, K.; Watanabe, M., *Chem. Lett.* **2013**, *42*, 1053.
86 Izutsu, K.; *Electrochemistry in Nonaqueous Solutions*, Wiley-VCH, **2002**.
87 Bockris, J. O'M.; Reddy, A. K. N., *Modern Electrochemistry 1: Ionics, (2nd Edition)* Plenum Press, **1998**.
88 Reichardt, C., *Solvents and Solvent Effects in Organic Chemistry*, Wiley-VCH*,* **2004**.
89 Aurbach, D., *Nonaqueous Electrochemistry*, Marcel Dekker Inc, **1999**.

90 Barthel, J.; Gores, H. –J.; Schmeer, G.; Wachter, R., *Non-Aqueous Electrolyte Solutions in Chemistry and Modern Technology*, Springer Press, **1983**.
91 Mandai, T; Yoshida, K.; Ueno, K.; Dokko, K.; Watanabe, M., *Phys. Chem. Chem. Phys.* **2014**, *16*, 8761.
92 Henderson, W. A., *J. Phys. Chem. B* **2006**, *110,* 13177.
93 Ueno, K.; Yoshida, K.; Tsuchiya, M.; Tachikawa, N.; Dokko, K.; Watanabe, M., *J. Phys. Chem. B* **2012**, *116*, 11323.
94 Conway, B. E.; Bockris, J. O'M. *Modern Aspects of Electrochemistry*, Plenum Press, **1979**.
95 Bruce, P. G.; Freunberger, S. A.; Hardwick, L. J.; Tarascon, J. –M., *Nat. Mat*. **2012**, *11*, 19.
96 Magasinski, A.; Dixon, P.; Herzberg, B.; Kvit, A.; Ayala, J.; Yushin, G. *Nat. Mater.* **2010**, *9*, 353.
97 Cheon, S. E.; Ko, K. S.; Cho, J. H.; Kim, S. W.; Chin, E. Y.; Kim, H. T., *J. Electrochem. Soc.*, **2003**, *150*, A796.
98 Ryu, H. S.; Ahn, H. J.; Kim, K. W.; Ahn, J. H.; Lee, J. Y.; Cairns, E. J., *J. Power Sources*, **2005**, *140*, 365.
99 Mikhaylik, Y.; Akridge, J. R., *J. Electrochem. Soc.*, **2004**, *151*, A1969.
100 Kumaresan, K.; Mikhaylik, Y.; White, R. E., *J. Electrochem. Soc.*, **2008**, *155*, A576.
101 Ji, X.; Lee, K. T.; Nazar, L. F. *Nat. Mater*. **2009**, *8*, 500.
102 Han, S. –C.; Song, M. –S.; Lee, H.; Kim, H. –S.; Ahn, H. –J.; Lee, J. –Y. *J. Electrochem. Soc.* **2003**, *150*, A889.
103 Zheng, W.; Liu, Y. W.; Hu, X. G.; Zhang, C. F. *Electrochim. Acta* **2006**, *51*, 1330.
104 Wang, H.; Yang, Y.; Liang, Y.; Robinson, J. T.; Li, Y.; Jackson, A.; Cui, Y.; Dai, H. *Nano Lett.* **2011**, *11*, 2644.
105 Ji, L.; Rao, M.; Zheng, H.; Zhang, L.; Li, Y.; Duan, W.; Guo, J.; Cairns, E. J.; Zhang, Y. *J. Am. Chem. Soc.*, 2011, 133, 18522.
106 Evers, S.; Nazar, L. F. *Chem. Commun.* **2012**, *48*, 1233.
107 Aurbach, D.; Pollk, E.; Elazari, R.; Salitra, G.; Kelley C. S.; Affinito, J. *J. Electrochem. Soc.* **2009**, *156*, A694.
108 Scheers, J.; Fantini, S.; Johansson, P. *J. Power Sources* **2014**, *255*, 204.
109 Park, J. –W.; Yamauchi, K.; Takashima, E.; Tachikawa, N.; Ueno, K.; Dokko, K.; Watanabe, M. *J. Phys. Chem. C* **2013,** *117*, 4431.
110 Ueno, K.; Park, J. –W.; Yamazaki, A.; Mandai, T.; Tachikawa, N.; Dokko, K.; Watanabe, M. *J. Phys. Chem. C* **2013,** *117*, 20509.
111 Suo, L.; Hu, Y. –S.; Li, H.; Armand, M.; Chen, L. *Nat. Commun.* **2013**, *4*, 1481.
112 Hassoun, J.; Scrosati, B. *Angew. Chem. Int. Ed*. **2010**, *49*, 2371.
113 Abraham, K. M.; Jiang, Z. *J. Electrochem. Soc.* **1996**, *143*, 1.
114 Mizuno, F.; Nakanishi, S.; Kotani, Y.; Yokoishi, S.; Iba, H. *Electrochemistry* **2010**, *78*, 403.
115 Veith, G. M.; Dudney, N. J.; Howe, J.; Nanda, J; *J. Phys. Chem. C* **2011**, *115*, 14325.
116 Xu, W.; Viswanathan, V. V.; Wang, D.; Towne, S. A.; Xiao, J.; Nie, Z.; Hu, D.; Zhang, J. *J. Power Sources* **2011**, *196*, 3894.
117 Freunberger, S. A.; Chen, Y.; Peng, Z.; Griffin, J. M.; Hardwick, L. J.; Bardé, F.; Novák, P.; Bruce, P. G. *J. Am. Chem. Soc.* **2011**, *133*, 8040.
118 Peng, Z.; Freunberger, S. A.; Chen, Y.; Bruce, P. G. *Science* **2012**, *337*, 563.
119 Xu, J.; Wang, Z.; Xu, D.; Zhang L.; Zhang, X. *Nat. Commun.* **2013**, *4*, 2438.
120 Sun, B.; Huang, X.; Chen, S.; Munroe, P.; Wang, G. *Nano Lett.* **2014**, *14*, 3145.

Chapter Two

Physicochemical Properties of the Glyme Based Solvents and Li Salt Mixtures

Abstract

A series of binary systems with ether solvents and Li salt mixtures were prepared. The effect of the solvent nature on the properties of [Li(glyme or THF)$_x$][TFSA] mixtures were studied over a wide range of Li[TFSA] concentrations. The physicochemical properties of these mixtures, such as thermal properties, density (ρ), ionic conductivity (σ), viscosity (η), and self-diffusion coefficient (D) have been investigated in detail. More specifically, the concentration dependency of self-diffusion coefficient of each chemical species in the electrolyte solutions were measured to investigate the interaction among the mixtures, where the stability of complex cations formed between Li^+ ions and solvents were evaluated by the ratio of diffusion coefficient (D_{sol}/D_{Li}). The ionicity reaches a maximum in the concentration range of 1.7−3.1 mol dm^{-3}, before decreasing again at more higher concentrations (>3 mol dm^{-3}) for all [Li(glyme or THF)$_x$][TFSA] mixtures. This behavior was further confirmed by means of Walden plot and Stokes-Einstein plot. It was established that the maximum ionicity occurs at an [O]/[Li^+] ratio of 4 or 5, which agrees well with the favorable coordination number for Li^+ ions in the electrolyte. The Raman spectra bands, where the active S-N stretching mode of $[TFSA]^-$ anion is sensitive to the association state, indicate that the number of either uncoordinated or SSIP-type $[TFSA]^-$ species increased upon dilution; and a significant break point was found at the [O]/[Li^+] ratio equal 4 to 6, which is according with the variation of ionicity.

Part of the work presented in this chapter has been published as:

Zhang, C.; Ueno, K.; Yamazaki, A.; Yoshida, K.; Moon, H.; Mandai, T.; Umebayashi, Y.; Dokko, K.; Watanabe, M. *J. Phys. Chem. B* **2014**, *118*, 5144-5153.

2.1. Introduction

Solvate ionic liquids are a new class of room-temperature ionic liquids (ILs) in which ligand molecules, as a third species of the liquids, strongly solvate the cations and/or anions of salts to form complex ions. The criteria for the formation of solvate ILs primarily depend on the formation of stable complex salts possessing a lower melting point. The basic concept of this new subclass of ILs was reported by Angell in 1965, who regarded the hydrated calcium cation as an independent cation in hydrated molten salts of $Ca(NO_3)_2 \cdot 4H_2O$.[1] Following this discovery, Angell *et al.* named this category of low-melting molten complexes as solvate ILs in their latest review article.[2] This concept is akin to that for common complex anions of ILs such as BF_4^-, PF_6^-, and $AlCl_4^-$; these ions are corresponding adducts of a Lewis acid (BF_3, PF_5, and $AlCl_3$) and a Lewis base (F^- and Cl^-) respectively, which are shown in **Scheme 2-1**.[3]

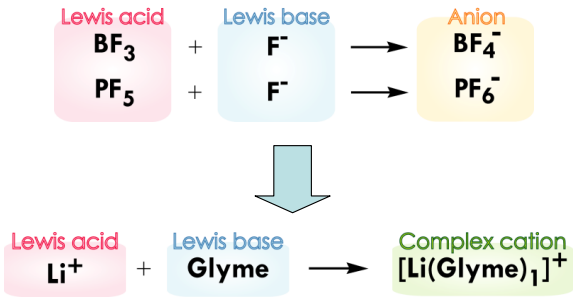

Scheme 2-1. Concept of complex cations in solvate ILs [3]

We have previously reported that molten complexes consisting of 1:1 equimolar mixtures of lithium bis(trifluoromethanesulfonyl)amide (Li[TFSA]) and triglyme (G3) or tetraglyme (G4) behave like typical ILs through the formation of crown ether-like complex cations $[Li(G3 \text{ or } G4)_1]^+$, and were thus judged as typical of solvate ILs.[4-6] Likewise, the Li^+ ions and the glymes represent as a Lewis acid and base, respectively, forming a complex $[Li(glyme)_1]^+$ cation (**Scheme 2-1**). The difference between these two examples is the glyme complexes are non-covalent compounds, whereas the former complexes like BF_4^- are covalent compounds.[3]

The lithium solvate ILs exhibit many desirable properties as a lithium-conducting electrolyte, including high lithium transference numbers, high Li^+ ion concentration, and improved oxidative stability,[6,7] in addition to commonly observed features of ILs such as low vapor pressure and high thermal stability. These characteristics allowed the successful operation of lithium ion batteries with various cathode and anode materials.[8,9] Furthermore, the lithium solvate ILs proved to be effective electrolytes for the suppression of undesired polysulfide dissolution in lithium sulfur batteries, leading to a noteworthy discharge capacity of ca. 700 mA h g^{-1} sulfur with high Coulombic efficiency (>98%),[10-12] even after 400 charge/discharge cycles. These extraordinary properties, such as enhanced oxidative stability,[13] the greatly

suppressed solubility of polysulfides[14,15] have also been found in highly concentrated Li[TFSA] electrolytes in low-molecular weight organic solvents, commonly used in lithium-ion battery electrolytes.

Given that solvate ILs and classical concentrated electrolyte solutions are considered very similar in composition—the number of solvent molecules and ions is comparable or almost equal for both systems—the categorization of these liquids is still ambiguous. To develop a basic understanding of solvate ILs and their unique properties, more elaborate criteria to divide solvate ILs from common electrolyte solutions are essential. In a previous study,[16] the anion-dependent properties of equimolar molten mixtures of different lithium salts (LiX) and G3/G4, [Li(G3 or G4)$_1$]X, were studied. [Li(G3 or G4)$_1$]X was classified as either a "concentrated solution" or a "solvate IL", depending on the stability of the [Li(G3 or G4)$_1$]$^+$ cation. There was crucial competition between Coulombic interactions (Li^+−X^-) and ion-dipole (induced dipole) interactions (Li^+−glyme) in highly concentrated [Li(G3 or G4)$_1$]X, and the stable complex cation were formed only when the former interaction overwhelmed the latter, in other words combined with weakly coordinating counter anions such as [TFSA]$^-$ (lower Li^+−X^- interactions).

In coordination chemistry, the stability of complex ions is strongly dictated by the structure of ligand molecules. To investigate the insight or criteria for solvate ILs, ion-ion interaction and ion-solvent interaction are two fundamental and important aspects. In our recent perspective paper, we classified the solvate ILs composed of a series of LiX salts and ligand molecules; only a few combinations of Li salts and ligand molecules can be classified as solvate ILs or concentrated solutions. The schematic model is shown in **Figure 2-1**.[3]

In this chapter, we will study the ion-solvent interaction in the mixtures of Li[TFSA] salts and various ligand molecules. We begin to investigate a structurally related series of concentrated mixtures of Li[TFSA] and oligoether solvents to clarify the effect of ion-dipole (or ion-induced dipole) interactions on the formation of solvate ILs. Whereas G3 and G4 possess 4 and 5 coordination sites, respectively, in each molecule to chelate the Li^+ ion, the number of oxygen atoms per molecule becomes smaller for diglyme (G2), monoglyme (G1), and tetrahydrofuran (THF). In addition, the mixtures with different types of organic solvent, such as amide or carbonate were prepared to study the solvent effect of the electrolytes. The main purpose of this investigation was to reveal the reflection of ion-solvent interactions in their transport properties of these mixtures with a large range of concentration.

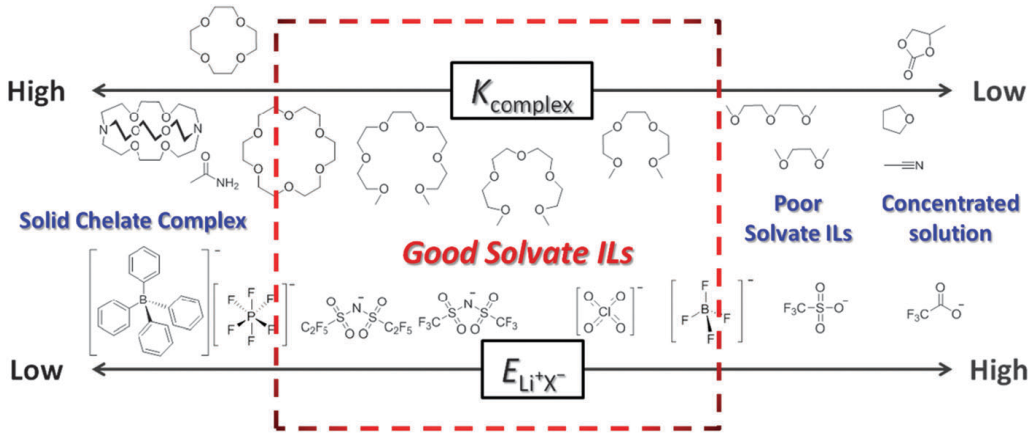

Figure 2-1. Schematic model of classification of solvate ionic liquids [3]

2.2. Experimental

2.2.1 Chemicals

Glymes with the chemical structure of $CH_3—O—(CH_2—CH_2—O)_n—CH_3$ (n = 1~4) are abbreviated as G1~G4 respectively. Monoglyme (G1), diglyme (G2) and triethyl phosphate (TEP) were purchased from Kishida Chemical (battery grade reagents), and super dehydrated tetrahydrofuran (THF) ([H_2O] <10 ppm) were purchased from Wako Pure Chemical. Triglyme (G3) and tetraglyme (G4) were obtained from Tokyo Chemical Industry and were distilled under reduced pressure over sodium metal. Dehydrated N-methyl-2-pyrrolidone (NMP) was purchased from Kanto Chemical. Li[TFSA] was obtained from Morita Chemical Industries and dried under vacuum at 120 °C before use.

2.2.2 Preparation of mixtures

The solutions were prepared by mixing the solvent and Li[TFSA] in different molar ratios and stirring overnight at room temperature to obtain homogeneous liquids. The mixtures were prepared, stored, and handled in an argon-filled glovebox (VAC, [H_2O] <1 ppm).

2.2.3.Methodology and Measurements

Ionic conductivities of the electrolyte solutions were determined by the complex impedance method using an AC impedance analyzer (Princeton Applied Research, VMP2) in a frequency range of 1 Hz–500 kHz at an amplitude of10mV. A conductivity cell possessing two electrodes of platinized platinum (TOA Electronics, CG-511B, cell constant = approximately 1 cm^{-1}) was used for conductivity measurements. The cell constant for the conductivity measurements was determined by calibration with a 0.01M KCl standard solution (Kanto Chemical). The cell was placed in a temperature-controlled chamber to ensure thermal

equilibrium for at least 60 min. The relative uncertainty for conductivity values was < 1%. The temperature dependence of viscosity and density were measured using an SVM3000 viscometer (Anton Paar). Uncertainty of density and viscosity values were ± 0.0005 gcm^{-3} and ± 0.35% respectively. Raman spectra were measured using a 532 nm laser RMP-300 Raman spectrometer (JASCO, Japan) at room temperature between 200−1700 cm^{-1}. All spectra were recorded in the liquid state. Raman spectral bands were analyzed for different concentrations with baseline correction using a JASCO spectra manager program.

Pulsed-field gradient spin echo (PGSE) NMR measurements were carried out to determine the self-diffusion coefficients of the components of the electrolyte solutions. A JEOL ECX-400 NMR spectrometer with a 9.4 T narrow-bore superconducting magnet and a pulsed-field gradient probe was used for the measurements. ^{1}H, ^{7}Li, and ^{19}F NMR spectra were recorded for the solvents, Li^{+}, and $[TFSA]^{-}$, respectively. The self-diffusion coefficients were measured via the use of a modified Hahn spin echo-based PGSE sequence incorporating a pulsed field gradient (PFG) in each τ period. The detailed measurement procedures for PGSE NMR are described elsewhere.[17] The free diffusion echo signal attenuation E is related to the experimental parameters by the Stejskal equation with sinusoidal PFG:[18]

$$\mathrm{In}(E) = \mathrm{In}(S / S_{\delta=0}) = \frac{-\gamma^2 g^2 D\delta^2 (4\Delta - \delta)}{\pi^2}$$

where S is the spin echo signal intensity, δ is the duration of the field gradient with magnitude g, γ is the gyromagnetic ratio, and Δ is the interval between the two gradient pulses. The value of Δ (50 ms) and δ (1−10 ms) were set at constant value, whereas g (0−13 T/m) was varied for the diffusion measurements. **Figure 2-2** shows the demonstration process of the diffusion measurements. All the results were well described by the Stejskal equation, and the standard deviations of the diffusion data were less than 5%. The PGSE NMR samples were inserted into a NMR micro-tube (BMS-005J, Shigemi) to a height of 3 mm to exclude convection. All measurements were performed at 30 °C.

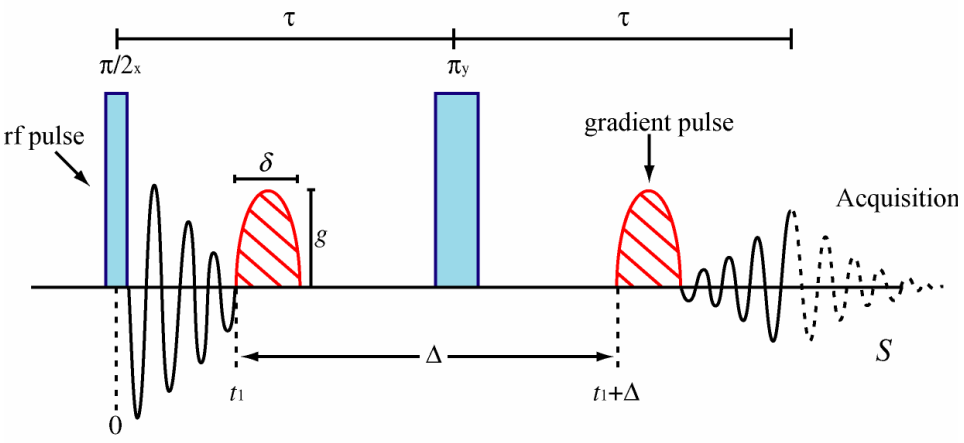

Figure 2-2. The demonstration process of the Pulsed-field gradient spin echo (PGSE) NMR measurements

2.3. Results and Discussions

2.3.1.Transport properties

Although our primary focus in this study concerned highly concentrated regions of the mixtures of Li[TFSA] and ether solvents, we first re-examined the transport properties of mixtures ranging from dilute (~0.01 mol dm^{-3}) and intermediate (~0.5 mol dm^{-3}) to extremely concentrated states (up to 3.7 mol dm^{-3}). **Figures 2-3** and **2-4** show the isothermal ionic conductivity and viscosity of [Li(glyme or THF)$_x$][TFSA] mixtures at 30°C. Similar to studies reported elsewhere,[19,20] the ionic conductivity increases as the concentration increases below 1 mol dm^{-3}, reaching a maximum at ca.1 mol dm^{-3}, and then decreases with further increases in the concentration. For [Li(G2)$_x$][TFSA] mixtures, limited data are shown in the concentrated regime because only a few appropriate ratios (G2/Li[TFSA] = 1:1, 4:3 and 4:1) yielded liquid samples at 30°C. In the dilute regime, the conductivity increases in the order of the ether solvents G1 > THF > G2 > G3 > G4 at the same concentration.

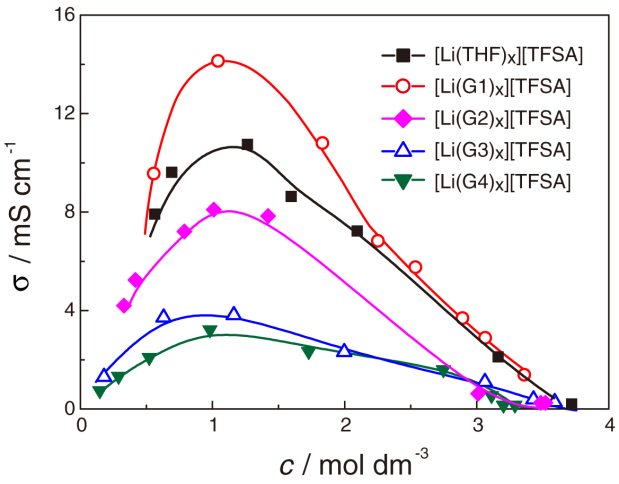

Figure 2-3. Concentration dependence ofionic conductivity for [Li(glyme or THF)$_x$][TFSA] mixtures at 30 °C. Lines in the figure are a guide to the eye.

The dependency of viscosity on concentration for [Li(glyme or THF)$_x$][TFSA] is shown in **Figure 2-4**, and is compared with the reported data for [Li(G3 or G4)$_x$][TFSA].[19] The viscosity is lower for the mixtures with shorter ethers (i.e., G1 and THF) at the same

concentration. The lower viscosity thus accounts for the higher ionic conductivity of $[Li(G1)_x][TFSA]$ compared to $[Li(G3 \text{ or } G4)_x][TFSA]$. As seen in **Figure 2-3**, however, the conductivity of $[Li(THF)_x][TFSA]$ is lower than those for $[Li(G1)_x][TFSA]$ despite the comparable viscosity for these solutions. Other factors such as the degree of dissociation or ionicity (correlation of ionic motion) may bring about differences in ionic conductivity among G1 and THF solutions (*vide infra*).

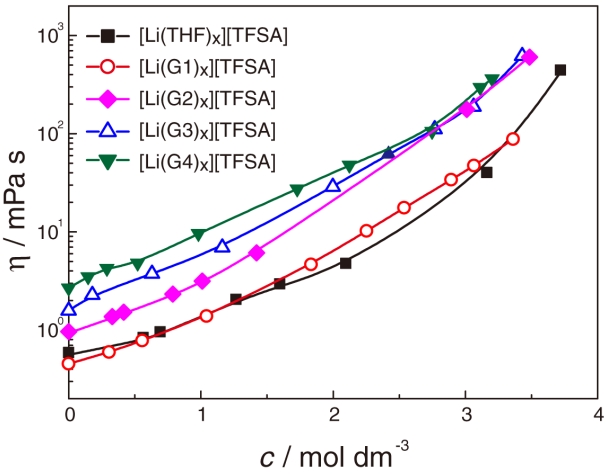

Figure 2-4. Concentration dependence of viscosity for $[Li(glyme \text{ or } THF)_x][TFSA]$ solutions at 30 °C. Lines are a guide to the eye.

The self-diffusion coefficients of the solvent, Li^+, and $[TFSA]^-$ were measured by PGSE NMR spectroscopy, and their concentration dependence is shown in the appendix of this chapter. Each diffusion coefficient decreased monotonically with increasing concentration. In the concentration range 0–2.0 mol dm^{-3}, the self-diffusion coefficients followed the order $D_{sol}>D_{TFSA}>D_{Li}$, which agrees well with the order of diffusion coefficients in conventional organic electrolytes, including the glymes.[19,21,22] However, D_{Li} became greater than D_{TFSA} in highly concentrated mixtures, implying that the coordination of Li^+ ions and their ionic diffusion differs from those in dilute systems.

In a previous study, we reported that the self-diffusion coefficient ratio of Li^+ ions and solvent molecules (D_{sol}/D_{Li}) is an effective metric to evaluate the stability of complex cations formed between Li^+ ions and the solvents G3 and G4.[16] In typical solvate ILs such as $[Li(G3)_1][TFSA]$ and $[Li(G4)_1][TFSA]$, the D_{sol}/D_{Li} ratio became unity, indicating that Li^+ and the glyme diffuse together and is therefore a good probe for confirming the formation of the long-lived complex cations $[Li(G3 \text{ or } G4)_1]^+$. Indeed, the PGSE NMR measurements were performed on the time scale of 10^{-2}–10^{-3} s, and the resulting D is given as the averaged value of both free and coordinated solvent to Li^+ ions on this time scale. **Figure 2-5** shows the D_{sol}/D_{Li} and D_{TFSA}/D_{Li} ratios of $[Li(glyme \text{ or } THF)_x][TFSA]$ depending on the concentration.

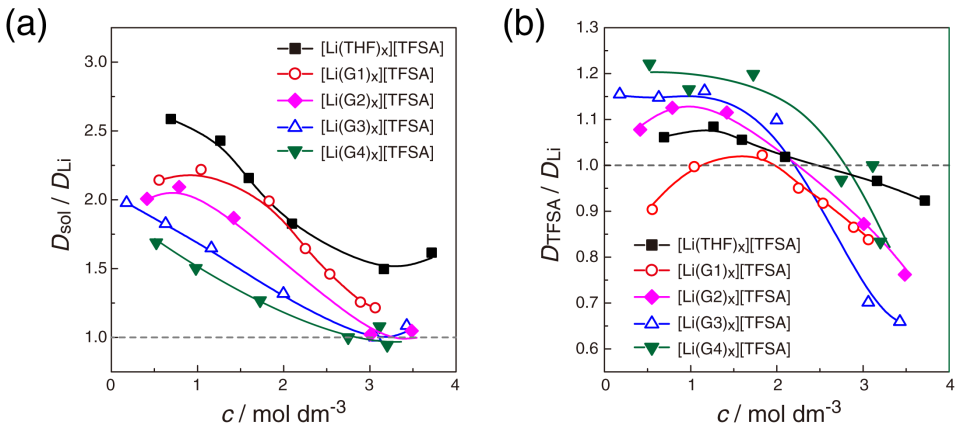

Figure 2-5. Concentration dependence of (a) D_{sol}/D_{Li} ratio and (b) D_{TFSA}/D_{Li} ratio at 30°C for [Li(glyme or THF)$_x$][TFSA] mixtures. Lines in the figure are a guide to the eye.

At lower concentrations (< 2 mol dm^{-3}), D_{sol}/D_{Li} and D_{TFSA}/D_{Li} are always greater than unity in all solvents, which is common for aprotic organic electrolyte solutions as noted above. At higher concentrations (>3 mol dm^{-3}), the D_{sol}/D_{Li} ratio of [Li(G1 or THF)$_x$][TFSA] levels off, but is still greater than unity, even if the molar concentration is as high as that of the solvate ILs [Li(G3 or G4)$_1$][TFSA]. In sharp contrast, the D_{sol}/D_{Li} ratios for [Li(G2)$_x$][TFSA] reach D_{sol}/D_{Li}~1 at higher concentration, similar to the previous results for [Li(G3 or G4)$_x$][TFSA].[19] As shown in **Figure 2-5b**, D_{TFSA}/D_{Li} becomes less than unity in the concentrated regime (>2 mol dm^{-3}) for all the [Li(glyme or THF)$_x$][TFSA] species studied in this work, indicating that Li^+ ions diffuse faster than $[TFSA]^-$. This suggests a different conduction mechanism in highly concentrated [Li(glyme or THF)$_x$][TFSA]. In dilute aprotic polar solvent solutions, it is generally assumed that solvate cations $[Li(glyme\ or\ THF)_x]^+$ and naked $[TFSA]^-$ diffuse through continuous glyme or THF with a viscosity η, as rationalized by the Stokes-Einstein equation. In such cases, the apparent hydrodynamic radius of the solvated Li^+ ion becomes larger than that of naked $[TFSA]^-$, which is a reason for a lower Li^+ transference number than 0.5 (D_{TFSA^-}/D_{Li^+} >1). On the contrary, in highly concentrated electrolytes such as ILs, the Stokes-Einstein equation has no physicochemical meaning, even if the equation appears to hold. For instance, we have reported that for imidazolium-based ILs, the cationic transference number becomes greater than 0.5 even when the cation is larger than the anion.[23] We observe that in highly concentrated [Li(glyme or THF)$_x$][TFSA] (> 2 mol dm^{-3}), D_{TFSA^-}/D_{Li^+} becomes less than unity (cationic transference number > 0.5). The lowest value of D_{TFSA^-}/D_{Li^+} for [Li(G3)$_1$][TFSA] (ca. 0.65) may not only be related to the compact solvate ion size, but also related to anomalies in the transport properties of ILs. We experimentally observe similar phenomena that cations move faster than the anion in conventional imidazolium-based ILs and in the concentrated [Li(glyme or THF)$_x$][TFSA] system.

Unique diffusivity (**Figure 2-5**) observed in the highly concentrated regime may be ascribed to the fact that certain solvates are formed through complexation between the solvent molecules and the Li salts, such that there is almost no free solvent. The differences in the properties among [Li(glyme or THF)$_x$][TFSA] were also more obvious in these concentrated mixtures. The solvate structure of the concentrated mixtures with specific [O]/[Li^+] ratio well be discussed in the next chapter.

2.3.2. Ionicity

The effect of the stability of complex cations on the dynamics of ionic transport is also of interest. Ionicity—also known as the molar conductivity ratio ($\Lambda_{imp}/\Lambda_{NMR}$)—has been used to estimate the degree of dissociation of lithium salts in dilute electrolytes,[21] and can also be a useful metric for quantifying the dissociativity or degree of correlative motion of ions, even in extremely concentrated systems like ILs.[24,25] Λ_{imp} is the molar conductivity measured by the AC impedance method, while Λ_{NMR} can be calculated from the ionic self-diffusion coefficients D_{Li} and D_{TFSA} (measured by PGSE NMR) using the Nernst-Einstein equation:

$$\Lambda_{NMR} = \frac{F^2}{RT}\left(D_{Li} + D_{TFSA}\right)$$

where F is the Faraday constant, R is the gas constant, and T is the absolute temperature. This equation postulates that all diffusing species detected by PGSE NMR contribute to the molar conductivity. In contrast, Λ_{imp} relies on the net migration of charged species in an electric field. Therefore, the ratio $\Lambda_{imp}/\Lambda_{NMR}$ accounts for the proportion of ions (charged species) that participate in ionic conduction from all diffusing species on the measurement timescale, enabling diagnosis of the correlation of ionic motion affected by ionic interactions.[26,27] $\Lambda_{imp}/\Lambda_{NMR}$ is often represented as Λ/Λ_{NE} in the literature,[28] and is reciprocal of well-known Haven ratio.[29,30]

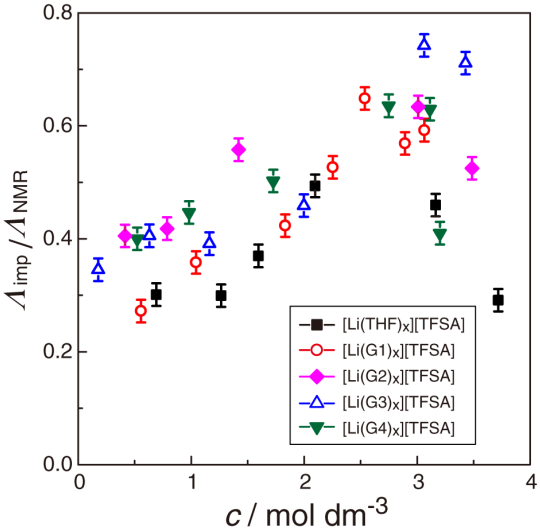

Figure 2-6. Ionicity ($\Lambda_{imp}/\Lambda_{NMR}$) at 30°C for [Li(glyme or THF)$_x$][TFSA] mixtures as a function of concentration.

In a previous study, we found that the ratio $\Lambda_{imp}/\Lambda_{NMR}$ exhibited its highest value at a 1:1 equimolar composition of [Li(G3 or G4)$_x$][TFSA] mixtures, which then decreased monotonically upon dilution. This phenomenon is opposite to that found in typical organic electrolytes—such as Li[TFSA] in propylene carbonate (PC)—in which the ionicity increased with decreasing salt concentration, as predicted by classical electrolyte theories.[31,32] In this

section, we re-examine our findings for various oligoether-based mixtures—including shorter glymes and THF—over a wide range of Li[TFSA] concentrations. **Figure 2-6** and **2-7** shows the ionicity of the [Li(glyme or THF)$_x$][TFSA] mixtures as functions of concentration and the [O]/[Li$^+$] ratio, respectively. Compared with other solvents (**Figure 2-6**), [Li(THF)$_x$][TFSA] mixtures tend to show lower ionicity, explaining the lower ionic conductivities of [Li(THF)$_x$][TFSA] than those of [Li(G1)$_x$][TFSA] (**Figure 2-3**). Similarly to the results previously reported for [Li(G3 or G4)$_x$][TFSA], $\Lambda_{imp}/\Lambda_{NMR}$ of [Li(G1, G2 or THF)$_x$][TFSA] became lower upon dilution when the concentration was lower than 3 mol dm^{-3}. More noteworthy is that the ionicity reached a maximum in the concentration range of 2–3.1 mol dm^{-3}, before decreasing again at higher concentrations (> 3 mol dm^{-3}) for all [Li(glyme or THF)$_x$][TFSA] mixtures. It was established for the first time in this study that the maximum ionicity occurs at an [O]/[Li$^+$] ratio of 4 or 5 (**Figure 2-7**). Although we do not have a clear rationale for this behavior, it should be noted that the [O]/[Li$^+$] ratio for the maximum ionicity agrees well with the favorable coordination number for Li$^+$ ions in the electrolyte. These results suggest that most uncorrelated cation-anion motions can be accomplished by the addition of a minimal amount of ether solvents that construct the first solvation shell of Li$^+$ ions (i.e., [O]/[Li$^+$] ~4 or 5).

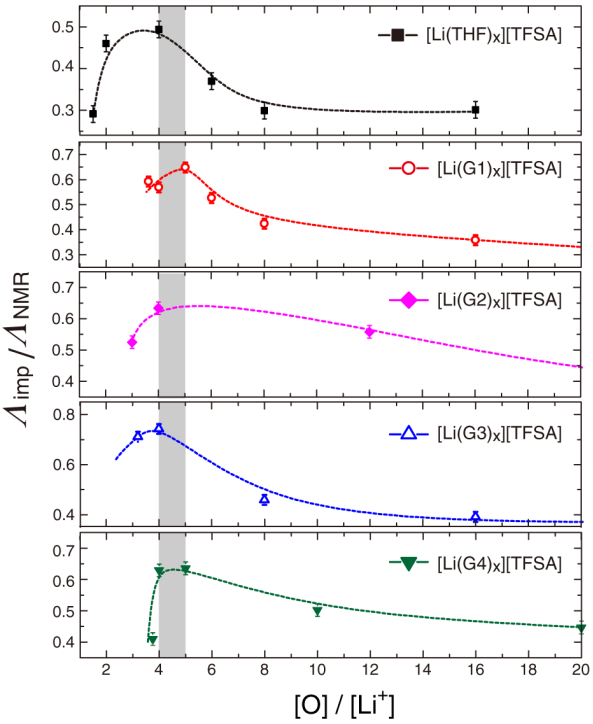

Figure 2-7. Ionicity ($\Lambda_{imp}/\Lambda_{NMR}$) at 30°C for [Li(glyme or THF)$_x$][TFSA] mixtures as a function of [O]/[Li$^+$] ratio. Lines in the figure are a guide to the eye.

2.3.3. Walden plot

Like ionicity obtained by the Nernst-Einstein equation, the Walden plot is another common method to investigate the dissociativity or degree of correlative motion of ions for ionic liquids or conventional solutions. Walden and his works provided valuable knowledge to us because in his earlier studies of aqueous solutions, he had formulated the Walden rule that relates the equivalent conductivity Λ of an ionically conducting liquid to its viscosity η.[33]

$$\Lambda\,\eta = \text{const.}$$

The rule has provided the basis for a very useful parameter of ionic liquids. Although the above equation worked reliably for aqueous solutions, the study on low-melting silver salts has been found that the rule broke down seriously and needed to be replaced by the fractional Walden rule where γ is a constant $0 < \gamma < 1$.[34]

$$\Lambda \eta^{\gamma} = \text{const.}$$

The fractional Walden rule implied that the Arrhenius activation energy for conductivity was lower than that for viscosity, which was readily interpreted in terms of the smaller silver ion slipping through the quasi-lattice of the larger halide ions, this rule being particularly clear in the case of the silver iodide which was a good conductor even in its crystalline state at temperatures near the melting point.[2] Such violations of the Walden rule are related to the unique transport properties of ILs. Angell *et al*. established a classification diagram of broad utility, now commonly referred to as a "Walden plot" based on Walden's rule.[35] Walden plot is a plot of $\log\Lambda$ vs. $\log(1/\eta)$ has been tested for ILs, in which data for a 0.01 M aqueous KCl solution were used as reference. Consequently, an "ideal" line represents the properties of an ideal electrolyte through the KCl point with slope of unity. The vertical distance from this ideal line at $\log(1/\eta)$ was utilized to classify ILs as *super*, *good*, *poor*, or *non-ionic*.[35, 36] Super protic ILs represents that proton transport likely follow Grotthuss mechanism leading to the position of data point above the ideal line. Good ILs are defined as the data point resided near the ideal line, on the other hand, a strong cation-anion interactions or incomplete proton transfer resulted poor IL that show moderate deviation from ideal KCl line, as well as non-ionic liquids that show largest deviation from ideal line.

Walden plot can also be use to evaluate the transport properties of solution electrolytes, for instant, lithium salt solutions with low permittivity solvent exhibit larger deviation from idea line comparing with the solutions containing high permittivity solvent at the same molar concentration, indicates the high permittivity solvent contained solutions regulate lower degree of ion association and higher dissociativity of the lithium salt. **Figure 2-8** shows the concentration dependent Walden plots for [Li(glyme or $THF)_x$][TFSA], by which we invited to reappraise the aforementioned ionicity plots. From **Figure 2-8** we could observe that none of the Walden plots showed linear behavior, and the variations of the slope in the Walden plots were very similar to those in the Stokes-Einstein plots of the ions. We could examine the consistency of the transport properties from dilute to extremely concentrated state. The break points also can be found in **Figure 2-8** at $[O]/[Li^+]$ ratio of 4 or 5 in the [Li(glyme or $THF)_x$][TFSA] mixtures, and the plots with $[O]/[Li^+]$ ~4 or 5 is much near to the ideal lines than the others, these behaviors are in accordance with the concentration dependence of the ratio of diffusion coefficients.

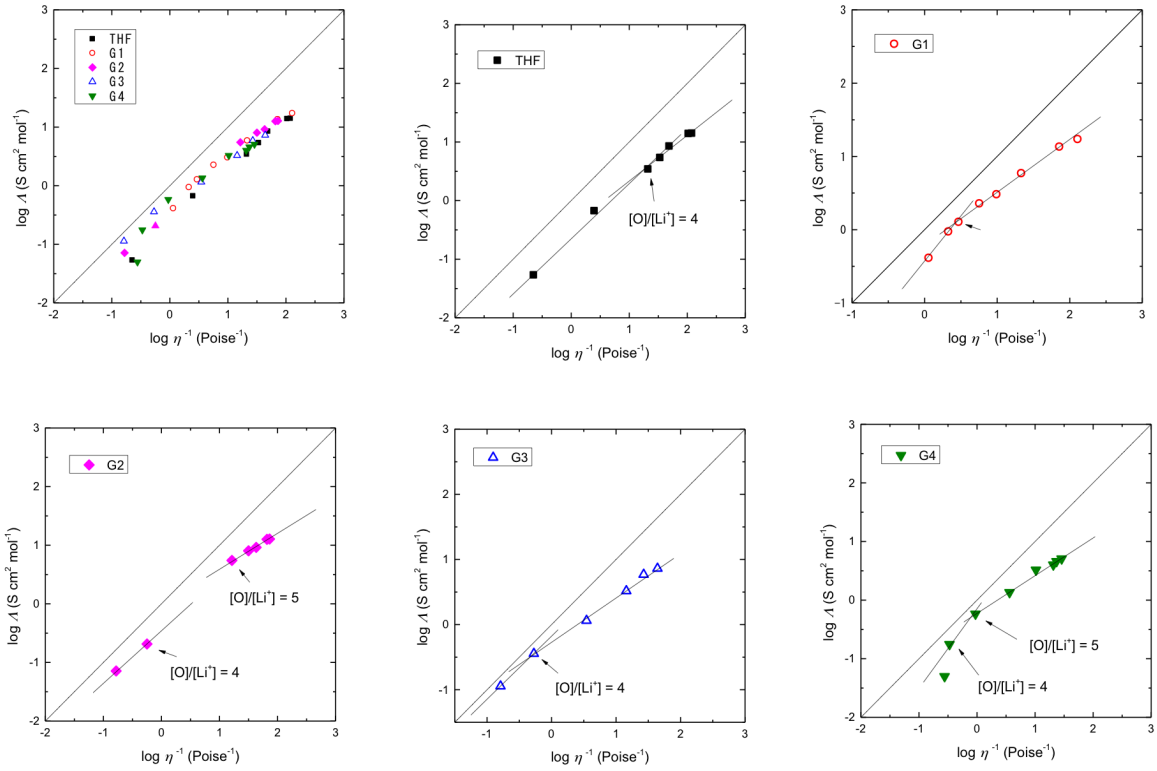

Figure 2-8. Concentration dependent Walden plots for [Li(glyme or THF)$_x$][TFSA] at 30 °C.

2.3.4. Raman spectroscopy

To further understanding transport properties and confusing ionicity behavior as well as the dynamical solution properties at a molecular level, the knowledge of the solvation structure of the solutes in the solutions by some spectroscopy methods is required. Raman spectra have been demonstrated as an important tool to study the interaction of the ions in the solution electrolytes. It was reported that the Raman bands of of 740–750 cm^{-1} wave number indicate the [TFSA]$^-$ anion; moreover, the relative greater wave number (~750 cm^{-1}) band is a measure of the concentration of Li$^+$–[TFSA]$^-$ associated species, contact ion-pairs (CIP) or aggregation state (AGG), on the other hand, the band around 740 cm^{-1} wave number originates from the solvent-separated ion-pairs (SSIP).[37] **Figure 2-9** illustrates the assignment of the Raman band for SNS and C–S stretching modes resolved into Gaussian–

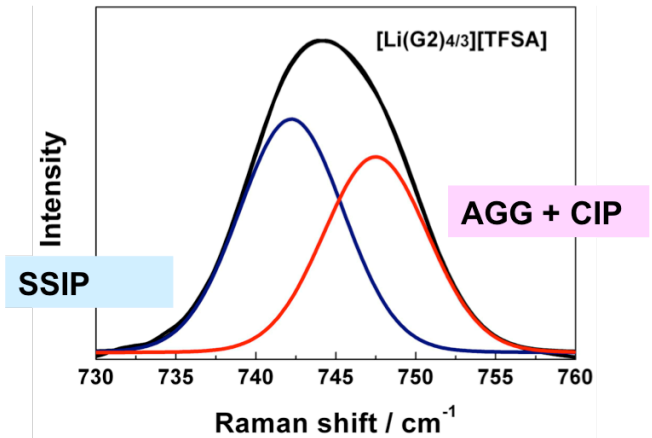

Figure 2-9. Raman spectra of [Li(G2)$_{4/3}$][TFSA] for SNS and C–S stretching modes resolved into Gaussian–Lorentzian bands.

Lorentzian bands in $[Li(G2)_{4/3}][TFSA]$.

Figure 2-10 summarizes the $[O]/[Li^+]$ ratio of the [Li(glyme or THF)][TFSA] mixtures against the variation of the relative intensity of the SSIP or AGG+CIP bands from Raman spectra, and **Figure 2-11** presents the illustrations of concentration dependence of Raman bands recorded from [Li(glyme or THF)][TFSA] mixtures. The observed perturbations of the S–N stretching mode are mostly due to anion–cation association because the anion only interacts weakly with the solvent. The intense of the AGG+CIP band decreased with the increasing of $[O]/[Li^+]$ ratio in both THF and glyme systems. Brouillette *et al*. reported the change from CIP or AGG to SSIP state of the Li[TFSA]/ G1 and G2 mixtures by the Raman spectra and they observed the $[O]/[Li^+]$ ratio is around 4–6.[37] Indeed at 30°C the $[O]/[Li^+]$ ratio of G2 system equal 5 or 6 ($[Li(G2)_{5/3}][TFSA]$ or $[Li(G2)_2][TFSA]$) is solid state and cannot gain the ionicity value from the measurement of liquid state samples to compare with the other samples. The change of the S–N mode bands were discontinuous when the number of $[O]/[Li^+]$ was less than 4. According to these results, we assume that when $[O]/[Li^+]$ was less than 4 or 5, the major association state of [Li(glyme or THF)][TFSA] mixtures are AGGs or CIPs and ion-ion interaction are prevailing. Otherwise, the ion-solvent interaction, the SSIPs state, would be in the majority with increase of the solvent to make $[O]/[Li^+]$ greater than 4 or 5.

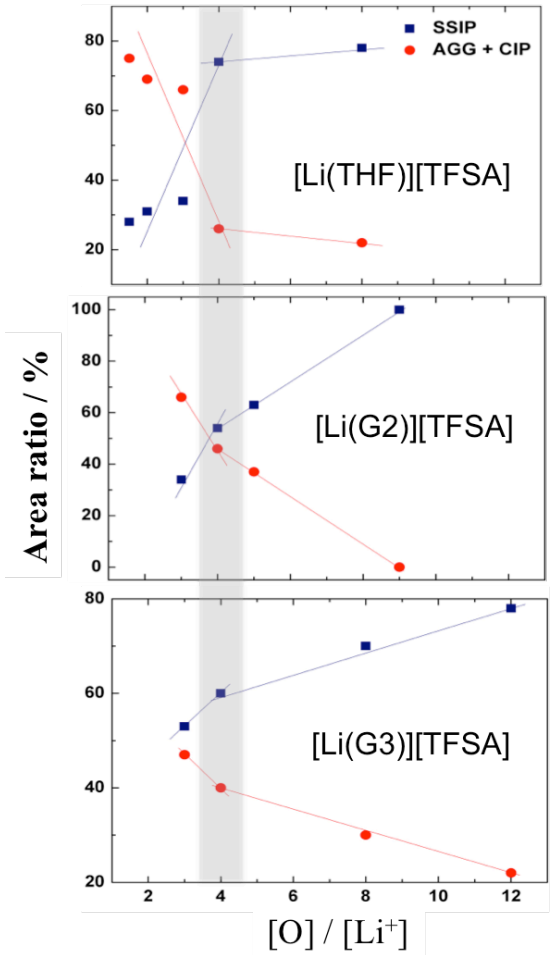

Figure 2-10. Variation of the relative intensity of the SSIP or AGG+CIP bands with $[O]/[Li^+]$ for [Li(glyme or THF)][TFSA] mixtures.

2.3.5. The ionicity behavior

The decrease in the ionicity upon dilution is likely common for ether-based $[Li(glyme\ or\ THF)_x][TFSA]$ mixtures, and independent of number of oxygen atoms in the molecules. This is reminiscent of our previous results found in aprotic ILs with the addition of solvents with relatively low polarity.[38,39] It was assumed that self-dissociable IL cations and anions form a relatively long-lived aggregate when diluted with low-polar solvents; cation-anion attractive forces would be enhanced in the presence of low-polarity solvents, rather than in neat ILs

with well-balanced ionic interactions. Given the maximum ionicity results from an [O]/[Li^+] ratio of ~4 or 5, these ratios may be sufficient for the dissociation of the solvated Li^+ and $[TFSA]^-$. In a similar fashion to the mixtures of aprotic ILs and low-polarity solvents, further addition of glymes or THF with low permittivity (ε = 7~8)[40] may bring about ionic association, where the excess solvent would serve as a low dielectric medium. As discussed above, Raman spectra of $[TFSA]^-$ in [Li(glyme or THF)$_x$][TFSA] (**Figure 2-10** and **2-11**) indicate that the number of either uncoordinated or SSIP-type $[TFSA]^-$ species increased upon dilution. Therefore, Raman spectra and the lowered ionicity would suggest that loosely-bound ion-pairs (or ionic aggregates) composed of solvated cations and [TFSA] (i.e., SSIPs) are formed in dilute [Li(glyme or THF)$_x$][TFSA] mixtures.

Such behavior is common for the oligoethers studied in this work. However, this is probably not the case for other non-aqueous aprotic solvents with higher permittivity—such as PC (ε ~64)—where Coulombic attractions between the solvated cation and the counter anions are more shielded.[41,42] In MD simulations by Borodin *et al*, a noticeable dynamic correlation of ionic motion was found in dilute Li[TFSA] solutions in less polar G1, while completely uncorrelated Li^+ and $[TFSA]^-$ motion was observed in dilute Li[TFSA] solutions in polar EC.[43,44]

The decrease in the ionicity at an [O]/[Li^+] ratio lower than 4 (highly concentrated regime) is probably due to the strong association of Li^+ with $[TFSA]^-$. In these extremely concentrated conditions, $[TFSA]^-$ must participate in the solvation of Li^+ to satisfy the lowest coordination number of 4 for Li^+ ions. This gives rise to a long-lived CIP or AGG, as evidencedby the Raman band of $[TFSA]^-$ in the range of 730–760 cm^{-1} further shifting to high frequency at an [O]/[Li^+] ratio less than 4 (**Figure 2-10** and **2-11**). Hence, Li^+ and $[TFSA]^-$ migrate collectively in the form of a CIP and/or AGG, leading to a drastic decrease in the ionicity.

Therefore, the ligands (the solvent or the anion) in the first coordination sphere of Li^+ ions are responsible for the ionicity value in highly concentrated regimes, whereas the dipolar properties of the solvent dominate the ionicity in dilute regimes.

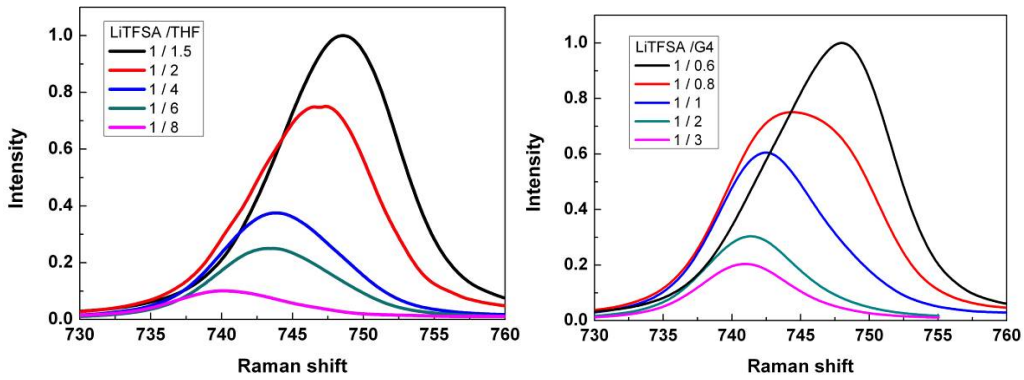

Figure 2-11. Raman spectra of (left) $[Li(THF)_x][TFSA]$ and (right) $[Li(G4)_x][TFSA]$.

2.3.6. The solvent effect on ionicity

As described above, the ionicity behavior of the binary system consisting of Li[TFSA] and solvents will change dependent on the type of the solvent. For the high permittivity solvent such as EC or PC, the ionicity of the solutions increase with decrease of the concentration, on the other hand, the ionicity exhibits a maximum value at $[O]/[Li^+]$~4 or 5 and further decreases by diluting in the ether (glymes or THF) contained solutions. It is well known that to the common organic solvent, the ion association constant decrease with dilution and ionicity should be increase due to the reducing of ion aggregation or cluster. Herein we prepared the mixtures of Li[TFSA] and different kinds of solvent to study the solvent effect on ionicity behaviour. **Figure 2-12** shows the ionicity change as a function of concentration and $[O]/[Li^+]$ ratio for the $[Li(solvent)_x][TFSA]$ mixtures, and solvents with various properties, such as permittivity and donor number (*DN*) were selected and investigated. The transport properties such as density, viscosity and ionic conductivity of these mixtures are listed in the appendix and only the dissociativity evaluated by PGSE NMR or Walden plot are summarized.

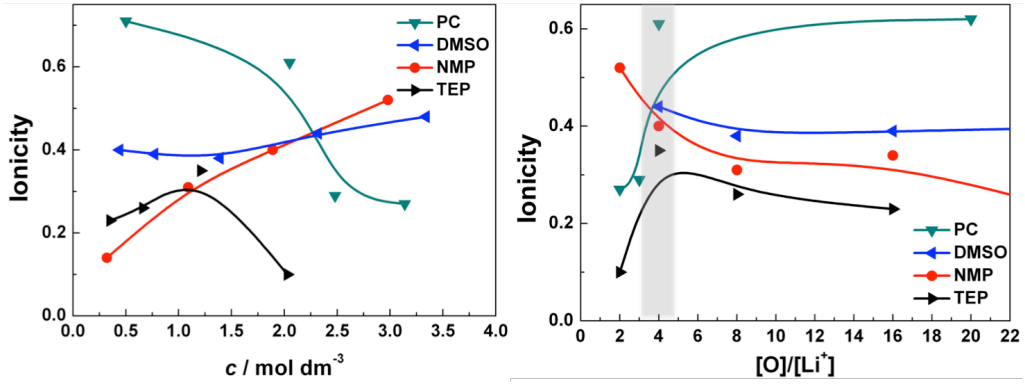

Figure 2-12. Ionicity ($\Lambda_{imp}/\Lambda_{NMR}$ or $\Lambda_{imp}/\Lambda_{ideal}$) at 30 °C for $[Li(solvent)_x][TFSA]$ mixtures as a function of (Left) molar concentration *c* and (Right) $[O]/[Li^+]$ ratio. Lines in the figure are just guides for the eye.

From **Figure 2-12** we could observe the change of ionicity dependent on the type of solvent. The $[Li(TEP)_x][TFSA]$ mixtures exhibits an similar plot as the $[Li(glyme\ or\ THF)_x][TFSA]$,

and the ionicity of the mixtures with NMP solvent decreases unilaterally upon diluting. It is very interesting to found that on the $[Li(DMSO)_x][TFSA]$ mixtures the ionicity does not charge so much at the concentration range from 0.3 mol dm^{-3} to 3.3 mol dm^{-3}. The mixtures with PC have an ionicity behavior as described before.[41] The permittivity of the solvent for TEP, NMP, DMSO and PC is 13.1, 32, 46.7 and 64 respectively. It is worth to note that at $[O]/[Li^+]$ ~4 the ionicity values of the mixtures follows that consequence of the permittivity of the solvents. The analogous change of ionicity for TEP and ethers such as THF and G1 may attribute to the comparable properties of the solvents. However, the unique plot of NMP or DMSO is rather difficult to explain. Although NMP and DMSO belong to the high permittivity aprotic solvent as well as carbonate such as PC and EC, diverse dissociativity especially in dilute regime may due to the difference of the permittivity. As we know that the permittivity of media influences the electrostatic interactions between electric charges, and the permittivity of a solvent has a decisive influence on the electrostatic ion-ion and ion-solvent interactions as well as on the dissolution and dissociation of the electrolytes. The difference of the ionicty behaviour would be determined by the different ion-solvent interactions, and the solvent effect may give a considerable affection on the solvation of the Li[TFSA]. Despite the ionicity behavior of the binary system consisting of Li[TFSA] and solvents is unclear, the solvent effect on ionicity of the solutions is observed and further study is requisite to reveal this phenomenon.

2.4. Conclusions

In conclusion, in order to understand type of solvent and ion-solvent interaction on the properties of [Li(glyme or THF)][TFSA] mixtures, a binary system consisting of Li[TFSA] and solvents (glyme or THF) covering a continuous range of Li[TFSA] concentrations were prepared. The ionic conductivity of [Li(THF or glyme)][TFSA] solutions changed depending on the Li[TFSA] concentration and passed through a maximum at ca. 1 mol dm^{-3} and the viscosity of the solutions monotonically increased as the concentration of Li[TFSA] increased. The self-diffusion coefficient of each chemical species in the electrolyte solutions increased as the concentration decreased. D_{sol} in excess glyme solutions was higher than D_{Li} and D_{TFSA}. The maximum ionicity ($\Lambda_{imp}/\Lambda_{NMR}$) of $[Li(glyme\ or\ THF)_x][TFSA]$ mixtures was found at a concentration range of $[O]/[Li^+]$ ~4 or 5, and the ionicity decreased both in the higher and lower concentration range. To understand this ionicity behaviour, two solvent effects were considered: the solvating effect of the ligands (the solvent and/or the anion) in the first coordination shell for the concentrated regime, and the dipolar effect of the solvent in the dilute regime.

2.5. References

1 Angell, C. A. *J. Electrochem. Soc.* **1965**, *112*, 1224.
2 Angell, C. A.; Ansari, Y.; Zhao, Z. *Faraday Discuss.* **2012**, *154*, 9.
3 Mandai, T.; Yoshida, K.; Ueno, K.; Dokko, K.; Watanabe, M. *Phys. Chem. Chem. Phys.* **2014**, *16*, 8761.
4 Tamura, T.; Hachida, T.; Yoshida, K.; Tachikawa, N.; Dokko, K.; Watanabe, M. *J. Power Sources* **2010**, *195*, 6095.
5 Tamura, T.; Yoshida, K.; Hachida, T.; Tsuchiya, M.; Nakamura, M.; Kazue, Y.; Tachikawa, N.; Dokko, K.; Watanabe, M. *Chem. Lett.* **2010**, *39*, 753.
6 Yoshida, K.; Nakamura, M.; Kazue, Y.; Tachikawa, N.; Tsuzuki, S.; Seki, S.; Dokko, K.; Watanabe, M. *J. Am. Chem. Soc.* **2011**, *133*, 13121.
7 Yoshida, K.; Tsuchiya, M.; Tachikawa, N.; Dokko, K.; Watanabe, M. *J. Electrochem. Soc.* **2012**, *159*, A1005.
8 Seki, S.; Takei, K.; Miyashiro, H.; Watanabe, M. *J. Electrochem. Soc.* **2011**, *158*, A769.
9 Orita, A.; Kamijima, K.; Yoshida, M.; Dokko, K.; Watanabe, M. *J. Power Sources* **2011**, *196*, 3874.
10 Tachikawa, N.; Yamauchi, K.; Takashima, E.; Park, J. -W.; Dokko, K.; Watanabe, M. *Chem. Commun.* **2011**, *47*, 8157.
11 Dokko, K.; Tachikawa, N.; Yamauchi, K.; Tsuchiya, M.; Yamazaki, A.; Takashima, E.; Park, J. -W.; Ueno, K.; Seki, S.; Serizawa, N.; Watanabe, M. *J. Electrochem. Soc.* **2013**, *160*, A1304.
12 Ueno, K.; Park, J. -W.; Yamazaki, A.; Mandai, T.; Tachikawa, N.; Dokko, K.; Watanabe, M. *J. Phys. Chem. C* **2013**, *117*, 20509.
13 McOwen, D. W.; Seo, D. M.; Borodin, O.; Vatamanu, J.; Boyle, P. D.; Henderson, W. A. *Energy Environ. Sci.* **2014**, *7*, 416.
14 Suo, L.; Hu, Y.-S.; Li, H.; Armand, M.; Chen, L. *Nat. Commun.* **2013**, *4*, 1481.
15 Shin, E. S.; Kim, K.; Oh, S. H.; Cho, W. I. *Chem. Commun.* **2013**, *49*, 2004.
16 Ueno, K.; Yoshida, K.; Tsuchiya, M.; Tachikawa, N.; Dokko, K.; Watanabe, M. *J. Phys. Chem. B* **2012**, *116*, 11323.
17 Tokuda, H.; Hayamizu, K.; Ishii, K.; Abu Bin Hasan Susan, M.; Watanabe, M. *J. Phys. Chem. B* **2004**, *108*, 16593.
18 Price, W. S. *NMR Studies of Translational Motion: Principles and Applications*; Cambridge University Press, **2009**.
19 Yoshida, K.; Tsuchiya, M.; Tachikawa, N.; Dokko, K.; Watanabe, M. *J. Phys. Chem. C* **2011**, *115*, 18384.
20 Brouillette, D.; Perron, G.; Desnoyers, J. E. *J. Solut. Chem.* **1998**, *27*, 151.
21 Hayamizu, K.; Aihara, Y.; Arai, S.; Martinez, C. G. *J. Phys. Chem. B* **1999**, *103*, 519.
22 Hayamizu, K.; Akiba, E.; Bando, T.; Aihara, Y. *J. Chem. Phys.* **2002**, *117*, 5929.
23 Tokuda, H.; Hayamizu, K.; Ishii, K.; Susan, M.; Watanabe, M. *J. Phys. Chem. B* **2005**, *109*, 6103.
24 Tokuda, H.; Tsuzuki, S.; Susan, M.; Hayamizu, K.; Watanabe, M. *J. Phys. Chem. B* **2006**, *110*, 19593.
25 Ueno, K.; Tokuda, H.; Watanabe, M. *Phys. Chem. Chem. Phys.* **2010**, *12*, 1649.
26 Harris, K. R. *J. Phys. Chem. B* **2010**, *114*, 9572.
27 Kashyap, H. K.; Annapureddy, H. V. R.; Raineri, F. O.; Margulis, C. J. *J. Phys. Chem. B* **2011**, *115*, 13212.
28 MacFarlane, D. R.; Forsyth, M.; Izgorodina, E. I.; Abbott, A. P.; Annat, G.; Fraser, K. *Phys. Chem. Chem. Phys.* **2009**, *11*, 4962.
29 Murch, G. E. *Solid State Ionics* **1982**, *7*, 177.

30 Fromling, T.; Kunze, M.; Schonhoff, M.; Sundermeyer, J.; Roling, B. *J. Phys. Chem. B* **2008**, *112*, 12985.
31 Robinson, R. A.; Stokes, R. H. *Electrolyte Solutions*; Dover Publications, **1970**.
32 Bockris, J. O. M.; Reddy, A. K. N. *Modern Electrochemistry 1: Ionics*; Springer, **1998**.
33 Walden, P. *Bull. Acad. Imper. Sci.* **1914**, 405.
34 Hurley, F. H.; Wier, T. P. *J. Electrochem. Soc.* **1951**, *98*, 203.
35 Xu, W.; Cooper, E. I.; Angell, C. A. *J. Phys. Chem. B* **2003**, *107*, 6170.
36 Yoshizawa, M.; Xu, W.; Angell, C. A. *J. Am. Chem. Soc.* **2003**, *125*, 15411.
37 Brouillette, D.; Irish, D. E.; Taylor, N. J.; Perron, G.; Odziemkowski, M.; Desnoyers, J. E. *Phys. Chem. Chem. Phys.* **2002**, *4*, 6063.
38 Tokuda, H.; Baek, S. J.; Watanabe, M. *Electrochemistry* **2005**, *73*, 620.
39 Borodin, O.; Henderson, W. A.; Fox, E. T.; Berman, M.; Gobet, M.; Greenbaum, S. *J. Phys. Chem. B* **2013**, *117*, 10581.
40 Choquette, Y.; Brisard, G.; Parent, M.; Brouillette, D.; Perron, G.; Desnoyers, J. E.; Armand, M.; Gravel, D.; Slougui, N. *J. Electrochem. Soc.* **1998**, *145*, 3500.
41 Aihara, Y.; Sugimoto, K.; Price, W. S.; Hayamizu, K. *J. Chem. Phys.* **2000**, *113*, 1981.
42 Takeuchi, M.; Kameda, Y.; Umebayashi, Y.; Ogawa, S.; Sonoda, T.; Ishiguro, S. -i.; Fujita, M.; Sano, M. *J. Mol. Liq.* **2009**, *148*, 99.
43 Borodin, O.; Smith, G. D. *J. Solut. Chem.* **2007**, *36*, 803.
44 Borodin, O.; Smith, G. D. *J. Phys. Chem. B* **2006**, *110*, 4971.

Appendix

Physicochemical properties of [Li(glyme or THF)$_x$][TFSA] mixtures at 30 °C.

	η /mPa s	d /gcm^{-3}	c /mol dm^{-3}	σ /mS cm^{-1}	Λ_{imp}	$\Lambda_{imp}/\Lambda_{NMR}$	Diffusion coefficient/10^{-7}cm^{2}s^{-1}		
							D_{sol}	D_{cation}	D_{anion}
[Li(THF)$_{3/2}$][TFSA]	444.34	1.4697	3.72	0.20	0.05	0.29	0.42	0.26	0.24
[Li(THF)$_2$][TFSA]	40.18	1.3643	3.16	2.11	0.67	0.46	2.99	2.00	1.93
[Li(THF)$_4$][TFSA]	4.77	1.2066	2.09	7.23	3.45	0.49	17.10	9.37	9.54
[Li(THF)$_6$][TFSA]	2.95	1.1486	1.60	8.63	5.41	0.37	41.58	19.27	20.34
[Li(THF)$_8$][TFSA]	2.05	1.0932	1.27	10.74	8.49	0.30	89.51	36.85	39.95
[Li(THF)$_{16}$][TFSA]	0.96	0.9963	0.69	9.61	13.90	0.30	156.80	60.64	64.34
[Li(THF)$_{20}$][TFSA]	0.84	0.9751	0.55	7.91	14.03	-	-	-	-

	η /mPas	d /gcm^{-3}	c /mol dm^{-3}	σ /mS cm^{-1}	Λ_{imp}	$\Lambda_{imp}/\Lambda_{NMR}$	Diffusion coefficient/10^{-7}cm^{2}s^{-1}		
							D_{sol}	D_{cation}	D_{anion}
[Li(G1)$_{3/2}$][TFSA]	87.70	1.4193	3.36	1.38	0.41	-	-	-	-
[Li(G1)$_{9/5}$][TFSA]	47.11	1.3773	3.07	2.88	0.94	0.59	2.84	2.34	1.96
[Li(G1)$_2$][TFSA]	33.93	1.3523	2.89	3.69	1.27	0.57	4.08	3.25	2.81
[Li(G1)$_{5/2}$][TFSA]	17.67	1.2998	2.54	5.75	2.27	0.65	7.21	4.94	4.58
[Li(G1)$_3$][TFSA]	10.21	1.2561	2.25	6.82	3.03	0.53	13.12	7.98	7.58
[Li(G1)$_4$][TFSA]	4.65	1.1873	1.83	10.80	5.89	0.42	37.06	18.63	19.04
[Li(G1)$_8$][TFSA]	1.39	1.0510	1.04	14.13	13.55	0.36	113.80	51.31	51.15
[Li(G1)$_{16}$][TFSA]	0.78	0.9630	0.56	9.56	17.16	0.27	192.20	89.73	81.07
[Li(G1)$_{30}$][TFSA]	0.60	0.9165	0.31	-	-	-	-	-	-

	η /mPas	d /gcm^{-3}	c /mol dm^{-3}	σ /mS cm^{-1}	Λ_{imp}	$\Lambda_{imp}/\Lambda_{NMR}$	Diffusion coefficient/10^{-7}cm^{2}s^{-1}		
							D_{sol}	D_{cation}	D_{anion}
[Li(G2)$_1$][TFSA]	602.20	1.4680	3.48	0.25	0.07	0.53	0.22	0.21	0.16
[Li(G2)$_{4/3}$][TFSA]	176.90	1.4027	3.01	0.62	0.21	0.63	0.48	0.47	0.41
[Li(G2)$_4$][TFSA]	6.10	1.1734	1.42	7.84	5.52	0.56	23.66	12.67	14.13
[Li(G2)$_6$][TFSA]	3.16	1.1049	1.01	8.10	8.02	-	-	-	-
[Li(G2)$_8$][TFSA]	2.33	1.0681	0.79	7.21	9.16	0.42	58.41	27.92	31.42
[Li(G2)$_{16}$][TFSA]	1.52	1.0075	0.42	5.24	12.61	0.41	81.42	40.58	43.73
[Li(G2)$_{20}$][TFSA]	1.37	0.9909	0.33	4.20	12.73	-	-	-	-

	η	d	c	σ	Λ_{imp}	$\Lambda_{imp}/\Lambda_{NMR}$	Diffusion coefficient/10^{-7}cm^{2}s^{-1}		
	/mPas	/gcm^{-3}	/mol dm^{-3}	/mS cm^{-1}			D_{sol}	D_{cation}	D_{anion}
[Li(G3)$_{4/5}$][TFSA]	617.44	1.4736	3.43	0.39	0.11	0.71	0.28	0.26	0.17
[Li(G3)$_1$][TFSA]	187.68	1.4247	3.06	1.10	0.36	0.74	0.77	0.77	0.54
[Li(G3)$_{6/5}$][TFSA]	110.98	1.3871	2.77	-	-	-	-	-	-
[Li(G3)$_{3/2}$][TFSA]	61.65	1.3414	2.42	-	-	-	-	-	-
[Li(G3)$_2$][TFSA]	28.73	1.2860	2.00	2.31	1.16	0.46	4.28	3.25	3.57
[Li(G3)$_4$][TFSA]	6.92	1.1610	1.16	3.81	3.28	0.39	17.30	10.50	12.20
[Li(G3)$_8$][TFSA]	3.74	1.0800	0.63	3.71	5.88	0.41	33.40	18.30	21.00
[Li(G3)$_{30}$][TFSA]	2.27	1.0060	0.18	1.30	7.28	0.35	52.40	26.50	30.60

	η	d	c	σ	Λ_{imp}	$\Lambda_{imp}/\Lambda_{NMR}$	Diffusion coefficient/10^{-7}cm^{2}s^{-1}		
	/mPas	/gcm^{-3}	/mol dm^{-3}	/mS cm^{-1}			D_{sol}	D_{cation}	D_{anion}
[Li(G4)$_{3/4}$][TFSA]	361.97	1.4534	3.20	0.16	0.05	0.41	0.17	0.18	0.15
[Li(G4)$_{4/5}$][TFSA]	297.10	1.4471	3.11	0.55	0.18	0.63	0.41	0.38	0.38
[Li(G4)$_1$][TFSA]	106.00	1.4000	2.75	1.60	0.58	0.64	1.26	1.26	1.22
[Li(G4)$_{3/2}$][TFSA]	47.92	1.3171	2.12	-	-	-	-	-	-
[Li(G4)$_2$][TFSA]	27.46	1.2640	1.73	2.34	1.35	0.50	4.21	3.32	3.98
[Li(G4)$_4$][TFSA]	9.66	1.1550	0.98	3.22	3.28	0.45	13.80	9.18	10.70
[Li(G4)$_8$][TFSA]	4.83	1.0780	0.52	2.09	4.00	0.40	20.60	12.20	14.90
[Li(G4)$_{15}$][TFSA]	4.26	1.4080	0.29	1.33	4.60	-	-	-	-
[Li(G4)$_{30}$][TFSA]	3.50	1.0260	0.15	0.75	5.08	-	-	-	-

	η /mPa・s	d /gcm^{-3}	M /mol dm^{-3}	m /mol kg^{-1}	σ /mS cm^{-1}	Λ_{imp}	$\Lambda_{imp}/\Lambda_{ideal}$
[Li(TEP)$_2$][TFSA]	31.26	1.31	2.03	1.56	0.67	0.33	0.10
[Li(TEP)$_4$][TFSA]	11.9	1.21	1.21	0.99	3.51	2.91	0.35
[Li(TEP)$_8$][TFSA]	3.7	1.15	0.66	0.58	4.63	7.02	0.26
[Li(TEP)$_{16}$][TFSA]	2.2	1.11	0.35	0.31	3.54	10.23	0.23

	η /mPa・s	d /gcm^{-3}	M /mol dm^{-3}	m /mol kg^{-1}	σ /mS cm^{-1}	Λ_{imp}	$\Lambda_{imp}/\Lambda_{ideal}$
[Li(DMSO)$_2$][TFSA]	367.87	1.45	3.34	2.30	0.44	0.13	0.48
[Li(DMSO)$_4$][TFSA]	25.2	1.37	2.32	1.69	4.03	1.73	0.44
[Li(DMSO)$_8$][TFSA]	5.3	1.25	1.39	1.11	9.79	7.05	0.38
[Li(DMSO)$_{16}$][TFSA]	3.1	1.18	0.77	0.65	9.86	12.74	0.39
[Li(DMSO)$_{30}$][TFSA]	2.41	1.14	0.44	0.38	7.15	16.44	0.40

	η /mPa・s	d /gcm^{-3}	M /mol dm^{-3}	m /mol kg^{-1}	σ /mS cm^{-1}	Λ_{imp}	$\Lambda_{imp}/\Lambda_{ideal}$
[Li(NMP)$_2$][TFSA]	451.82	1.42	2.98	2.10	0.34	0.11	0.52
[Li(NMP)$_4$][TFSA]	24.7	1.28	1.89	1.48	3.07	1.62	0.40
[Li(NMP)$_8$][TFSA]	5.3	1.17	1.09	0.93	6.37	5.83	0.31
[Li(NMP)$_{16}$][TFSA]	2.9	1.10	0.59	0.54	6.91	11.68	0.34
[Li(NMP)$_{30}$][TFSA]	1.79	1.04	0.32	0.31	2.44	7.65	0.14

	η /mPa・s	d /gcm^{-3}	M /mol dm^{-3}	m /mol kg^{-1}	σ /mS cm^{-1}	Λ_{imp}	$\Lambda_{imp}/\Lambda_{ideal}$
[Li(DEC)$_2$][TFSA]	24.9	1.33	2.58	1.94	1.07	0.41	0.10
[Li(DEC)$_4$][TFSA]	4.7	1.20	1.59	1.33	2.96	1.86	0.09
[Li(DEC)$_8$][TFSA]	1.9	1.10	0.90	0.82	2.30	2.57	0.05
[Li(DEC)$_{16}$][TFSA]	1.2	1.04	0.48	0.46	0.73	1.54	0.02

Chapter Three

Ion-Solvent Interaction and Solvate-Structure Stability of the Glyme Based Solvents and Li Salt Mixtures

Abstract

In the concentrated regions where the [O]/[Li^+] ratio was adjusted to be 4 or 5, the mixtures yielding the solvate ILs could be easily distinguished from the concentrated solutions by analyzing the self-diffusion coefficient ratio of D_{sol}/D_{Li}. D_{sol}/D_{Li} was always greater than 1 in concentrated solutions ([Li(G1 or $THF)_x$][TFSA] mixtures) even when the molar concentration was higher than 3 mol dm^{-3}, whereas the solvate ILs ([Li(G3 or $G4)_1$][TFSA] and [$Li(G2)_{4/3}$][TFSA]) showed a D_{sol}/D_{Li} of ~1, indicating the presence of long-lived complex cations. The different stabilities of the complex cations of [Li(glyme or $THF)_x$][TFSA] mixtures with an [O]/[Li^+] ratio of ~4 or 5 could be explained by the chelate effect, where longer glymes are liable to form stable solvate cations, affording a high thermal and electrochemical stability. Interestingly, compared to the fact that notable decomposition occurred in concentrated [$Li(THF)_4$][TFSA] and [$Li(G1)_2$][TFSA] solutions at lower potentials, the oxidative decomposition was greatly suppressed in the solvate ILs [$Li(G3)_1$][TFSA] and [$Li(G2)_{4/3}$][TFSA]. In addition, the solvent dependence of solvate-structure stability was studied by comparing the thermal stability and transport properties of a series of [Li(solvent)$_x$][TFSA] mixtures with an [O]/[Li^+] ratio of ~4.

Part of the work presented in this chapter has been published as:

Zhang, C.; Ueno, K.; Yamazaki, A.; Yoshida, K.; Moon, H.; Mandai, T.; Umebayashi, Y.; Dokko, K.; Watanabe, M. *J. Phys. Chem. B* **2014**, *118*, 5144-5153.

3.1. Introduction

Understanding the physicochemical properties as well as the internal structure of liquid electrolyte has long been an important subject of research on solution chemistry.[1-3] Especially in extremely concentrated electrolytes, the internal forces such as ion-ion, ion-solvent, and their mutual interactions are very complicated, thus currently no credible valid model can give a reasonable account for the experimental results.[3,4] Although the theoretical works based on empirical extensions of equations for dilute solutions or the structure resembling a crystal lattice can be applied to the concentrated solutions, numerous limitation and enormous gulf between the conceivable model and practical variants still remain. Furthermore, the importance of the highly dense electrolyte systems has been becoming a compelling topic in recent year. In particular concerning the high energy-density storage devices, in which the high ionic conductive electrolyte with other extraordinary properties such as high electrochemical stability, non-volatility, and non-flammability is considered as an important factor.[5-8]

Ionic liquids (ILs) are promising as alternative electrolytes to conventional organic solvents for future power sources and other applications owing to their outstanding physicochemical properties.[9,10] Owing to their remarkable features such as high thermal and chemical stability, negligible vapour pressure, and high ionic conductivity, ILs have attracted much attention as a new class of electrolyte candidates used in electrochemical devices including batteries and electrochemical capacitors.[11-13] What's more, the significance of ILs appears on both theoretical and practical aspect. For the theoretical study, these solvent-free ILs can be regarded as the extreme case, so that much effort has been devoted to cognition of the fundamental electrolyte properties and internal interaction.[14-19] In more practical topic, lithium-conducting, IL-based electrolyte has great potential for the substitution of hazardous electrolytes in order to address recent glowing demand for the safety of lithium-ion batteries.

We have previously found that certain equimolar mixtures of oligoethers (glymes) and certain Li salts (LiX) yielded a low-melting (or glass-forming) complex abbreviated as $[Li(glyme)_1]X$,[20,21] in which strong complexation occurred between all glyme molecules and Li^+ cations involved, being in form of $[Li(glyem)_1]^+$ that behaves like organic cations in typical ILs. In recent review paper by Angell et al.,[22] ILs have been classified into four groups: existing "aprotic", "protic", "inorganic" ILs, and a novel, "solvate (or chelate)" ILs. Out of these IL families, the "solvate" ILs, for which ligand molecules as a third component strongly coordinate the cation and/or anion of salts to form the complex ions, would be an important class of the ILs which contains metal cations.

In coordination chemistry, the stability of complex ions is strongly dictated by the structure and property of ligand molecules. **Table 3-1** shows the physical properties of some common organic solvents.[23] As oppose to rich in expertise for a wide variety of

ligand-metal salts complexes based on coordination chemistry, little is known about the impact of solvent type or feature on the solvate formation and electrolyte properties in fused state.[24] In this study, we investigate type of solvent and properties of a series of concentrated Li salt solutions to understand the ion-solvent interaction and criteria for characterizing the solvate ILs. The physicochemical properties of glymes or other solvent solutions containing Li[TFSA] are explored and especially the samples have similar $[O]/[Li^+]$ ratios in stoichiometry and the transport properties were systematically studied. Although the enhanced stability of complex ions with multidentate ligands is well known through the chelate effect, the studies have been generally performed in dilute solutions or in the crystalline state. The main purpose of this investigation was to study the dynamics of the chelate effect on the stability of lithium complex cations (i.e., the formation of solvate ILs) in extremely concentrated liquid states. The physicochemical properties of the concentrated mixtures were explored at constant $[O]/[Li^+]$ ratios of 4 or 5, and compared with those for the previously reported solvate IL $[Li(G3 \text{ or } G4)_1][TFSA]$. The study demonstrates that the stabilities of complex cations are clearly reflected in their thermal and electrochemical properties, as well as the transport properties of these concentrated electrolytes.

Table 3-1. Physical properties of some solvents[23]

Solvent	MW / $gmol^{-1}$	*d* / gml^{-1}	ε_r / -	η_0 / $mPas^{-1}$	*DN* / -	*mp* / °C	*bp* / °C
Ethylene cabonate (EC)	88.06	1.322 (40 °C)	89.6	1.85	16.4	37	238
Propylene cabonate (PC)	102.09	1.21	64.4	2.51	15.1	-47	238
Butylene cabonate (BC)	116.12	1.15	53.0	3.20		-53	240
γ-Butylrolactane (GBL)	86.1	1.01	39.1	1.73	18.0	-44	205
g-Valerolactane (GVL)	100.12	1.06	34.0	2.00		-31	208
1,2-Dimethoxyethane (G1)	90.1	0.867	7.20	0.46	20.0	-58	84
Diglyme (G2)	134.2	0.943	7.27	1.00		-64	162
Triglyme (G3)	178.2	0.986	7.51	2.01		-45	216
N-methyl-2-pyrrolidone (NMP)	99.13	1.028	32.0	1.67	27.3	-24	202
Tetrahydrofuran (THF)	72.11	0.889	7.40	0.46	20.0	-109	66
1,3-Dioxane (DOL)	74.08	1.06	7.10	0.59		-95	78
Dimethyl carbonate (DMC)	90.08	1.07	3.10	0.59		3	90
Diethyl carbonate (DEC)	118.13	1.01	2.90	0.65		-55	108

3.2. Experimental

3.2.1. Materials

Glymes with the chemical structure of $CH_3—O—(CH_2—CH_2—O)_n—CH_3$ (n = 1~5) are abbreviated as G1~G5 respectively. Monoglyme (G1) and diglyme (G2) were purchased from Kishida Chemical (battery grade reagents), and super dehydrated tetrahydrofuran (THF) ([H_2O] <10 ppm) was purchased from Wako Pure Chemical. Triglyme (G3) and tetraglyme (G4) were obtained from Tokyo Chemical Industry and were distilled under reduced pressure over sodium metal. Purified pentaglyme (G5) was kindly supplied by Nippon Nyukazai and used as received. Dehydrated N-methyl-2-pyrrolidone (NMP) was purchased from Kanto Chemical. Li[TFSA] was obtained from Morita Chemical Industries and dried under vacuum at 120 °C before use.

3.2.2 Preparation of mixtures

The solutions were prepared by mixing the solvent and Li[TFSA] in different molar ratios and stirring overnight at room temperature to obtain homogeneous liquids. The mixtures were prepared, stored, and handled in an argon-filled glovebox (VAC, [H_2O] <1 ppm).

3.2.3. Methodology and measurements

^{1}H NMR spectra were recorded by an FT-NMR spectrometer (JEOL JNM-AL 400) at 30 °C. Chemical shifts for the C-H proton of the pure solvent or the mixtures were determined using a double tube (inner: pure solvents or mixtures, outer: DMSO with TMS, Shigemi, Tokyo). Raman spectra were measured using a 532 nm laser RMP-300 Raman spectrometer (JASCO, Japan) at room temperature between 200−1700 cm^{-1}. All spectra were recorded in the liquid state. Raman spectral bands were analyzed for different concentrations with baseline correction using a JASCO spectra manager program.

Thermogravimetric analysis was performed using a TG/TDA 6200 apparatus (Hitachi High-tech Science) under a nitrogen atmosphere from room temperature to 550 °C at a heating rate of 10 °C min^{-1}. In this study, the thermal decomposition temperature (T_d) was defined as the temperature of a 5% mass loss in the thermogravimetric curves. Thermal properties such as melting were explored using differential scanning calorimetry (DSC) with a Seiko Instruments DSC 220C under N_2 atmosphere. The samples were tightly sealed within aluminum pans in an argon-filled glovebox. The samples were first cooled to −150 °C and then heated to 30 °C at heating and cooling rates of 10 °C min^{-1}. The DSC was recorded during the heating scans.

The temperature dependence of viscosity and density were measured using an SVM3000 viscometer (Anton Paar). Uncertainty of density and viscosity values were ± 0.0005 g cm^{-3} and ± 0.35% respectively. Ionic conductivities of the electrolyte solutions were determined by the complex impedance method using an AC impedance analyzer

(Princeton Applied Research, VMP2) in a frequency range of 1 Hz–500 kHz at an amplitude of 10mV. A conductivity cell possessing two electrodes of platinized platinum (TOA Electronics, CG-511B, cell constant = approximately 1 cm^{-1}) was used for conductivity measurements. The cell constant for the conductivity measurements was determined by calibration with 0.01 M KCl standard solution (Kanto Chemical). The cell was placed in a temperature-controlled chamber to ensure thermal equilibrium for at least 60 min. The relative uncertainty for conductivity values was < 1%.

The PGSE-NMR measurements were carried out on a JEOL ECX-400 NMR spectrometer with a 9.4 T narrow-bore superconducting magnet and a pulsed-field gradient probe. The self-diffusion coefficients were measured via the use of a modified Hahn spin echo-based PGSE sequence incorporating a pulsed field gradient (PFG) in each τ period. The value of Δ (50 ms) and δ (1−10 ms) were set at constant value, whereas g (0−13 T/m) was varied for the diffusion measurements. All the results were well described by Stejskal equation, and the standard deviations of the diffusion data were less than 5%. The PGSE NMR samples were inserted into a NMR micro-tube (BMS-005J, Shigemi) to a height of 3 mm to exclude convection. All measurements were performed at 30 °C.

The oxidative electrochemical stabilities of the binary Li[TFSA]/ether mixtures were studied using linear sweep voltammetry (LSV) at a scan rate of 1 mV s^{-1} in a three-electrode cell, with Li metal foil as the counter electrode, and a platinum disk (diameter 1 mm) encapsulated in a shrinkable fluorinated tube as the working electrode. The reference electrode was Li metal soaked in 1 mol dm^{-3} Li[TFSA]/G3 solution, confined in a glass tube equipped with a liquid junction (Vycor glass).

3.3. Results and discussion

3.3.1. Structures of molten crystalline solvates and relevant highly concentrated mixtures

Mixtures of glymes or THF and Li[TFSA] form crystalline solvates in the concentrated regime. Longer glymes such as G3, G4, and G5 tend to form a stable solvate in a 1:1 ratio with Li[TFSA].[25-27] Crystalline $[Li(G3)_1][TFSA]$ and $[Li(G5)_1][TFSA]$ possess melting points of 20 °C and 67 °C, respectively (**Figure 3-1**). However, $[Li(G4)_1][TFSA]$ did not exhibit any thermal events other than a glass transition, which may be due to crystallinity gap behavior as reported in related PEO-Li[TFSA] systems.[28] The mixtures with the shorter G1 and G2 involve a series of intermediate crystalline solvates. The previous reports suggested the formation of stable solvates in a 3:1 (T_m = 29 °C), 2:1 (T_m = 20 °C), and 1:1 ratio (T_m = 56 °C) for G1-Li[TFSA] mixtures; and a 2:1 (T_m = 83 °C), 1:1 (T_m = 22 °C), and 1:2 ratio (T_m: not reported) for G2-Li[TFSA] mixtures.[29,30] In crystalline solvates with THF reported in the literature,[31,32] Li^+ ions are mostly solvated by four THF molecules (four-fold coordination) in the form of $[Li(THF)_4]^+$ complex cations.

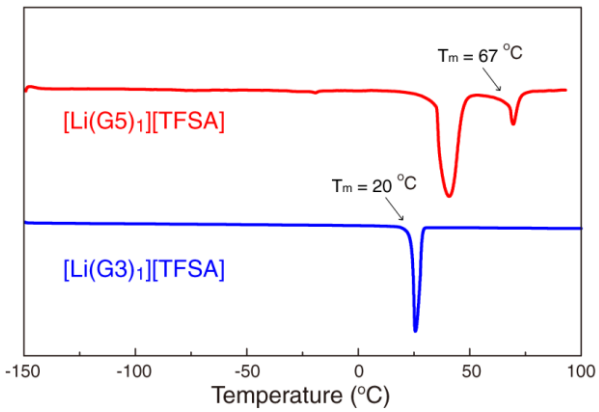

Figure 3-1. DSC thermogram of $[Li(G5)_1][TFSA]$ and $[Li(G3)_1][TFSA]$

Whereas a favorable coordination number for Li^+ ions is known to be 4-5 in solution,[33] complexes with six-fold coordination via the oxygen atoms of ether solvents, as observed in $[Li(G1)_3][TFSA]$, $[Li(G2)_2][TFSA]$, and $[Li(G5)_1][TFSA]$, seem to be more stable in the crystalline state. Indeed, they generally possess a higher melting point than other solvates that exhibit four- or five-fold coordination. Because the solvates with four- or five-fold coordination possess low melting points, they are appropriate for the prime focus of this study. **Table 3-2** summarizes the electrolyte properties (viscosity η, density ϱ, molar concentration, and ionic conductivity σ) of $[Li(glyme\ or\ THF)_x][TFSA]$ for which the ratio of Li^+ ions and oxygen atoms of the solvent ($[O]/[Li^+]$) is 4 or 5. $[Li(THF)_4][TFSA]$, $[Li(G1)_2][TFSA]$, and $[Li(G2)_{4/3}][TFSA]$ possess the same $[O]/[Li^+]$ ratio as that of $[Li(G3)_1][TFSA]$. $[Li(G1)_{5/2}][TFSA]$ can be considered an analog of $[Li(G4)_1][TFSA]$. The density and molar concentration are in the order of $[Li(G3)_1]>[Li(G2)_{4/3}]>[Li(G1)_2]>[Li(THF)_4]$, which is in accordance with the number of the oxygen atoms in each ligand molecule. $[Li(G2)_{4/3}][TFSA]$ shows the lowest ionic conductivity, even with a comparable viscosity to that of $[Li(G3)_1][TFSA]$.

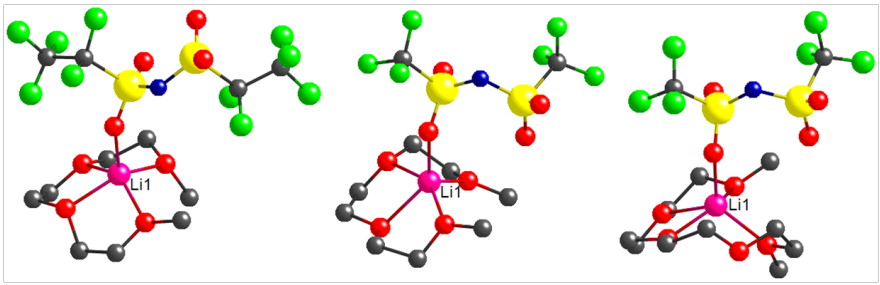

Figure 3-2. Solvate structures of $[Li(G3)_1][BETI]$ (left), $[Li(G3)_1][TFSA]$ (center) and $[Li(G4)_1][TFSA]$ (right). H atoms are omitted for clarity. Pink, Li; red, O; gray, C; blue, N; yellow, S; green, F.[8]

Table 3-2. Viscosity (η), density (ϱ), molar concentration (c), ionic conductivity (σ), and D_{sol}/D_{Li} of the [Li(glyme or THF)$_x$][TFSA] mixtures at 30 °C.

mixtures	[O]/[Li] (-)	η (mPa s)	ρ (g cm^{-3})	c (mol dm^{-3})	σ (mS cm^{-1})	D_{sol}/D_{Li} (-)
[Li(THF)$_4$][TFSA]	4	5	1.21	2.10	7.2	1.82
[Li(G1)$_2$][TFSA]	4	34	1.35	2.89	3.7	1.26
[Li(G2)$_{4/3}$][TFSA]	4	177	1.40	3.01	0.62	1.02
[Li(G3)$_1$][TFSA]	4	188	1.42	3.06	1.1	1.00
[Li(G1)$_{5/2}$][TFSA]	5	18	1.30	2.54	5.8	1.46
[Li(G4)$_1$][TFSA]	5	106	1.40	2.75	1.6	1.00

The crystal structures of [Li(G3 or G4)$_1$][TFSA] have not been revealed because of their low melting and glass forming character. While strong evidence for the complexation and the relevant remarkable properties has been demonstrated as mentioned above. As shown in **Figure 3-2**, the crystal structure of [Li(G3)$_1$][BETI] is available in literature, which is considered as an analog of [Li(G3)$_1$][TFSA].[34] In the crystalline [Li(G3)$_1$][BETI] all of the oxygen atoms in ligand was coordinated to Li^+ cation to form a 12-crown-4 ether like coordination geometry[35] and one oxygen atom from $[BETI]^-$ anion was also coordinated to Li^+ cation, which is defined as contact ion pair (CIP). On the other hand, the coordination structures of [Li(G3 or G4)$_1$][TFSA] optimized by *ab initio* molecular orbital calculation indicates that the glyme donates lone pairs of oxygen atoms to Li^+ cation, and the ligand wraps around the Li^+ cation to form a crown ether-like, one-to-one complex cation $[Li(glyme)_1]^+$.[21] The calculated structure of $[Li(G3)_1]^+$ complex cation is very similar to the crystalline [Li(G3)$_1$][BETI], and $[TFSA]^-$ anion is assumed that possesses the same chemical configuration with $[BETI]^-$ anion. In the light of the above we can speculate that the formation of complex cation $[Li(glyme)_1]^+$ is available in the equimolar mixture of G3 or G4 glyme and Li[TFSA].[8]

Meanwhile, in the reported single crystal structures of both $[Li(THF)_4]X$[31,32] and $[Li(G1)_2]X$[36,37] with different counter anions X, all the oxygen atoms of the solvent bind to the Li^+ ion to form the solvated cations $[Li(THF)_4]^+$ and $[Li(G1)_2]^+$. [Li(THF)$_4$][TFSA] and [Li(G1)$_2$][TFSA] would also possess a structurally similar complex cation to each analog in their crystalline states, although the actual crystal structure is unknown for these solvates. However, as shown in **Table 3-2**, the D_{sol}/D_{Li} ratios are greater than 1 for the

molten complexes $[Li(THF)_4][TFSA]$ and $[Li(G1)_2][TFSA]$, as well as the non-stoichiometric $[Li(G1)_{5/2}][TFSA]$. These results suggest that the complex cations are unstable in the melt, and they possess either uncoordinated solvents or short-lived complex cations where ligand exchange takes place rapidly between the solvent and the anion in the liquid state. In this respect, the molten state of stable THF and G1 solvates such as $[Li(THF)_4][TFSA]$ and $[Li(G1)_2][TFSA]$ may not be classified as solvate ILs. The coordinating or weakly coordinating (highly exchangeable) solvents can screen the strong interaction between the ions, thereby reducing the viscosity even in dense electrolytes such as $[Li(THF)_4][TFSA]$ and $[Li(G1)_2][TFSA]$ (see **Table 3-2**).

For $[Li(G2)_{4/3}][TFSA]$ (in which the mixed ratio is not stoichiometric to form the isolated solvates), the molten mixture of the stable complexes $[Li(G2)_2][TFSA]$ and $[Li(G2)_1][TFSA]$ may account for the almost equivalent diffusivity of the solvents and Li^+ ions. Because uncoordinated solvents with a long lifetime are scarcely present in the non-stoichiometric $[Li(G2)_{4/3}][TFSA]$, this molten mixture can be regarded as a solvate IL. In the $[Li(G2)_2][TFSA]$ crystal structure reported by Henderson et al,[27] the Li^+ ion is six-coordinate (by the two G2 molecules), while the $[TFSA]^-$ counter anion remains uncoordinated in the form of a solvent separated ion pair (SSIP). The crystal structure of $[Li(G2)_1][TFSA]$ was postulated based on the analogous single crystal structure $[Li(G2)_1][CF_3SO_3]$ consisting of binuclear $[Li_2(G2)_2]$ complexes cross-linked by the two anions; each five-coordinate Li^+ ion is coordinated by one G2 molecule and by two oxygen atoms from the two anions (one each from two anions).[38] This dimeric form may partially form in the liquid state, and would be responsible for the lower ionic conductivity (**Table 3-2**) and diffusion coefficients of the components in $[Li(G2)_{4/3}][TFSA]$, despite a comparable viscosity to that of $[Li(G3)_1][TFSA]$.

From the D_{sol}/D_{Li} results discussed above, $[Li(glyme\ or\ THF)_x][TFSA]$ mixtures with an $[O]/[Li^+]$ ratio of 4 or 5 can be classified into two liquids: concentrated solutions or solvate ILs. $[Li(THF)_4]^+$ and $[Li(G1)_2]^+$ solvate cations were not adequately stable in their molten states, and thus $[Li(THF)_4][TFSA]$ and $[Li(G1)_2][TFSA]$ showed ordinal electrolyte solution behavior. In contrast, $[Li(G3\ or\ G4)_1]^+$ complex cations adopting crown ether-like coordination geometries are long-lived, and behave like an independent cation in $[Li(G3\ or\ G4)_1][TFSA]$ solvate ILs.[39] Judging by the thermal stability of $[Li(G3\ or\ G4)_1][TFSA]$ solvate ILs,[4,5] there is no free glyme activity, and the lifetime of the solvates are long enough to call them solvate ILs. $[Li(G2)_{4/3}][TFSA]$ behaved as a solvate IL although it is not an isolated solvate. It is suggested that solvate ionic liquids are formed when Li[TFSA] is mixed with oligoethers possessing ethylene oxide units longer than G2 for the $[Li(glyme)_x][TFSA]$ mixtures at an $[O]/[Li^+]$ ratio of 4 or 5.

3.3.2. Chelate effect

It is clear that the D_{sol}/D_{Li} ratio correlates to the lifetime of the [Li(glyme or THF)]$^+$ complex cations in the liquid state. As mentioned in the previous chapter, the longer glymes yield more robust complex cations with Li^+, even at the same [O]/[Li] ratio. In this part of the study we verified that the chelate effect is effective for [Li(glyme or THF)]$^+$ complex cations in the concentrated liquid regime.

The complex formation constant K is an important parameter quantifying the chelate effect and the stability of complexes. Although there are no reports addressing these constants in concentrated [Li(glyme or THF)$_x$][TFSA] mixtures, some studies have reported K in dilute solutions. The K values for the systems involving lithium picrate (as a spectroscopic probe of lithium salts) and the glymes or THF (as a ligand) in 1,4-dioxane solutions have been studied by Tsvetanov *et al.*, and the K values were found to be 0.95, 2.1, 8.5, 17.0, and 24.5 M^{-1} for THF, G1, G2, G3, and G4, respectively.[40] Using fluorenyl lithium as another lithium salt probe, the K values of the glymes in 1,4-dioxane solutions were reported to be 0.055, 3.1, 130, and 240 M^{-1} for G1, G2, G3, and G4, respectively.[41,42] The K likely depends on various factors such as the lithium salt probe used, the solvent, and the Li salt concentration. Nevertheless, the D_{sol}/D_{Li} ratios in the concentrated regime and the K values studied in dilute solutions correlate well in terms of the number of oxygen atoms in the single ligands; significantly lower K values for THF and G1 may be the cause of the D_{sol}/D_{Li} ratio higher than 1, indicating the lower stability of the solvated Li^+ ions. This is supported by the stabilization energies (ΔE_{form}) studied by computational methods; ΔE_{form} for the formation of [Li(glyme)$_1$]$^+$ complexes with the glymes were in the same order: G4 > G3 > G2 > G1.[43] Molecular dynamics (MD) simulations have also shown that the solvent residence time near Li^+ ions was more than one order of magnitude longer for pentaglyme (G5) than for bidentate G1 and monodentate ethylene carbonate (EC) in dilute Li[TFSA] solutions.[44]

In a previous study, we estimated the ligand exchange time (τ_b) between the [Li(G3 or G4)$_1$]$^+$ complex and the free glymes in [Li(G3 or G4)$_2$][TFSA] mixtures from ^{1}H NMR spectra, where [Li(G3 or G4)$_2$][TFSA] were assumed to be 1:1 mixtures of [Li(G3 or G4)$_1$][TFSA] complexes and free glymes. The τ_b value can be estimated by the following equation in limited situations ($\tau_b << (2\pi\delta\nu)^{-1}$):[45]

$$\tau_b = \frac{2(W - W_0)}{\pi(\delta\nu)^2}$$

Where W_0 and W are the full width at half-maximum (fwhm) of the NMR signals of the terminal glyme methoxy proton and [Li(G3 or G4)$_2$][TFSA], respectively. $\delta\nu$ is the difference in the chemical shift of the end methoxy proton of [Li(G3 or G4)$_1$][TFSA] and pure glyme. The τ_b value for the G3 or G4 systems are 1.9×10^{-4} and 3.6×10^{-4} s

respectively.[39] We applied the same procedure to the concentrated mixtures of the shorter glymes, and the NMR results are shown in **Figure 3-3**. However, the above equation may be invalid for $[Li(G2)_{4/3}][TFSA]$ because of its non-stoichiometric composition. Furthermore, we encountered experimental difficulties in NMR measurements of $[Li(G2)_x][TFSA]$ because the concentrated mixtures were prone to solidification at room temperature. For $[Li(G1)_2][TFSA]$, τ_b can be approximated to a timescale of 10^{-5}–10^{-6} s using the above equation, which is much shorter than those reported for [Li(G3 or $G4)_1][TFSA]$. It is known that water exchange timescale on Li^+ is extremely fast ($\tau_b \sim 10^{-9}$ s).[46] Likewise, it can be assumed that τ_b for the mixtures with monodentate THF is even shorter than that for the mixtures with G1 although it is impossible to follow the exchange for THF on Li^+ by NMR. Thus, we can conclude the order of the lifetimes is G4 > G3 >> G1 >> THF.

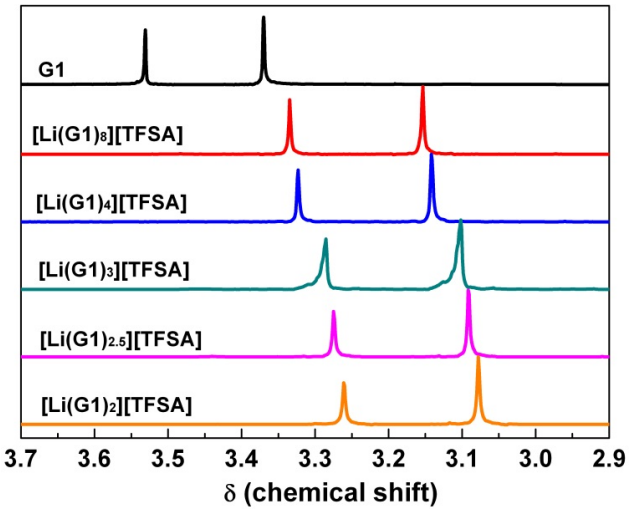

Figure 3-3. ^{1}H NMR spectra for $[Li(G1)_x][TFSA]$ at 30 °C. The terminal methoxy protons ($-OCH_3$) of the glymes were used for the calculation of τ_b. W_0: full width at half-maximum (fwhm) of the NMR signal for pure G1, W: the fwhm of the NMR signal for $[Li(G1)_x][TFSA]$ (x = 3–8), δv: the difference in the chemical shift of the end methyl proton of $[Li(G1)_2][TFSA]$ and pure G1.

The different ion-solvent interactions based on the chelate effect would also be reflected in ion-ion interactions in concentrated mixtures, because there is competition between the solvent and $[TFSA]^-$ for the interaction with Li^+ ions. **Figure 3-4** presents Raman spectra ranging from 730 to 760 cm^{-1} for $[Li(glyme\ or\ THF)_x][TFSA]$ at an $[O]/[Li^+]$ ratio of 4. The peaks at this frequency range have been assigned to the CF_3 bending vibration coupled with the S-N stretching vibration of $[TFSA]^-$, and is very sensitive to the Li^+–$[TFSA]^-$ interaction.[47] The band corresponding toa SSIP or an uncoordinated $[TFSA]^-$ anion appears at 739–742 cm^{-1}, whereas the band between 745–755 cm^{-1} originates from $[TFSA]^-$ bound directly to Li^+ ions in the form of a contact ion pair (CIP) or aggregate coordination (AGG).[30,48] As shown in **Figure 3-4**, the peak shifted to higher frequency in the sequence $[Li(THF)_4]$ < $[Li(G3)_1]$ < $[Li(G2)_{4/3}]$ < $[Li(G1)_2]$. Except for

$[Li(THF)_4][TFSA]$, this order correlates with the number of ethylene oxide units in the glyme, suggesting that the association of $[TFSA]^-$ with Li^+ ions is more predominant in $[Li(G1)_2][TFSA]$ than in $[Li(G3)_1][TFSA]$, even at the same $[O]/[Li^+]$ ratio. This is corroborated by weaker ion-solvent interactions for the shorter G1, as discussed in the studies on D_{sol}/D_{Li} and K. The lowest peak frequency for $[Li(THF)_4][TFSA]$ was probably due to its lower concentration (2.09 mol dm^{-3}) compared to the other mixtures (~3 mol dm^{-3}). The steric hindrance of $[Li(THF)_4]^+$—being less crowded than the glyme-based complex cations when interacting with $[TFSA]^-$—was also reflected by the lowest peak frequency. When the Raman spectra were compared at commensurate concentrations of ~3 mol dm^{-3}, the peak shifted to higher frequency with decreasing number of oxygen atoms in the solvent: $[Li(G3)_1] < [Li(G2)_{4/3}] < [Li(G1)_2] < [Li(THF)_2]$.

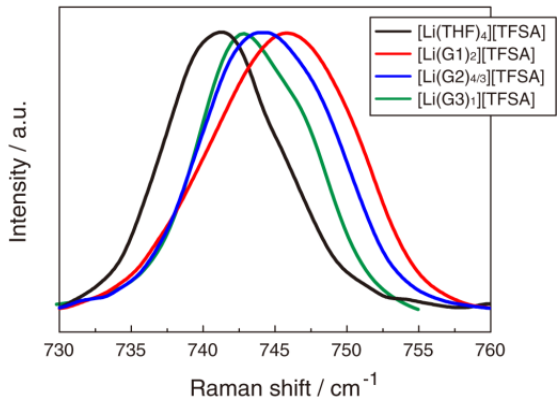

Figure 3-4. Raman spectra of $[Li(glyme\ or\ THF)_x][TFSA]$ mixtures at an $[O]/[Li^+]$ ratio of 4.

3.3.3. The chelate effect on physicochemical properties

In this section, we demonstrate how the stability of the complex cation arising from the chelate effect correlates with the properties of the concentrated $[Li(glyme\ or\ THF)_x][TFSA]$ mixtures. Generally, solvate ILs should possess high thermal stability—as is typical for ILs— owing to the strong complexation between Li^+ ions and the ligands. The thermal decomposition temperature (T_d) and its difference (ΔT_d) from T_d of the pure solvents of the $[Li(glyme\ or\ THF)_x][TFSA]$ mixtures at $[O]/[Li^+]$ ratio of 4 or 5 were studied by thermogravimetric analysis, and are shown in **Figure 3-5**. It is apparent that the relatively low T_d and ΔT_d values for $[Li(THF)_x][TFSA]$ and $[Li(G1)_x][TFSA]$—which are not solvate ILs—are attributed to the high volatility of the uncoordinated or weakly interacting solvents found in these solution-like mixtures. However, for the other mixtures exhibiting D_{sol}/D_{Li} ~1, ΔT_d is more pronounced, and the thermal stability is dramatically improved by the strong complexation between Li^+ ions and the longer glymes such as G2, G3, and G4, yielding solvate ILs. The ΔT_d of $[Li(G3)_1][TFSA]$ ($[O]/[Li^+] = 4$) was slightly higher than that of $[Li(G4)_1][TFSA]$ ($[O]/[Li^+] = 5$), implying that the coordination number of 4 offers the most thermally stable conditions.

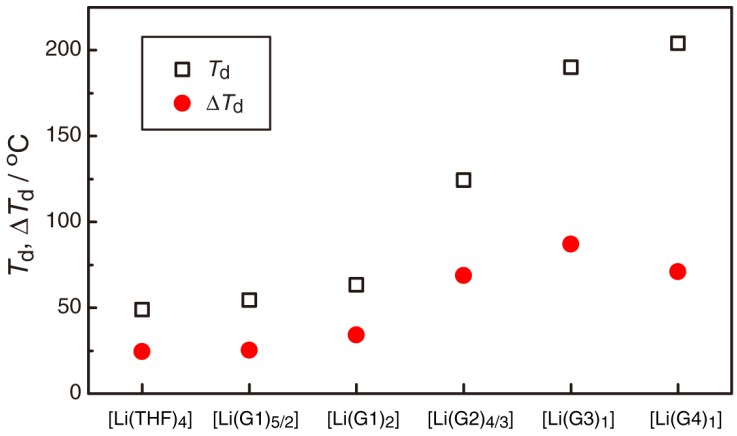

Figure 3-5. The thermal decomposition temperature (T_d) and its difference (ΔT_d) from T_d of the pure solvents of [Li(glyme or THF)$_x$][TFSA] mixtures.

Figure 3-6 illustrates linear sweep voltammograms at a Pt electrode for the [Li(glyme or THF)$_x$][TFSA] concentrated mixtures. Interestingly, almost no current is detected below 4.5 V vs. Li/Li$^+$ for the solvate ILs [Li(G2)$_{4/3}$][TFSA] and [Li(G3)$_1$][TFSA], whereas obvious current flow can be seen at potentials higher than 4 V vs. Li/Li$^+$ for [Li(THF)$_4$][TFSA] and [Li(G1)$_2$][TFSA]. The ether solvents oxidatively decomposed at lower potentials in the solution-like [Li(THF)$_4$][TFSA] and [Li(G1)$_2$][TFSA]. However, the formation of the stable complex cation in the lithium solvate ILs [Li(G2)$_{4/3}$][TFSA] and [Li(G3)$_1$][TFSA] lowers the HOMO energy level of the oligoether solvents, and thus effectively suppresses the oxidative decomposition.[5]

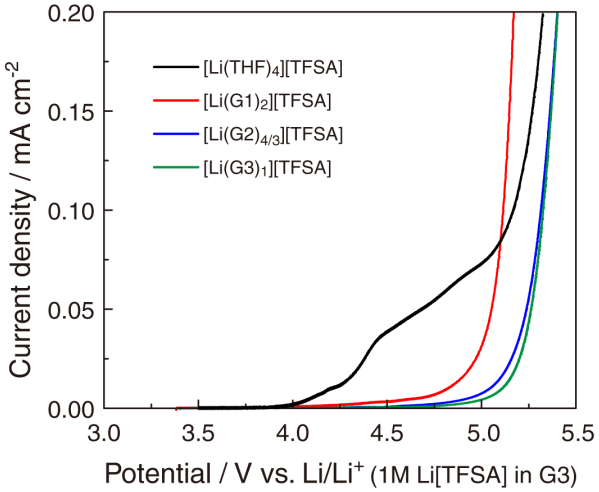

Figure 3-6. Linear sweep voltammograms of [Li(glyme or THF)$_x$][TFSA] at scan rate 1 mV s^{-1} at 30 °C.

The properties of [Li(G2)$_{4/3}$][TFSA] and [Li(G3 or G4)$_1$][TFSA] discussed above are all ascribed to the formation of stable complex cations. Therefore, the present lithium solvate ILs have many desirable properties such as high thermal and electrochemical stability, and high Li$^+$ concentration; they are therefore promising electrolytes for not only lithium ion

batteries, but also high-energy density batteries such as lithium-sulfur and lithium-air batteries.

3.3.4. The physicochemical properties of other mixtures

Because some solvents such as THF have high electron pair donor ability, the mixture of alkali metal salts and these solvent molecules with/without some ligands often construct a characteristic complex.[49-51] Regarding these circumstances on the basis of coordination chemistry, it can be anticipated that other solvent with high donor ability also coordinate to Li^+ cation resulting in formation of a complex, and a system involving solvated Li^+ cations and dissociated anions may be able to count as a kind of solvate ionic liquid. **Table 3-1** in the introduction section lists the physical properties of some common solvents for electrolyte and most of them exhibit high donor ability.

The mixtures of solvent and Li[TFSA] are prepared with $[O]/[Li^+]$ ~4, and transport properties of these samples are shown in **Table 3-3**. Comparing with typical solvate ILs, these mixtures show low lithium concentration, low viscosity and high ionic conductivity. As well as we know there is no report addressing the ionic nature of these extremely condensed electrolyte solutions with such solvent compounds minutely and systemically. Herein we discussed the binary mixtures of Li[TFSA] and various kinds of solvent as an archetype of extremely concentrated carbonate-Li salt electrolyte systems from the viewpoint of coordination chemistry. The practical solvent, such as NMP shows higher donor capability than glymes and THF, from which one may expect that the concentrated NMP-Li salt solutions may has stable complex cations like solvate ILs.

Table 3-3. Viscosity (η), density (ϱ), molar concentration (c), ionic conductivity (σ) and ionicity ($\Lambda_{imp}/\Lambda_{NMR}$ or $\Lambda_{imp}/\Lambda_{ideal}$) of the $[Li(solvent)_x][TFSA]$ mixtures at 30 °C.

mixtures	[O]/[Li] (-)	η (mPa s)	ρ (g cm^{-3})	c (mol dm^{-3})	σ (mScm^{-1})	$\Lambda_{imp}/\Lambda_{NMR}$ (-)
$[Li(DEC)_4][TFSA]$	4	4.7	1.20	1.59	1.07	0.09
$[Li(THF)_4][TFSA]$	4	4.77	1.21	2.09	7.23	0.49
$[Li(G1)_2][TFSA]$	4	34	1.35	2.89	3.7	0.58
$[Li(NMP)_4][TFSA]$	4	24.7	1.28	1.89	3.1	0.40
$[Li(PC)_4][TFSA]$	4	60.4	1.43	2.05	2.34	0.61

We selected the thermal properties of the mixtures to exam the stability of the solvate cations, which has been demonstrated in the aforementioned section. The thermal stability studied by thermogravimetric analysis are summarized and shown in **Figure 3-7**. The

difference of the thermal decomposition temperature (ΔT_d) for [Li(solvent)$_x$][TFSA] mixtures versus the donor number (*DN*) of the solvent has been revealed. It is interesting to find that there is a correlation for donor ability of the solvent and improvement of the thermal stability of the solvent contained mixtures, and thus the enhanced thermal stability of the mixture could be attribute to the formation of stable solvate in the mixtures. As we know, *DN* is a value come from an empirical semi-quantitative measure of the nucleophilic properties of the solvents and indicates the electron pair donor ability of the ligand in the formed complex. The formation of the solvent-Li solvation contributes to improving the solvate stability, and the solvate-structural stability is also corresponding to the ion-solvent interaction. It is noteworthy that in **Figure 3-7** the plots of solvate ILs are upon the trend line, which means the chelate effect in solvate ILs reinforce the stability of the complex cation although the glymes have relative lower *DN* than some other solvents. In the cases of solvate ILs, Li^+ solvation with glymes (i.e. G3 or G4) occurs intramolecularly and the activation energy was ca. 68 kJmol^{-1}.[52] The desolvation process of the solvate cations Li(G3 or G4)$_1$]$^+$ should be difficult that the desolvation reactions of the glymes occur step by step, and the last desolvation process between Li^+ and an ether-oxygen dipole appears to be the activation barrier for the reactions.

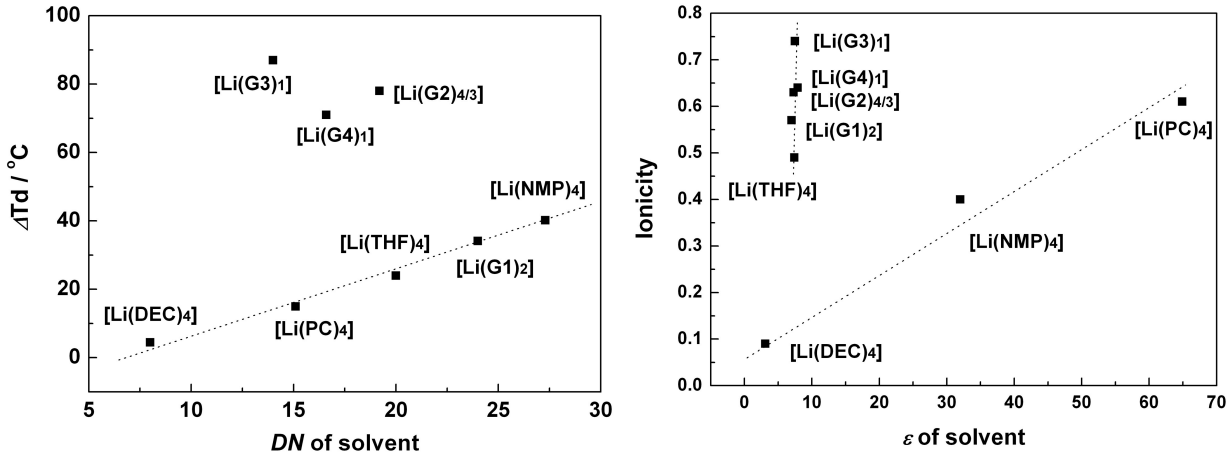

Figure 3-7. (Left) Difference of the thermal decomposition temperature (ΔT_d) for [Li(solvent)$_x$][TFSA] mixtures versus the donor number (*DN*) of the solvent. (Right) Ionicity ($\Lambda_{imp}/\Lambda_{NMR}$ or $\Lambda_{imp}/\Lambda_{ideal}$) of the [Li(solvent)$_x$][TFSA] mixtures versus the dielectric constant (ε) of the solvent. Lines in the figure are just guides for the eye.

For the compare of the dissociativity, another trend line is drawn in the ionicity ($\Lambda_{imp}/\Lambda_{NMR}$ or $\Lambda_{imp}/\Lambda_{ideal}$) of the [Li(solvent)$_x$][TFSA] mixtures versus the dielectric constant (ε) of the solvent (**Figure 3-7**). High ionicity (> 0.6) can be achieved in solvate ILs with high molar concentration of lithium. On the other hand, the concentrated mixtures have a lower ionicity even including some high permittivity solvent such as PC or NMP. Indeed the ionicity is high related to the solvent in the dilute Li[TFSA] contained electrolytes.[53] However, in extreme concentrated electrolytes most of the solvent molecules was served

as ligands rather than solvents and took part in formation the complex cations. The stable complex cations in solvate ILs may reduce the degree of ion association, and the ligands (the solvent or the anion) in the first coordination sphere of Li^+ are responsible for the ionicity value in these mixtures. Although we do not understand these unique behaviors of ionicity and dissociation mechanism clearly, high ionicity is beneficial in some aspect because it can cover the slower lithium transport caused by high viscosity and would be a favorable aspect for alternative lithium battery electrolytes to replace common non-aqueous systems.

3.4. Conclusions

In this study, the effect of the solvent nature on the properties of [Li(glyme or $THF)_x$][TFSA] mixtures were studied. In concentrated regions where the [O]/[Li^+] ratio was adjusted to be 4 or 5, the mixtures yielding the solvate ILs could be distinguished from the concentrated solutions by analyzing the self-diffusion coefficient ratio D_{sol}/D_{Li}; the ratio was always greater than 1 in concentrated solutions ([Li(G1 or $THF)_x$][TFSA] mixtures) even when the molar concentration was higher than 3mol dm^{-3}, whereas the solvate ILs ([Li(G3 or $G4)_1$][TFSA] and [$Li(G2)_{4/3}$][TFSA]) showed a D_{sol}/D_{Li} of ~1, indicating long-lived complex cations. The chelate effect explained differences in the stability of the complex cations amongst [Li(glyme or $THF)_x$][TFSA] mixtures with an [O]/[Li^+] ratio of ~4 or 5. The stable solvate cations could be formed with longer glymes, and afforded high thermal and electrochemical stability. The solvate ILs [$Li(G3)_1$][TFSA] and [$Li(G2)_{4/3}$][TFSA] significantly suppressed oxidative decomposition, whereas notable decomposition occurred in concentrated [$Li(THF)_4$][TFSA] and [$Li(G1)_2$][TFSA] solutions at lower potentials. It was also revealed that the effect of solvent (or ion-solvent interaction) on the stability of the solvate cations in the concentrated [Li(solvent)$_x$][TFSA] mixtures.

3.5. References

1 Onsager, L. *Chem. Rev.* **1933**, *13*, 73.
2 Robinson, R. A.; Stokes, R. H. *Electrolyte Solutions*; Dover Publications, **1970**.
3 Reichardt, C.; Welton, T. In *Solvents and Solvent Effects in Organic Chemistry*; Wiley-VCH Verlag GmbH & Co. KGaA: **2010**, p 7.
4 Bockris, J. O. M.; Reddy, A. K. N. *Modern Electrochemistry 1: Ionics*; Springer, **1998**.
5 Choi, N. -S.; Chen, Z.; Freunberger, S. A.; Ji, X.; Sun, Y.-K.; Amine, K.; Yushin, G.; Nazar, L. F.; Cho, J.; Bruce, P. G. *Angew. Chem. Int. Ed.* **2012**, *51*, 9994.
6 Armand, M.; Tarascon, J. M. *Nature* **2008**, *451*, 652.
7 Bruce, P. G.; Freunberger, S. A.; Hardwick, L. J.; Tarascon, J. -M. *Nat. Mater.* **2012**, *11*, 19.
8 Mandai, T.; Yoshida, K.; Ueno, K.; Dokko, K.; Watanabe, M. *Phys. Chem. Chem. Phys.* **2014**, *16*, 8761.
9 Wasserscheid, P.; Welton, T. *Ionic Liquids in Synthesis, 2 Volume Set*; Wiley, **2007**.
10 Ohno, H. *Electrochemical Aspects of Ionic Liquids*; Wiley, **2011**.
11 Lewandowski, A.; Swiderska-Mocek, A. *J. Power Sources* **2009**, *194*, 601.
12 Galinski, M.; Lewandowski, A.; Stepniak, I. *Electrochim Acta* **2006**, *51*, 5567.
13 Armand, M.; Endres, F.; MacFarlane, D. R.; Ohno, H.; Scrosati, B. *Nat. Mater.* **2009**, *8*, 621.

14 Xu, W.; Cooper, E. I.; Angell, C. A. *J. Phys. Chem. B* **2003**, *107*, 6170.
15 Noda, A.; Hayamizu, K.; Watanabe, M. *J. Phys. Chem. B* **2001**, *105*, 4603.
16 Tokuda, H.; Hayamizu, K.; Ishii, K.; Abu Bin Hasan Susan, M.; Watanabe, M. *J. Phys. Chem. B* **2004**, *108*, 16593.
17 Tokuda, H.; Hayamizu, K.; Ishii, K.; Susan, M.; Watanabe, M. *J. Phys. Chem. B* **2005**, *109*, 6103.
18 Tokuda, H.; Ishii, K.; Susan, M.; Tsuzuki, S.; Hayamizu, K.; Watanabe, M. *J. Phys. Chem. B* **2006**, *110*, 2833.
19 Miran, M. S.; Kinoshita, H.; Yasuda, T.; Susan, M. A. B. H.; Watanabe, M. *Phys. Chem. Chem. Phys.* **2012**, *14*, 5178.
20 Tamura, T.; Hachida, T.; Yoshida, K.; Tachikawa, N.; Dokko, K.; Watanabe, M. *J. Power Sources* **2010**, *195*, 6095.
21 Yoshida, K.; Nakamura, M.; Kazue, Y.; Tachikawa, N.; Tsuzuki, S.; Seki, S.; Dokko, K.; Watanabe, M. *J. Am. Chem. Soc.* **2011**, *133*, 13121.
22 Angell, C. A.; Ansari, Y.; Zhao, Z. *Faraday Discuss.* **2012**, *154*, 9.
23 Park, J. -W. *Ph. D. Thesis,* Yokohama National University **2013**.
24 Pappenfus, T. M.; Henderson, W. A.; Owens, B. B.; Mann, K. R.; Smyrl, W. H. *J. Electrochem. Soc* **2004**, *151*, A209.
25 Henderson, W. A.; Brooks, N. R.; Brennessel, W. W.; Young, V. G. *Chem. Mat.* **2003**, *15*, 4679.
26 Henderson, W. A.; Brooks, N. R.; Young, V. G. *Chem. Mat.* **2003**, *15*, 4685.
27 Henderson, W. A.; McKenna, F.; Khan, M. A.; Brooks, N. R.; Young, V. G.; Frech, R. *Chem. Mat.* **2005**, *17*, 2284.
28 Lascaud, S.; Perrier, M.; Vallee, A.; Besner, S.; Prud'homme, J.; Armand, M. *Macromolecules* **1994**, *27*, 7469.
29 Henderson, W. A. *J. Phys. Chem. B* **2006**, *110*, 13177.
30 Brouillette, D.; Irish, D. E.; Taylor, N. J.; Perron, G.; Odziemkowski, M.; Desnoyers, J. E. *Phys. Chem. Chem. Phys.* **2002**, *4*, 6063.
31 Serrano, C. B.; Less, R. J.; McPartlin, M.; Naseri, V.; Wright, D. S. *Organometallics* **2010**, *29*, 5754.
32 Sazama, G. T.; Betley, T. A. *Inorg. Chem.* **2010**, *49*, 2512.
33 Kameda, Y.; Umebayashi, Y.; Takeuchi, M.; Wahab, M. A.; Fukuda, S.; Ishiguro, S.-i.; Sasaki, M.; Amo, Y.; Usuki, T. *J. Phys. Chem. B* **2007**, *111*, 6104.
34 Henderson, W. A.; McKenna, F.; Khan, M. A.; Brooks, N. R.; Young, V. G.; Frech, R. *Chem. Mat.* **2005**, *17*, 2284.
35 Su, J.; Goodwin, S. D.; Li, X.-W.; Robinson, G. H. *J. Am. Chem. Soc.* **1998**, *120*, 12994.
36 Becker, G.; Eschbach, B.; Mundt, O.; Reti, M.; Niecke, E.; Issberner, K.; Nieger, M.; Thelen, V.; Nöth, H.; Waldhör, R.; Schmidt, M. *Z. Anorg. Allg. Chem.* **1998**, *624*, 469.
37 Henderson, W. A.; Brooks, N. R.; Brennessel, W. W.; Young, V. G. *J. Phys. Chem. A* **2003**, *108*, 225.
38 Rhodes, C. P.; Frech, R. *Macromolecules* **2001**, *34*, 2660.
39 Yoshida, K.; Nakamura, M.; Kazue, Y.; Tachikawa, N.; Tsuzuki, S.; Seki, S.; Dokko, K.; Watanabe, M. *J. Am. Chem. Soc.* **2011**, *133*, 13121.
40 Tsvetanov, C. B.; Petrova, E. B.; Dimov, D. K.; Panayotov, I. M.; Smid, J. *J. Solut. Chem.* **1990**, *19*, 425.
41 Chan, L. -L.; Smid, J. *J. Am. Chem. Soc.* **1967**, *89*, 4547.
42 Chan, L. -L.; Wong, K. H.; Smid, J. *J. Am. Chem. Soc.* **1970**, *92*, 1955.
43 Tsuzuki, S.; Shinoda, W.; Seki, S.; Umebayashi, Y.; Yoshida, K.; Dokko, K.; Watanabe, M. *ChemPhysChem* **2013**, *14*, 1993.
44 Borodin, O.; Smith, G. D. *J. Solut. Chem.* **2007**, *36*, 803.
45 Allerhand, A.; Gutowsky, H. S.; Jonas, J.; Meinzer, R. A. *J. Am. Chem. Soc.* **1966**, *88*, 3185.
46 Helm, L.; Merbach, A. E. *Chem. Rev.* **2005**, *105*, 1923.
47 Umebayashi, Y.; Mitsugi, T.; Fukuda, S.; Fujimori, T.; Fujii, K.; Kanzaki, R.; Takeuchi, M.; Ishiguro, S. -I. *J. Phys. Chem. B* **2007**, *111*, 13028.
48 Seo, D. M.; Borodin, O.; Han, S. -D.; Boyle, P. D.; Henderson, W. A. *J. Electrochem. Soc.* **2012**, *159*, A1489.
49 Seo, D. M.; Boyle, P. D.; Henderson, W. A. *Acta Crystallogr., Sect. E* **2011**, *67*, m1148.

50 Guzei, I. A.; Spencer, L. C.; Su, J. W.; Burnette, R. R. *Acta Crystallogr., Sect. B* **2007**, *63*, 93.
51 Izod, K.; Clark, E. R.; Clegg, W.; Harrington, R. W. *Organometallics* **2011**, *31*, 246.
52 Yoshida, K.; Tsuchiya, M.; Tachikawa, N.; Dokko, K.; Watanabe, M. *J. Phys. Chem. C* **2011**, *115*, 18384.
53 Hayamizu, K.; Aihara, Y.; Arai, S.; Martinez, C. G. *J. Phys. Chem. B* **1999**, *103*, 519.

Chapter Four

Application of Glyme Based Solvents and Li Salt Mixtures for Rechargeable Lithium Batteries

Abstract

The [Li(glyme or THF)$_x$][TFSA] mixtures were then investigated as electrolytes for Li-ion and Li-S batteries. The oxidative stability of molten solvates of [Li(glyme or THF)$_x$][TFSA] ([O]/[Li$^+$] ~ 4) changes depending on the structural stability of [Li(glyme or THF)$_x$]$^+$. For instance, comparing with [Li(G1)$_2$]$^+$ and [Li(THF)$_x$]$^+$, complex cation [Li(G3)$_1$]$^+$ with tetradentate ligands is rather stable owing to the chelate effect. The performance of Li-$LiCoO_2$ cell is affected significantly by the oxidative stability of the electrolytes. The cell with [Li(G3)$_1$][TFSA] electrolyte showed a good cycle stability with a high Coulombic efficiency, while the degradation of performance due to the oxidative decomposition of the solvents was observed in the case of [Li(THF)$_4$][TFSA] and [Li(G1)$_2$][TFSA]. In addition to the oxidative stability, the corrosion of the Al current collector is also affected by the solvate cation stability of [Li(glyme or THF)$_x$][TFSA]. The surface reactions at the Al current collector were investigated by cyclic voltammetry (CV) and scanning electron microscope (SEM). The result indicated that the corrosion process involves the electrochemical oxidation of the ether solvents on Al/Al_2O_3 and the dissolution of Al (III) compounds in the electrolyte. The rate of corrosion reaction in [Li(THF)$_4$][TFSA] and [Li(G1)$_2$][TFSA] is much faster than that in [Li(G3)$_1$][TFSA]. Consequently, the corrosion of the Al current collector in Li-$LiCoO_2$ cell causes the fade of discharge capacity and the low Coulombic efficiency of charge-discharge of the cell. The solubility of Li_2S_m, which is a reaction intermediate of sulfur cathode of Li-S battery, changes dramatically depending on the stability of complex [Li(glyme or THF)$_x$]$^+$ cation in the electrolyte. The stable molten [Li(G3)$_1$][TFSA] solvate has a very low solubility of Li_2S_m, while the unstable molten solvates such as [Li(THF)$_4$][TFSA] and [Li(G1)$_2$][TFSA] can dissolve Li_2S_m in high concentrations. The free or highly exchangeable solvent molecules in [Li(THF)$_4$][TFSA] and [Li(G1)$_2$][TFSA] are expected to contribute to the solvation of the Li_2S_m. In contrast, the [Li(G3)$_1$][TFSA] hardly contains free solvent to dissolve Li_2S_m. The solubility of Li_2S_m affects the charge-discharge efficiency of Li-S cell because the dissolved Li_2S_m behaves as a redox shuttle between cathode and anode, leading to a low Coulombic efficiency and capacity decay during charge-discharge cycles. The suppressed solubility of Li_2S_m in [Li(G3)$_1$][TFSA] electrolyte is favorable for the stable operation of a Li-S battery.

Part of the work presented in this chapter has been published as:

Zhang, C.; Yamazaki, A.; Murai, J.; Park, J. –W.; Mandai, T.; Ueno, K.; Dokko, K.; Watanabe, M. *J. Phys. Chem. C* **2014**, *118*, 17362-17373.

4.1. Introduction

Ethers have been widely used as non-aqueous solvents for electrolyte solutions of various metal salts because of their relatively strong solvation ability. In solutions, the lone pairs of ether oxygens are donated to the metal cation, forming solvate cations. Glymes are oligoethers with multiple ether-oxygens in a single molecular structure. They are chemically stable, less volatile, and capable of dissolving Li salts in high concentrations. Recently, glymes have attracted much attention as electrolyte solvents in Li-ion batteries[1] and high energy density batteries such as Li-S[2] and Li-O_2.[3] In these batteries, chemical stability to reactive intermediates and low volatility are essential properties for the electrolyte. Mixtures of glymes and Li salts have long been studied as a model of poly(ethyleneoxide) (PEO)-based polymer electrolytes.[4-6] Interestingly, appropriate combinations of glymes and Li salts yield isolated solvates in certain molar ratios. Henderson et al. systematically studied the crystal structures of these solvates in the solid state,[7-11] and they determined that the coordination number of Li^+ in the glyme-Li salts binary mixtures is in the range of 4–6.

Our group has focused on the solvates composed of glymes and alkali metal salts in a "molten" state.[12-14] Glyme-based solvates tend to be low melting, and some mixtures are liquid at room temperature. This is significantly different from the properties of well-known crown ether complexes[15-17] and allows us to apply these molten complexes to battery electrolytes.[18] Among the molten complexes, the most representative is the equimolar mixture of triglyme (G3) and lithium bis(trifluoromethanesulfonyl)amide (Li[TFSA]), abbreviated as $[Li(G3)_1][TFSA]$ (melting point T_m = 23 °C).[19] G3 with four coordination sites per molecule adopts a crown ether-like conformation to form a 1:1 complex cation $[Li(G3)_1]^+$.As the long-lived $[Li(G3)_1]^+$ behaves as an independent cation in the molten state, $[Li(G3)_1][TFSA]$ showed properties similar to those of conventional ionic liquids (ILs), such as non-flammability, negligible vapor pressure (at lower than 100 °C), relatively high ionic conductivity, and a wide electrochemical window.[13] These types of room-temperature molten complexes were recently named "solvate" ILs.[20] We have demonstrated that the solvate ILs can be used as efficient electrolytes for Li-ion,[21,22] Li-S,[23,24] Li-O_2[25] batteries, and other electrochemical devices.

Understanding the structure-property relationships for solvate ILs is important in the development of more effective electrolytes for high-energy storage batteries, especially for Li-S and Li-O_2 cells, where conventional carbonate-based organic electrolyte solutions cannot be used. To this end, a variety of concentrated mixtures with different Li salts and glymes have been investigated. The counter anion, X^-, of Li salts has a crucial effect on the stability (lifetime) of the complex $[Li(glyme)_1]^+$ cation[26] because the solvent and X^- compete for

interactions with the Li^+ ions. The complex cation became more stable (with longer lifetime) as the Lewis basicity of X^- decreased.

In addition to the anionic effect, the stability of the complex cations was also governed by ligand species (or solvents). In earlier work, we prepared a series of highly concentrated, binary mixtures of glymes (monoglyme (G1), diglyme (G2), triglyme (G3), tetraglyme (G4), or pentaglyme (G5)) and Li[TFSA].[27] For comparison, tetrahydrofuran (THF)-Li[TFSA] binary mixtures were also studied. Owing to the chelate effect, the longer glymes formed more stable complex $[Li(glyme)_x]^+$ cations with longer lifetimes in the molten solvates. Although well-defined crystalline structures were reported in stoichiometric compositions with shorter glymes (such as G1),[7] the complex cations were no longer stable in the melt. The structural stability of the complex cations was found to have a significant influence on the physicochemical properties such as thermal stability, oxidative stability, and transport properties of the binary mixtures.[27]

However, to gain further insight into the effects of the structural stability of glyme-Li^+ solvates in electrolytes on the electrochemical reactions in Li batteries, more detailed investigations are required. Herein, we report that the oxidative stability of [Li(glyme or THF)$_x$][TFSA] has an effect on the charge-discharge cycle stability of the Li-$LiCoO_2$ cell ($LiCoO_2$ is a popular cathode material of Li-ion batteries). Furthermore, we found that a side reaction, corrosion of the Al current collector of the cathode, takes place depending on the composition of the electrolytes. The electrochemical reactions in Li-S cells were also investigated. The solubility of lithium polysulfides (Li_2S_m, $2 \le m \le 8$), which are intermediate products during discharge reactions in Li-S cells, is governed by the stability of the complex $[Li(glyme)_x]^+$ cation in the electrolytes, and this consequently affects the charge-discharge efficiency of the Li-S cell. This study demonstrates that the stability of complex $[Li(glyme)_x]^+$ cations in electrolytes has a significant impact on the performance of Li batteries.

4.2. Experimental

4.2.1. Electrolytes

Purified glymes (G1, G2, and G3) were purchased from Kishida Chemical, and super dehydrated THF ($[H_2O] < 10$ ppm) was purchased from Wako Pure Chemical. Li[TFSA] was purchased from Morita Chemical Industries and dried under high vacuum at 120 °C prior to use. The electrolytes were prepared by mixing the appropriate amount of solvent (glyme or THF) and Li[TFSA], and the mixtures were stirred overnight at room temperature to obtain homogeneous liquids. Hereafter, the electrolytes are abbreviated as [Li(glyme or THF)$_x$][TFSA]. The electrolytes were prepared, stored, and handled in an argon-filled glove box (VAC, $[H_2O] < 1$ ppm).

4.2.2. $LiCoO_2$ Composite Electrode

$LiCoO_2$ powder was kindly supplied by AGC Seimi Chemical and used as received. Acetylene black (AB, Denki Kagaku Kogyo) and poly(vinylidene fluoride) (PVDF, Kureha Chemical) were used as an electrically conductive additive and a binder polymer, respectively. The preparation procedure for the composite electrode was described elsewhere.[13] The mass ratio of $LiCoO_2$/AB/PVDF was 85:9:6, and a $LiCoO_2$–AB–PVDF composite slurry was spread on an Al foil current collector and dried completely. The prepared $LiCoO_2$–AB–PVDF composite/Al sheet was cut into a circular shape (16 mm diameter) and subjected to a battery test. The thickness of the prepared electrode was ~17 μm, and the mass of the active material was ~5.9 mg.

4.2.3. Carbon/Sulfur Composite Electrode

Ketjen black (KB, Lion Corporation), a porous carbon with high specific surface area of 1270 m^2g^{-1}, and elemental sulfur (Wako Pure Chemical Industries) were used to prepare the C/S porous composite electrode. Poly(vinyl alcohol) (PVA, average degree of polymerization 3100–3900, saponification degree 86–90 mol%, Wako Pure Chemical Industries) was used as a binder polymer. The procedure for the electrode preparation was described in detail in our previous papers.[28,29] The mass ratio of S/KB/PVA was 60:30:10, and an S–KB–PVA composite slurry was spread on an Al foil current collector and dried completely. The prepared composite sheet was cut into a circular shape (16 mm diameter) and compressed at 100 kg f cm^{-2} using a hydraulic press. The thickness of the composite sheet on the Al was ~15 μm, and the mass of S on the sheet electrode was ~1.2 mg.

4.2.4. Battery Test

Coin cells (2032 type) were fabricated in the Ar-filled glovebox. A cathode sheet, porous glass separator (GA 55, Advantec), Li foil anode, and an electrolyte were encapsulated in a coin cell. The electrolyte penetrated into the voids of the porous separator and porous composite cathode during cell fabrication. The total electrolyte volume is ca. 36μL in the cells. The galvanostatic charge-discharge measurements for Li-$LiCoO_2$ and Li-S cells were conducted using electrochemical analyzers (VMP2, BioLogic and BTS-2004, Nagano) at 30 °C. In the case of the Li-$LiCoO_2$ cell, the cell was prepared in a fully discharged state. The specific capacity of the cell was calculated based on the mass of $LiCoO_2$. Based on the mass of $LiCoO_2$, the gravimetric current density of 137 mA g^{-1} was defined as a 1 C rate, which corresponds to a geometric current density of 0.4 mA cm^{-2}. In the case of the Li-S cell, the cell was prepared in a fully charged state, and the charge-discharge cycle is defined as follows: first discharge → second charge → second discharge → third charge → third discharge, and so on. The Coulombic efficiency was defined as: (Nth discharge capacity) / (Nth charge

capacity). The specific capacity of the cell was calculated based on the mass of sulfur, and the gravimetric current density of 1672 mA g^{-1} was defined as the 1 C rate, which corresponds to a geometric current density of ~1 mA cm^{-2}. The surface morphology change of the Al current collector by corrosion was observed using a scanning electron microscope (SEM) (S-2000, Hitachi High-Technologies).

4.2.5. Estimation of Solubility of Lithium Polysulfide

The solubility of $S_8$and Li_2S_m in the electrolytes were determined using a UV-Vis spectrophotometer (UV-2500PC, Shimadzu).[28] The absorbance at 266 nm correlates linearly with the concentrations of S_8. The electrolytes were saturated by mixing them with an excessive amount of S_8 at 60 °C for 24 h with vigorous stirring and then maintaining them at 30 °C for 48 h without stirring. The electrolytes saturated with Li_2S_m were prepared as follows. Appropriate amounts of S_8 and Li_2S powder were placed in a vial containing an electrolyte and reacted at 60 °C for 100 h with stirring. Li_2S_m was generated during the stirring owing to the direct reaction of Li_2S with S_8 ($8Li_2S + (m - 1)\ S_8 \rightarrow 8Li_2S_m$).[30] After that, the electrolyte was maintained at 30 °C for 48 h without stirring, and the electrolytes were then assumed to be saturated with Li_2S_m based on the precipitation observed at the vial bottom. The supernatant liquid was subjected to UV-Vis spectroscopic analysis. The solubility limit of Li_2S_m was measured by the reported procedure with a two-compartment cell and electrochemical oxidation of Li_2S_m to S_8 followed by quantification of the converted S_8 using UV-Vis spectroscopy.[28]

4.3. Results and Discussion

4.3.1. Electrolytes for Li-$LiCoO_2$Cells

To comparatively study electrochemical reactions in cells with different electrolytes, the ratio of ether-oxygen atoms and Li^+ ([O]/[Li]) in the electrolytes was adjusted to four. A favorable coordination number for Li^+ ions is known to be between four and five in solution.[31,32] Therefore, all the solvent molecules in the [Li(glyme or THF)$_x$][TFSA] with [O]/[Li] = 4 were expected to be involved in the solvation of Li^+ ion. In previous work, we reported the fundamental transport properties of [Li(glyme or THF)$_x$][TFSA] with [O]/[Li] = 4.[27] The ionic conductivities (30 °C) were 7.2, 3.7, 0.62, and 1.0 S cm^{-1} for $[Li(THF)_4]^+$, $[Li(G1)_2]^+$, $[Li(G2)_{4/3}]^+$, and $[Li(G3)_1]^+$, respectively. The higher conductivity of [Li(glyme or THF)$_x$][TFSA] with shorter ethers arose from their lower viscosities: 4.8, 34, 177, and 184 mPa s at 30 °C for $[Li(THF)_4]^+$, $[Li(G1)_2]^+$, $[Li(G2)_{4/3}]^+$, and $[Li(G3)_1]^+$, respectively.

Figure 4-1 shows the galvanostatic charge/discharge curves of [Li anode │[Li(glyme or THF)$_x$][TFSA] electrolytes │ $LiCoO_2$ cathode] cells measured in the cell voltage range from

3.0 V to 4.2 V. Because of its low conductivity, a cell test with $[Li(G2)_{4/3}][TFSA]$ was not performed. The theoretical capacity of $LiCoO_2$ in this voltage range is 137 mA h g^{-1} based on the electrochemical reaction:

$$LiCoO_2 \rightleftarrows Li_{0.5}CoO_2 + 0.5Li^+ + e^-$$

Charge/discharge measurements were carried out at a gravimetric current density of 17 mA g^{-1}, which corresponds to a geometric current density of 50 μA cm^{-2}. During the charge/discharge, the Li^+ ions are reversibly extracted/inserted from/into the layered structure of the $LiCoO_2$. The cells with $[Li(G1)_2][TFSA]$ and $[Li(G3)_1][TFSA]$ showed reversible and stable charge/discharge behaviors, and the charge and discharge capacities are close to the theoretical value, although the former cell exhibited rapid capacity decay. As can be seen in **Figure 4-1**, the charge and discharge voltage plateaus of the cell with $[Li(G3)_1][TFSA]$ are slightly higher and lower, respectively, than those of the cell with $[Li(G1)_2][TFSA]$. This suggests that the internal resistance of the cell with $[Li(G3)_1][TFSA]$ is higher than that with $[Li(G1)_2][TFSA]$.This can be attributed to the lower ionic conductivity of $[Li(G3)_1][TFSA]$ compared to $[Li(G1)_2][TFSA]$.[27] In contrast to the reversible charge/discharge behavior observed in cells with $[Li(G1)_2][TFSA]$ and $[Li(G3)_1][TFSA]$, cells with $[Li(THF)_4][TFSA]$ had capacities that rapidly decayed through repeated charge/discharge reactions (*vide infra*).

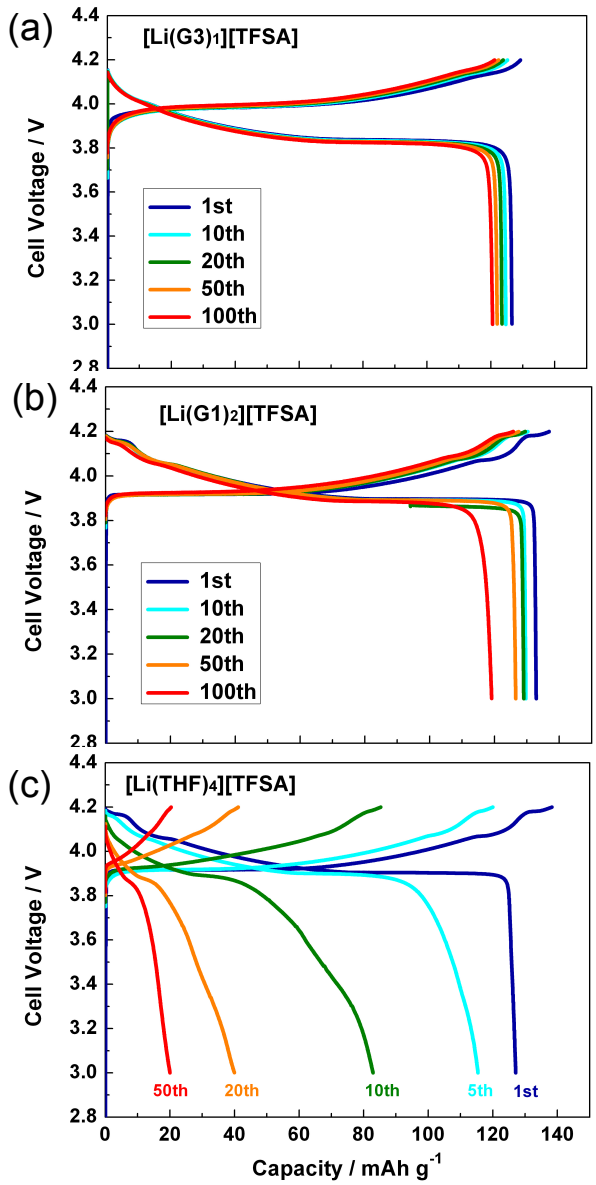

Figure 4-1. Charge/discharge curves of Li metal anode |[Li(glyme or THF)$_x$][TFSA] electrolyte| $LiCoO_2$ cathode cells with a constant current density of 50 μA cm^{-2} (1/8 Crate) at 30°C; (a) $[Li(G3)_1][TFSA]$, (b) $[Li(G1)_2][TFSA]$, (c) $[Li(THF)_4][TFSA]$.

It is well known that ethers oxidatively decompose at ~4V versus Li/Li^+.[1] Therefore, ether-based electrolytes have not been used for practical 4 V class Li ion batteries. However, the cells with $[Li(G1)_2][TFSA]$ and $[Li(G3)_1][TFSA]$ could be charged and discharged repeatedly for more than 100 cycles (**Figure 4-1a** and **b**). This suggests that undesirable oxidative decomposition was greatly suppressed in those cells. In the case of the equimolar complex of $[Li(G3)_1][TFSA]$, the strong electric field of the Li^+ ion polarizes the glyme oxygens through complexation, and lowers the HOMO energy level of the glyme.[13] Additionally, free (un-coordinating) G3 scarcely exists in $[Li(G3)_1][TFSA]$ at a 1:1 composition. Therefore, $[Li(G3)_1][TFSA]$ does not decompose even at a high electrode potential of ~4.5 V versus Li/Li^+, resulting in stable operation of the $LiCoO_2$ cathode, but the cell with $[Li(G3)_4][TFSA]$ containing excess glymes cannot be operated because of the decomposition of the un-coordinating G3, as shown before.[13] Likewise, the oxidative stability of G1 can be enhanced in the form of $[Li(G1)_2]^+$. The anodic limit of $[Li(G1)_2][TFSA]$ was ~4.3 V,[27] which is higher than the charging potential of the Li-$LiCoO_2$ cell. However, the anodic limit of $[Li(G1)_2][TFSA]$ is lower than that of $[Li(G3)_1][TFSA]$. This is due to the instability of the solvate structure of $[Li(G1)_2]^+$ compared to that of $[Li(G3)_1]^+$. The lower oxidative stability of the G1-based solvate leads to a lower Coulombic efficiency for the discharge/charge capacities of the Li-$LiCoO_2$ cell (*vide infra*).

As pointed out above, the charge and discharge capacities of the cell with $[Li(THF)_4][TFSA]$ faded rapidly as the cycle number increased, suggesting unfavorable side reactions took place in the cell (**Figure 4-1c**). One may expect that all of the THF molecules participate in the solvation of Li^+, and no free THF exist in $[Li(THF)_4][TFSA]$. However, as reported in our previous paper,[27]the lifetimes of $[Li(G1)_2]^+$ and $[Li(G3)_1]^+$ in solutions with an excess of glymes were estimated to be in the ranges of $10^{-6} \sim 10^{-5}$ s and $10^{-4} \sim 10^{-3}$ s, respectively.Clearly, the smaller the number of ether oxygens the solvent has, the faster the ligand exchange rate becomes. This implies that the lifetime of $[Li(THF)_4]^+$ with a monodentate ligand is much shorter than 10^{-6} s. Even in further concentrated $[Li(THF)_3][TFSA]$ and $[Li(THF)_2][TFSA]$ systems, the ligand exchange rate would be faster than that in $[Li(G3)_1][TFSA]$.[27] This is attributed to the instability and short lifetime of the solvate structure of $[Li(THF)_x]^+$. During fast ligand exchange in $[Li(THF)_4][TFSA]$, free THF should be generated, and the free THF can be electrochemically oxidized at a lower electrode potential. The oxidative decomposition of $[Li(THF)_4][TFSA]$ started at an electrode potential of 4.0 V versus Li/Li^+.[27] As a result, the free THF cannot withstand the charging potential (4.2 V) of the $LiCoO_2$ cathode, and this is a possible reason for the cell performance degradation (**Figure 4-1c**). The Coulombic efficiencies of the charge/discharge capacity of Li-$LiCoO_2$ cells are shown in **Figure 4-2**. The cell with $[Li(G3)_1][TFSA]$ exhibited a Coulombic

efficiency higher than 99% throughout the 100 cycles. For the initial 50 cycles, the Coulombic efficiency of the cell with $[Li(THF)_4][TFSA]$ was lower than 97%, while that of the cell with $[Li(G1)_2][TFSA]$ was greater than 99%. This result clearly indicates that the stability of the solvate structure of $[Li(glyme\ or\ THF)_x]^+$ has an important impact on the oxidative stability of the electrolyte and charge/discharge cycle stability of the battery. After 50 cycles, the Coulombic efficiency of the cell with $[Li(G1)_2][TFSA]$ also decreased gradually, indicating irreversible side reactions in the cell. This result can be attributed to poor anodic stability of $[Li(G1)_2][TFSA]$ on $LiCoO_2$ or Li_xCoO_2, which is well-known in conventional electrolytes for Li-ion batteries.[1,33]

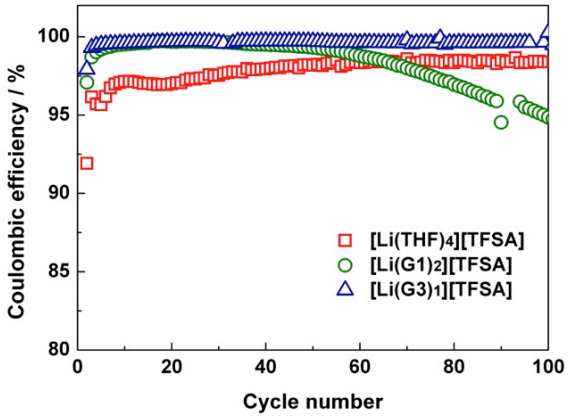

Figure 4-2. Coulombic efficiency of Li metal anode |$[Li(glyme\ or\ THF)_x][TFSA]$ electrolyte| $LiCoO_2$ cathode cells with a constant current density of 50 μA cm^{-2} (1/8 Crate) at 30°C.

4.3.2. Corrosion of Al Current Collector

In addition to the irreversible decomposition of the electrolytes, the corrosion of the Al current collector in the cathode may take place in Li-$LiCoO_2$ cells. It is well known that Al electrode corrodes at ~3.8 V versus Li/Li^+ in Li[TFSA]-containing electrolytes,[34-36] which prevents the practical use of Li[TFSA]-containing electrolytes for lithium ion batteries. Nevertheless, as shown in **Figure 4-1a**, the Li-$LiCoO_2$ cell can operate with the solvate IL, $[Li(G3)_1][TFSA]$, for more than 100 cycles. The severe Al corrosion was inhibited in this electrolyte. This fact prompted us to investigate whether Al corrosion can be suppressed in the electrolyte containing $[TFSA]^-$ and if the corrosion rate may be affected by the electrolyte composition.

To examine Al corrosion, cyclic voltammetry of Al foil was carried out using a cell with $[Li(glyme\ or\ THF)_x][TFSA]$ electrolyte, as shown in **Figure 4-3**. Almost no current was detected below 5.5 V versus Li/Li^+ for $[Li(G3)_1][TFSA]$, whereas obvious onsets of anodic reaction can be seen at 4.2 V and 4.7 V versus Li/Li^+ for $[Li(THF)_4][TFSA]$ and$[Li(G1)_2][TFSA]$, respectively. The anodic limit of Al in each electrolyte was higher than

that with a Pt electrode.[27] The Al surface was covered with the natural passivation film of Al_2O_3, whereas no passivation films exist on the Pt surface because of its noble nature. The Al_2O_3 film makes the Al surface inert, and the oxidative decomposition of the electrolytes was suppressed. However, the anodic current at higher potentials suggests that the passivation film was destroyed, and the anodic dissolution of Al(III) compounds and oxidative decomposition of electrolytes on the fresh Al surface occur simultaneously.

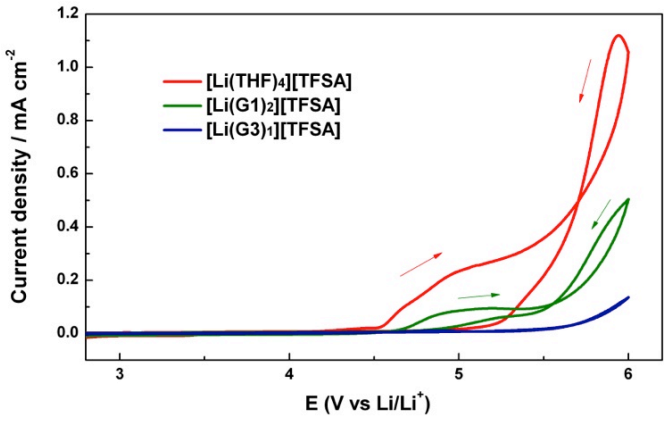

Figure 4-3. Cyclic voltammograms (1st cycle) in [Li(glyme or THF)$_x$][TFSA] mixtures at [O]/[Li^+] ratio of 4 at a scan rate of 5 mV sec^{-1} at 30°C. Al foil was used as working electrode, while Li metal was used as reference and counter electrode.

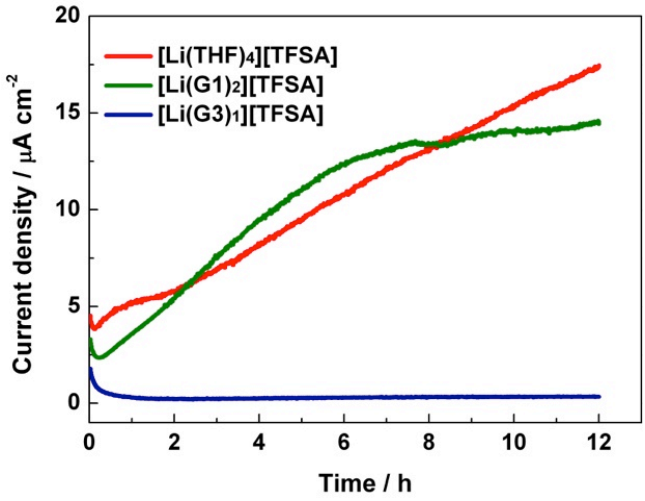

Figure 4-4. Chronoamperograms of Al electrodes recorded during prolonged polarization at 4.8 V versus Li/Li^+ in [Li(glyme or THF)$_x$][TFSA] mixtures at 30 °C. Li foil was used as the reference and counter electrode.

Figure 4-4 illustrates the chronoamperograms for an Al electrode measured at a constant cell voltage of 4.8 V. The anodic current for $[Li(G3)_1][TFSA]$ rapidly decayed, suggesting that the Al corrosion and decomposition of electrolyte were effectively suppressed. However, the anodic currents for $[Li(THF)_4][TFSA]$ and $[Li(G1)_2][TFSA]$ were continuously observed for

12 h. According to recent reports, the corrosion of Al is assumed to proceed in Li[TFSA] containing electrolytes as follows:[37] (1) the passivation film Al_2O_3 is destroyed, (2) the oxidation of Al takes place to produce Al^{3+}, and (3) Al^{3+} forms complexes with $[TFSA]^-$. Then, the resulting $Al[TFSA]_3$ or other Al-[TFSA]-based products dissolve in the electrolytes. In the case of $[Li(THF)_4][TFSA]$ and $[Li(G1)_2][TFSA]$, a certain amount of un-coordinating THF and G1 molecules can exist in the liquids (*vide supra*). These solvents are capable of dissolving Al-[TFSA] complexes. On the other hand, un-coordinating G3 is negligible in $[Li(G3)_1][TFSA]$, and thus, the dissolution of Al-[TFSA] complexes can be suppressed. When Al-[TFSA] complexes are insoluble, they may contribute to the formation of a stable protective layer, which prevents further Al corrosion.[38]

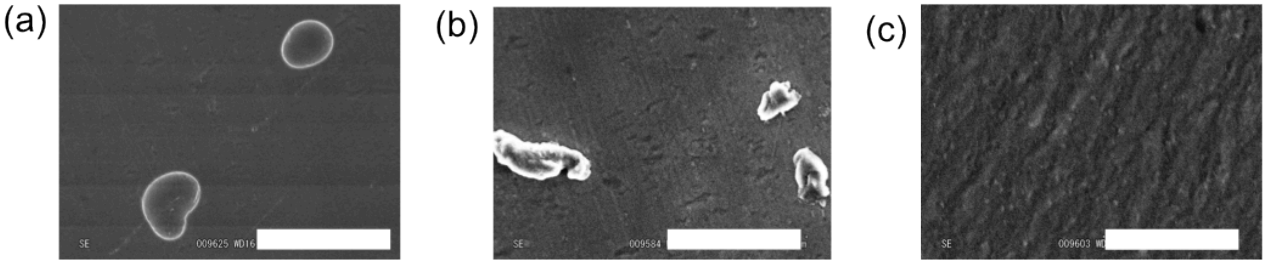

Figure 4-5.SEM images of Al electrodes polarized for 12h at 4.8 V versus Li/Li^+ in $[Li(glyme\ or\ THF)_x][TFSA]$ mixtures at 30 °C. (a) $[Li(THF)_4][TFSA]$, (b) $[Li(G1)_2][TFSA]$, (c) $[Li(G3)_1][TFSA]$. Scale bar in each image is 50 μm.

To check the morphology changes of the Al foil from corrosion reactions, the surface was observed by SEM. **Figure 4-5** shows SEM images of Al foils after the polarization at 4.8 V for 12 h. The pitting corrosion of Al was observed in $[Li(THF)_4][TFSA]$ and $[Li(G1)_2][TFSA]$, but the morphology change was not significant in $[Li(G3)_1][TFSA]$. The anodic currents in $[Li(THF)_4][TFSA]$ and $[Li(G1)_2][TFSA]$ gradually increased as the polarization time increased (**Figure 4-4**), indicating that the Al corrosion and electrolyte oxidation were enhanced over the course of time. As can be seen in **Figure 4-5**, the surface roughness of Al was increased by corrosion, and this increment of the surface area accelerates the anodic dissolution of Al and electrolyte oxidation.

Although the charge/discharge tests of Li-$LiCoO_2$ cells were carried out in the potential range of 3.0–4.2 V, Al corrosion can gradually proceed even at 4.2 V. Therefore, the Al corrosion in $[Li(THF)_4][TFSA]$ and $[Li(G1)_2][TFSA]$ during charge-discharge tests of Li-$LiCoO_2$ cells can account for the gradual decay of Coulombic efficiency (**Figure 4-2**). In addition, Al corrosion would destroy the current-collection path from $LiCoO_2$ particles, leading to a decrease in the discharge capacity of the cells (**Figure 4-1**). A similar suppression of Al corrosion was reported for highly concentrated electrolytes of Li[TFSA] in ethylene carbonate (EC)/diethyl

carbonate (DEC) mixtures[39] and in pure EC.[40] In those works, the concentration (c) of Li[TFSA] was a key factor in determining the Al corrosion suppression. However, our results here demonstrate that the structural stability of complex cations also affects the Al corrosion even at similar Li[TFSA] concentrations: c ~2.9 and 3.1 mol dm^{-3} for [Li(G1)$_2$][TFSA] and [Li(G3)$_1$][TFSA], respectively.[27] The absence of un-coordinating solvents, either in the solvate ILs or extremely highly concentrated Li[TFSA] electrolytes, hampers the dissolution of Al-[TFSA] complexes and explains the suppression of persistent Al corrosion.

The trigger for Al corrosion is the breakdown of the passivation film of Al_2O_3. The details of the breakdown mechanism of Al_2O_3 film in organic electrolytes are not clear at present; however, this phenomenon may be correlated with the oxidation of solvent molecules on Al/Al_2O_3. The anodic limits of the Al electrode in different electrolytes have the same order of oxidative stability as the electrolytes do when using a Pt electrode: [Li(G3)$_1$][TFSA] > [Li(G1)$_2$][TFSA] > [Li(THF)$_4$][TFSA]. Certain intermediates in the oxidative decomposition process may attack Al_2O_3 and cause the film to dissolve into the electrolyte. Further investigations may be needed to clarify a detailed corrosion mechanism.

4.3.3. Solubility limits of sulfur and lithium ploysulfides

The Li-S battery has attracted much attention as a next-generation energy storage device because of its high energy density.[41,42] Elemental sulfur (S_8) can be electrochemically reduced to Li_2S in aprotic electrolytes, as shown by the following equation.

$$S_8 + 16Li^+ + 16e^- \rightleftarrows 8Li_2S$$

This electrochemical reaction is reversible, and the theoretical discharge capacity of sulfur is 1672 mA h g^{-1}, which is much larger than that of conventional cathode materials such as $LiCoO_2$ and $LiFePO_4$ used in current lithium ion batteries. However, Li-S batteries generally suffer from several problems such as low active material utilization in the cathode and dissolution of lithium polysulfides (Li_2S_m) into the electrolyte during charge and discharge cycles. Lithium polysulfides are reaction intermediates of the S cathode, and the dissolution of Li_2S_m causes a rapid capacity fade and poor charge/discharge cycle stability of the cell. In addition, the dissolved Li_2S_m acts as a redox shuttle between the cathode and anode, resulting in low Coulombic efficiency for the discharge/charge of the cell.[43-45] In previous work, we revealed that the compositions of G3- or G4-Li salt electrolytes have a great impact on the electrochemical reactions of the S cathode. As the molar ratio (x) of the glymes to Li[TFSA] in [Li(G3 or G4)$_x$][TFSA] became smaller, the solubility of Li_2S_m drastically decreased.[24] Furthermore, the counter anion, X^-, of Li salt in [Li(G3 or G4)$_1$]X also affected the solubility of Li_2S_m and the reversibility of the electrochemical reaction at the S cathode.[46] As a result, we found that the redox shuttle mechanism in a Li-S cell can be effectively inhibited by using

equimolar [Li(G3 or G4)$_1$][TFSA] complex electrolytes. [Li(G3 or G4)$_1$][TFSA] allowed for a stable charge-discharge cycle of a Li-S cell for over 400 cycles with a high Coulombic efficiency (> 98%) and discharge capacity of ~800 mA h g^{-1}.[24]

In this study, we report the effect of solvent (ligand) structures in [Li(glyme or THF)$_x$][TFSA] on the charge-discharge properties of Li-S cells. As mentioned, the solubility of Li_2S_m has a significant impact on the redox reaction at the S cathode in the cell. To elucidate how the structural stability of the complex [Li(glyme or THF)$_x$]$^+$ cation affects the solubility of the reaction intermediates, lithium polysulfides (m = 2, 4, 6, and 8) were chemically prepared in [Li(glyme or THF)$_x$][TFSA] through the direct reaction between S_8 and Li_2S,[30] as shown below, and analyzed.

$$8Li_2S + (m - 1)\ S_8 \rightarrow 8Li_2S_m$$

Figure 4-6 shows UV-Vis spectra of saturated S_8 and Li_2S_m in [Li(glyme or THF)$_x$][TFSA]. The spectra of Li_2S_m (except for Li_2S_6) in [Li(G3)$_1$][TFSA] are reported elsewhere.[24] The spectral shape, especially the overall absorbance of Li_2S_m, changes greatly depending on the structure of the ligands. In addition, multiple peaks can be seen in each spectrum, suggesting that the solutions contain several polysulfide species with different chain lengths.[47] According to the literature, the assignment of the UV-Vis absorption bands of S_m^{2-} in organic solvents is as follows: 490−500 nm for S_8^{2-}, 450−470 nm for S_6^{2-}, ~420 nm for S_4^{2-}, 340 nm for S_3^{2-}, and ~280 nm for S_2^{2-}.[48,49] The Gibbs energies of formation for polysulfides with different chain lengths (Li_2S_m, $2 \le m \le 8$) are very close to each other.[50] Therefore, the disproportionation of S_m^{2-} can easily occur in the electrolytes, and several polysulfide species coexist. It was reported that the polysulfide species and their proportion are strongly affected by electrolyte qualities such as solvents (including ILs),[28,29,51,52] Li salt concentration,[24] and anion structure of Li salts.[46]

The total concentration of S_8 and Li_2S_m can be quantitatively evaluated, as reported previously in our paper, but it is difficult to determine the concentration of each polysulfide.[24,28,29] **Figure 4-7** shows the solubility limits of S_8 and Li_2S_m in [Li(glyme or THF)$_x$][TFSA]([O]/[Li] = 4). The solubility is represented as the total atomic S concentration. Li_2S hardly dissolves in each electrolyte, and the concentration was less than 1 mM. The solubility of S_8 is also relatively low. [Li(THF)$_4$][TFSA] can dissolve at 30 mM, however, the solubility limits of pure sulfur in [Li(G1)$_2$][TFSA], [Li(G2)$_{4/3}$][TFSA], and [Li(G3)$_1$][TFSA] are less than 10 mM. Compared to the low solubility of Li_2S and S_8, the solubility of Li_2S_m is rather high. Especially, Li_2S_m with a nominal composition of $4 \le m \le 8$ is highly soluble. The negative charges of S_m^{2-} are more delocalized on longer polysulfides. Therefore, the interaction between Li^+ and the polysulfide

becomes weaker as the chain length of S_m^{2-} increases. As a result, the longer Li_2S_m easily dissociates to dissolve in the electrolytes.

The solubility of Li_2S_m changes greatly depending on the ligand structure in [Li(glyme or THF)$_x$][TFSA]. Clearly, the solubility of Li_2S_m tends to decrease as the ligand length increases, despite the same [O]/[Li] ratio in the electrolytes. Amazingly, the solubility limits of Li_2S_m in $[Li(THF)_4][TFSA]$ and $[Li(G1)_2][TFSA]$ are 1−2 orders of magnitude higher than those in $[Li(G2)_{4/3}][TFSA]$ and $[Li(G3)_1][TFSA]$.

For the dissolution process, Li_2S_m is presumed to dissociate into Li^+ and S_m^{2-},andthe generated Li^+ ion should be stabilized by solvation. In the cases of $[Li(THF)_4][TFSA]$ and $[Li(G1)_2][TFSA]$ electrolytes, the lifetimes of $[Li(THF)_4]^+$ and $[Li(G1)_2]^+$ in the electrolytes are very short when compared to those of $[Li(G2)_{4/3}][TFSA]$ and $[Li(G3)_1][TFSA]$ (*vide supra*). Therefore, a certain amount of free solvent is present in $[Li(THF)_4][TFSA]$ and $[Li(G1)_2][TFSA]$. This can contribute to the solvation of Li_2S_m, resulting in the high solubility of Li_2S_m. In contrast, the lifetimes of $[Li(G2)_{4/3}]^+$ and $[Li(G3)_1]^+$ are rather long, and free G2 and G3 molecules scarcely exist in the electrolyte, resulting in the relatively low solubility of Li_2S_m.

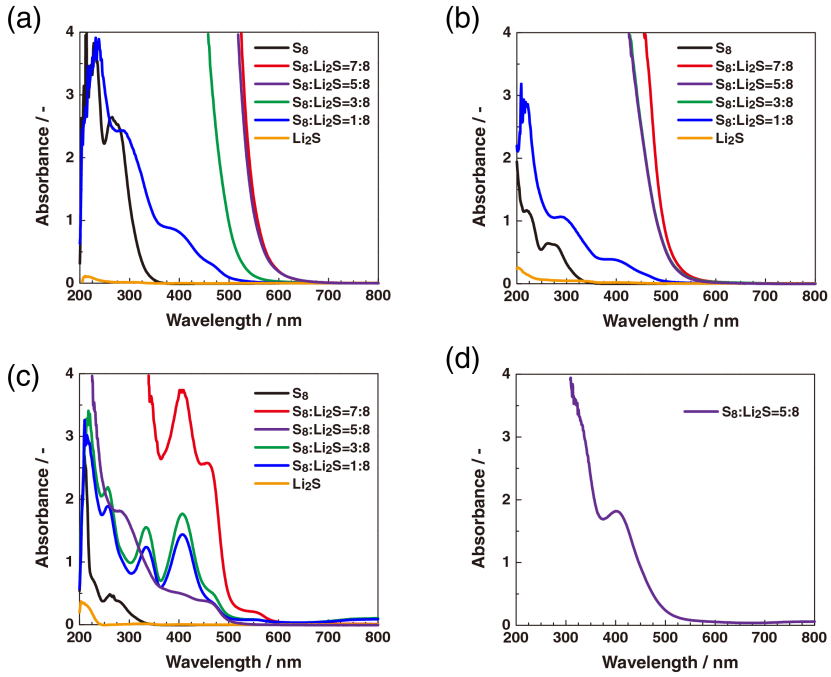

Figure 4-6. UV-vis spectra of saturated solutions of S_8, Li_2S_8, Li_2S_6, Li_2S_4 and Li_2S_2 in [Li(glyme or THF)$_x$][TFSA] mixtures. Li_2S_m (m = 8, 6, 4, 2) is the nominal formula and the actual polysulfides in each electrolyte are mixtures of several species with different chain lengths. (a) $[Li(THF)_4][TFSA]$; (b) $[Li(G1)_2][TFSA]$; (c) $[Li(G2)_{4/3}][TFSA]$; (d) $[Li(G3)_1][TFSA]$ (only for Li_2S_6).

In a previous paper, we reported that complex $[Li(G3 \text{ or } G4)_1]^+$ cations became unstable when combined with strongly Lewis basic X^-.[26] Indeed, the dissolution of Li_2S_m was more pronounced in $[Li(G3 \text{ or } G4)_1]X$ with the strongly Lewis basic X^- such as NO_3^- and $CF_3SO_3^-$.[46] Overall, the solubility of Li_2S_m in the molten $[Li(glyme \text{ or } THF)_x]X$ solvates is greatly affected by the structural stability of the complex cation, and the stable and unstable molten $[Li(glyme \text{ or } THF)_x]X$ solvates poorly and highly solubilize Li_2S_m, respectively.

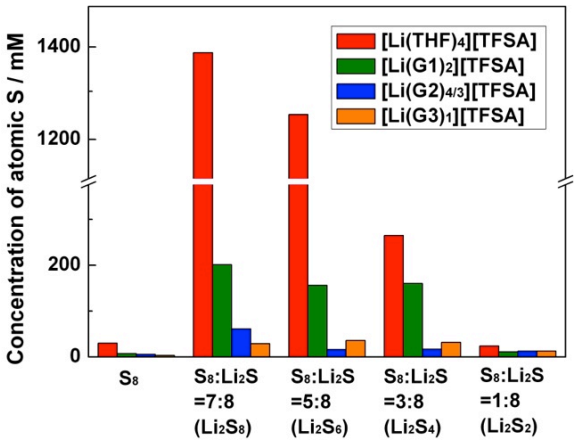

Figure 4-7. Saturation concentrations of S_8, Li_2S_8, Li_2S_6, Li_2S_4 and Li_2S_2 represented in units of total atomic-S concentration in $[Li(glyme \text{ or } THF)_x][TFSA]$ mixtures. Li_2S_m (m = 8, 6, 4, 2) is the nominal formula and the actual polysulfides in each electrolyte are mixtures of several species with different chain lengths.

To investigate the effects of physicochemical properties of electrolytes and solubility of Li_2S_m on the electrochemical reaction at the S cathode, coin-type Li-S cells were fabricated. **Figure 4-8** shows galvanostatic charge-discharge curves of Li-S cells with $[Li(THF)_4][TFSA]$, $[Li(G1)_2][TFSA]$, $[Li(G2)_{4/3}][TFSA]$, and $[Li(G3)_1][TFSA]$ and a low current rate of 139 mA g^{-1}-sulfur (1/12 C rate) was measured at 30 °C. Each cell shows reversible charge/discharge curves with two voltage regions, and the initial discharge capacity is within the range of 700–1000 mA h g^{-1}, corresponding to 40–60% of the theoretical capacity of elemental S. The voltage-sloping region of 2.4–2.0 V in the discharge curve is regarded as the reduction of S_8 into Li_2S_m ($m \geq 4$) through the formation of Li_2S_8, and the voltage plateau at ~2.0 V is ascribed to the reduction of Li_2S_4into Li_2S.[53,54] An increase in the overvoltage with the repeating charge-discharge cycles could be observed in the cells with $[Li(THF)_4][TFSA]$ and $[Li(G1)_2][TFSA]$ electrolytes (**Figure 4-8**). This can be attributed to side reactions on the electrodes accompanied by the dissolution of Li_2S_m (*vide infra*). During the charge-discharge process, the electrochemically generated Li_2S_m can dissolve in the electrolyte. The coin-type [Li| electrolyte with a glass separator| C/S] cells were used in this study, and the volume of electrolyte was limited to the void space of the porous separator and C/S composite cathode.

The concentration of Li_2S_m in the electrolyte was limited to the solubility limit (**Figure 4-7**). In the cases of the cells with $[Li(G2)_{4/3}][TFSA]$ and $[Li(G3)_1][TFSA]$, the maximum amount of dissolved Li_2S_8 was estimated to be 3 and 6% of the total amount of S originally loaded on the composite cathode respectively. This suggests that most of the Li_2S_m remains in a solid state. On the other hand, 100 % of S on the cathode was expected to be dissolved in the cell with $[Li(THF)_4][TFSA]$. Li_2S_8 can be moderately soluble in the cell with $[Li(G1)_2][TFSA]$ (19 % of total S on the cathode). The dissolved Li_2S_m reacts with the metallic lithium anode and partially forms insoluble byproducts. Moreover, the dissolved Li_2S_m can form electrochemically inactive precipitates on the cathode. These would be responsible for the increase in the cell resistance, leading to the observed over potential in the cell with $[Li(THF)_4][TFSA]$ and $[Li(G1)_2][TFSA]$.

4.3.4. Electrolytes for Li-S cells

Figure 4-8a shows the charge-discharge cycle performance of Li-S cells. The discharge capacity of each cell decreased as the cycle number increased. This degradation is probably caused by a volume change in the cathode active material. The volume of the active material theoretically becomes 1.8 times larger during the conversion reaction of sulfur ($S_8 + 16Li^+ + 16e^- \rightarrow 8Li_2S$). The repetition of the volume change of the active material during charge-discharge cycles may bring about loosing electrical contact between the active material and carbon support. The electrically isolated active material cannot contribute to the redox reaction, and the capacity of the cathode gradually decreases. In addition, the dissolution of Li_2S_m in the electrolyte may be partly responsible for the degradation, however, this factor would be minor for cells with $[Li(G2)_{4/3}][TFSA]$ and $[Li(G3)_1][TFSA]$ because of the low solubility of Li_2S_m.

As shown in **Figure 4-8a**, the discharge capacities of cells with $[Li(THF)_4][TFSA]$ and $[Li(G1)_2][TFSA]$ are higher than those of cells with $[Li(G2)_{4/3}][TFSA]$ and $[Li(G3)_1][TFSA]$. This could be because of the differences in viscosity and ionic conductivity of the electrolytes. The viscosities and ionic conductivities of $[Li(THF)_4][TFSA]$ and $[Li(G1)_2][TFSA]$ are low and high, respectively, in comparison to those of $[Li(G2)_{4/3}][TFSA]$ and $[Li(G3)_1][TFSA]$. The mass transport resistance within the pores of the C/S composite cathode should increase as the depth of the discharge increases because the volume fraction of the electrolyte in the composite cathode decreases because of volume expansion of the active material. The low viscosity of $[Li(THF)_4][TFSA]$ and $[Li(G1)_2][TFSA]$ would facilitate ionic conduction in the narrowed pores and increase utilization of the active material. In addition to the low mass transport resistance, the dissolution of Li_2S_m in $[Li(THF)_4][TFSA]$ and $[Li(G1)_2][TFSA]$ may enhance the kinetics of the redox reaction of sulfur (*vide infra*).

Figure 4-8b shows the Coulombic efficiency (discharge capacity/charge capacity) of the Li-S cells with different electrolytes. The Coulombic efficiency of the cells with $[Li(THF)_4][TFSA]$ (< 95%) and $[Li(G1)_2][TFSA]$ (~97%) is much lower than that of the cells with $[Li(G2)_{4/3}][TFSA]$ and $[Li(G3)_1][TFSA]$ (~99%). Clearly, the Coulombic efficiency is correlated to the solubility of Li_2S_m in the electrolytes. The dissolved Li_2S_m acts as a redox shuttle between the cathode and anode in cells. The electrochemically generated Li_2S_m in the C/S composite dissolves in the electrolyte, and Li_2S_m diffuses from the composite cathode to the Li metal anode. The Li_2S_m can be further reduced to Li_2S_l ($l<m$) on the Li surface, and Li_2S_l can diffuse back toward the composite cathode to be further reduced when the cell is discharging and oxidized when the cell is charging. This redox shuttle mechanism during a charge-discharge cycle causes low Coulombic efficiency in the cell.[55-57] In addition, the shuttle mechanism may cause a self-discharge of the cell. Therefore, inhibition of the shuttle is essential to achieve a high Coulombic efficiency and stable operation of Li-S cells. In the case of $[Li(THF)_4][TFSA]$ and $[Li(G1)_2][TFSA]$, the solubility of $Li_2S_m$is rather high.

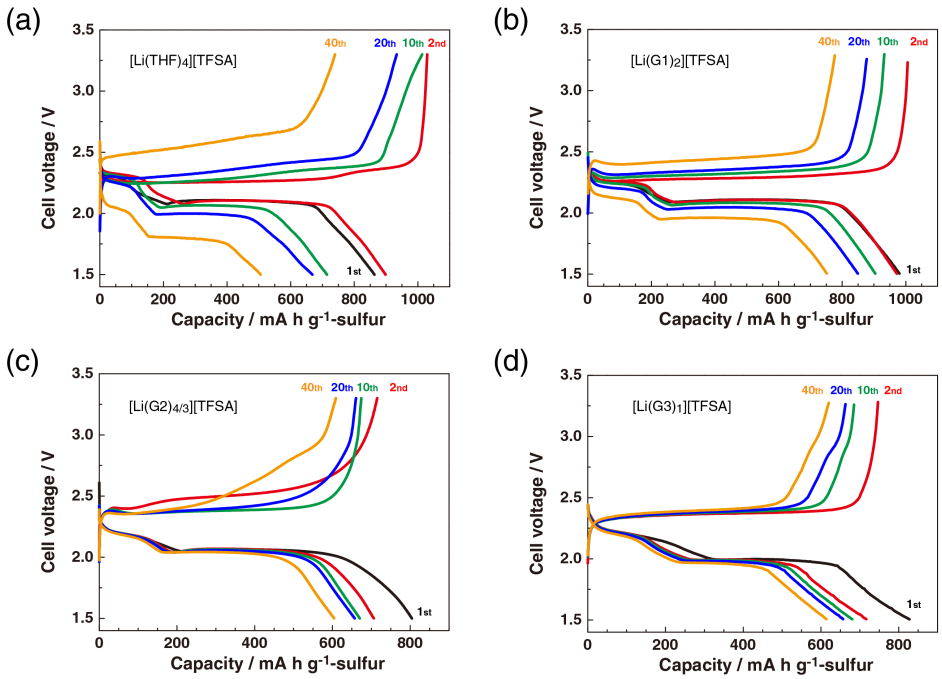

Figure 4-8. Galvanostatic charge/discharge curves of Li-S cells with $[Li(glyme\ or\ THF)_x][TFSA]$ measured at a current density of 139 mA g^{-1} -sulfur at 30 °C; (a) $[Li(THF)_4][TFSA]$, (b) $[Li(G1)_2][TFSA]$, (c) $[Li(G2)_{4/3}][TFSA]$, (d) $[Li(G3)_1][TFSA]$.

As we demonstrated, the charge-discharge cycle stability of a Li-S cell is strongly affected by the physicochemical properties of the electrolyte and solubility of Li_2S_m.[24] The electrode kinetics of the S cathode can also be affected by electrolytes. To investigate the kinetics of the

C/S cathode, charge and discharge measurements of Li-S cells were carried out at various current densities (**Figure 4-9**). The discharge capacities of the cells decreased as the current density increased. The cells with $[Li(THF)_4][TFSA]$ and $[Li(G1)_2][TFSA]$ had better charge-discharge rate capacities than cells with $[Li(G2)_{4/3}][TFSA]$ and $[Li(G3)_1][TFSA]$. This suggests that the rate capability of the Li-S cell is mainly dominated by the transport properties of the electrolyte, although the rate capability is affected by several factors. The relatively low ionic conductivity and high viscosity of $[Li(G2)_{4/3}][TFSA]$ and $[Li(G3)_1][TFSA]$ would cause a high mass transport resistance within the porous C/S composite cathode. In the $[Li(THF)_4][TFSA]$ and $[Li(G1)_2][TFSA]$ systems, the mass transport resistance should be low because of their relatively high ionic conductivities and low viscosities. Furthermore, the dissolution of Li_2S_m ($4 \leq m \leq 8$) probably accelerates the redox reaction rate of the composite cathode. The dissolved Li_2S_m does not block the ionic conduction path within the composite cathode. Moreover, the charge transfer reaction at the active material/electrolyte interface is presumed to be assisted by the dissolution of Li_2S_m because the Li^+ ion can diffuse in the liquid and easily approach the surface of the active material. On the other hand, in the case of $[Li(G2)_{4/3}][TFSA]$ and $[Li(G3)_1][TFSA]$, Li_2S_m ($1 \leq m \leq 8$) mainly remains in the solid state because of its low solubility (*vide supra*), and the Li^+ ion should diffuse in the solid state to complete the redox reaction of the active material. This would lead to a relatively high resistance in the cells with $[Li(G2)_{4/3}][TFSA]$ and $[Li(G3)_1][TFSA]$.

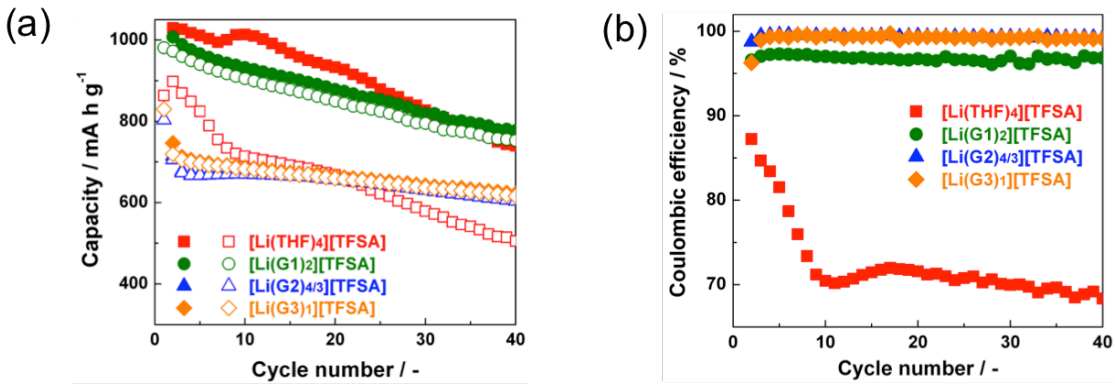

Figure 4-9. Cycle performance of Li-S cells with $[Li(glyme\ or\ THF)_x][TFSA]$ measured at a current density of 139 mA g^{-1} -sulfur at 30 °C; (a) Capacity, (b) Coulombic efficiency. Closed and open plots represent charge and discharge capacity, respectively.

As shown in **Figure 4-11**, the discharge capacity of each cell in the voltage sloping region of 2.4–2.0 V is nearly independent of the current density. This suggests that the electrochemical reactions ($S_8 \rightarrow Li_2S_8 \rightarrow 2Li_2S_4$) in the voltage sloping region are relatively fast. However, the discharge capacity of the voltage plateau at 2.0 V rapidly decreased as the current density

increased, and the kinetics of reactions ($2Li_2S_4 \rightarrow 4Li_2S_2 \rightarrow 8Li_2S$) at the voltage plateau is rather slow. The negative charge density of S_m^{2-} becomes higher as the ionic size of S_m^{2-} becomes smaller, resulting in low electron acceptability of S_m^{2-}. The electron acceptability of S_8 and long S_m^{2-} ($4<m\leq8$) is relatively high compared with that of short S_m^{2-} ($2\leq m\leq4$). The high electron acceptability of long S_m^{2-} ($4<m\leq8$) would result in the relatively fast electrochemical reactions in the voltage sloping region of 2.4–2.0 V, while the reaction kinetics at the 2.0 V plateau is sluggish due to the low electron acceptability of short S_m^{2-} ($2\leq m\leq4$). Furthermore, the volume expansion of the active material takes place, and the mass transport resistance within the pores of the composite cathode is increased as the depth of the discharge increases (*vide supra*). Therefore, the discharge capacity of the voltage plateau at 2.0 V was decreased as increasing the current density.

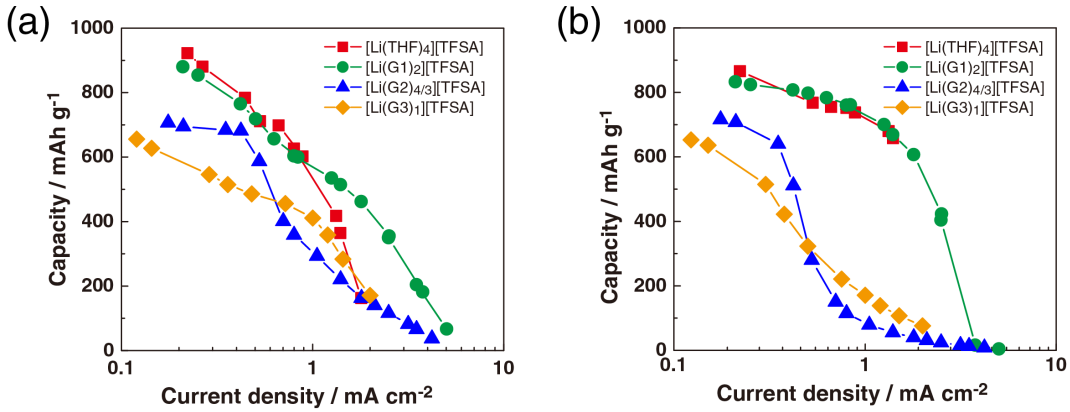

Figure 4-10. Rate capabilities of Li-S cells with [Li(glyme or THF)$_x$][TFSA] measured at various current density at 30 °C; (a) Discharge, (b) Charge.

In **Figure 4-10**, there are differences in the rate capabilities of Li-S cells in charging and discharging processes. The difference may be originated from the different reaction kinetics of charging and discharging processes. As observed in **Figure 4-8**, the discharge profile of each cell shows a voltage sloping region (2.4–2.0 V) and a voltage plateau at 2 V, however, the charge profile of the cell shows onlyone voltage plateau at 2.3 V. As discussed above, the reaction rate of the 2 V plateau in discharge process is slower than that of the voltage sloping region (2.4–2.0 V). The slow kinetics of the low voltage region may induce the mixed high and lowvoltage reactions during the charging at the 2.3 V plateau. However, further investigation is needed to understand the kinetics of electrochemical reaction of sulfur cathode.

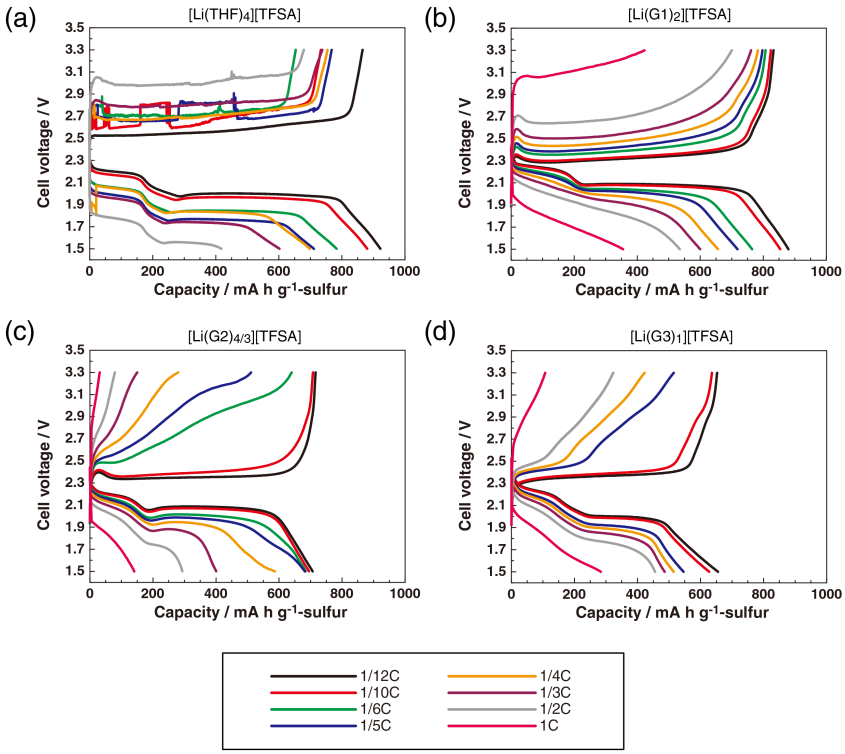

Figure 4-11. Discharge and charge curves of Li-S cells measured at various current densities with the (a) $[Li(THF)_4][TFSA]$, (b) $[Li(G1)_2][TFSA]$, (c)$[Li(G2)_{4/3}][TFSA]$, and (d) $[Li(G3)_1][TFSA]$ electrolytes at 30 °C.

It has been reported that the high lithium concentration in the electrolytes could inhibit the dissolution of lithium polysulfides,[58,59] which indicates that the solubility of Li_2S_mcould be suppressed by using concentrated electrolytes such as $[Li(THF)_x][TFSA]$ ($x \leq 3$) and $[Li(G1)_x][TFSA]$ ($x < 2$). F**igure 4-12** shows the Li-S cell performance byusing extreme concentrated $[Li(THF)_x][TFSA]$ electrolytes ($1.5 \leq x \leq 3$), reversible charge-discharge curves is achieved and the Coulombic efficiency of the Li-S cell can be increased comparing with $[Li(THF)_4][TFSA]$. This is because free THF molecules scarcely exist in $[Li(THF)_x][TFSA]$ ($1.5 \leq x \leq 2$), and the solubility of Li_2S_m is effectively suppressed. This is also true for the cases of $[Li(G2)_{4/3}][TFSA]$ and $[Li(G3)_1][TFSA]$. Indeed, we found some other factors, such as the anionic effects[46] and the chelate effects in the electrolytes, as shown in this study, are also important factors for determining the solubility of Li_2S_m. In our previous work we demonstrated that the stability of solvate cations of $[Li(THF)_x]^+$ is very low even in the extremely high concentration electrolyte (~3.7 mol/L), which is due to highly exchangeable property of THF solvent in the mixtures.[27] Although $[Li(THF)_x][TFSA]$ (x = 1.5 or 2) electrolyte could show reversible charge-discharge cycles and high capacity retention in Li-S cell test, the Coulombic efficient is still lower (~97%) than typical solvate IL electrolytes. It is noteworthy that the chelate effect or stability of solvate cations is quite important for the

electrolyte of Li-S batteries. Unstable $[Li(THF)_x]^+$cations, which will dissolve polysulfides, are not desirable for practical applications.

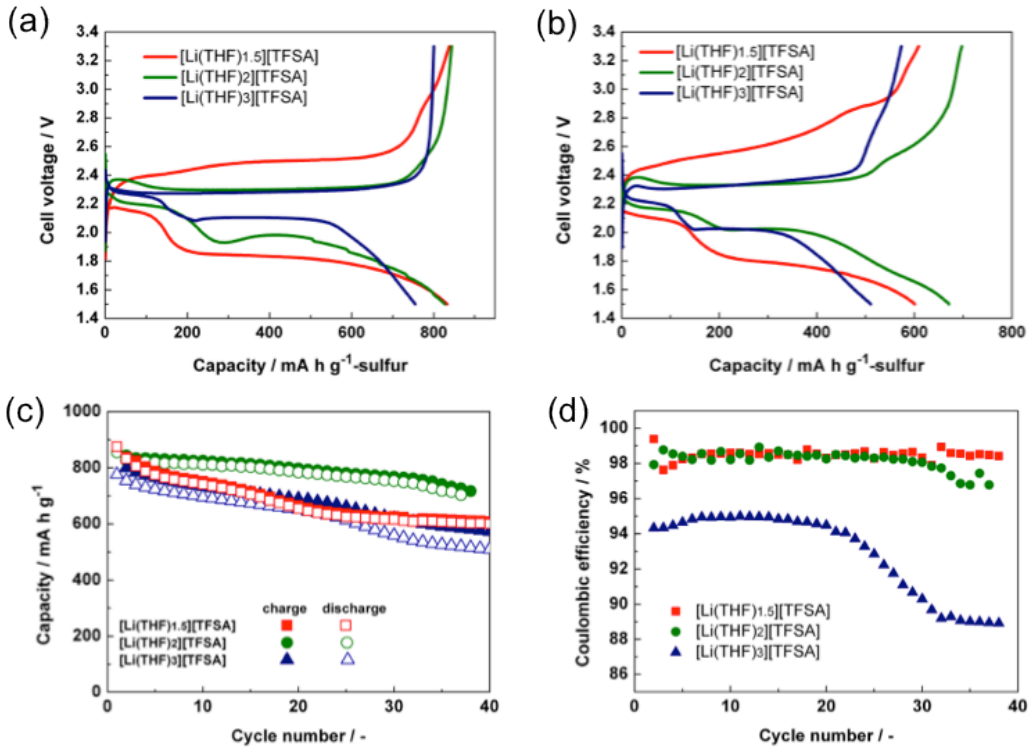

Figure 4-12. Galvanostatic charge-discharge curves of Li-S cells with $[Li(THF)_x][TFSA]$ (x = 1.5, 2 and 3) measured at a current density of 139 mA g^{-1} -sulfur at 30 °C; (a) 2nd charge-discharge curves, (b) 40th charge-discharge curves, (c) Capacity, (d) Coulombic efficiency. Closed and open plots represent charge and discharge capacity, respectively.

The solvent in the electrolyte has been expected as a key factor on the electrochemical performance of the Li-S cells. Such as carbonate-based solvents could react with the intermediate lithium polysulfides and almost no discharge capacity was observed by using the carbonate-based solvent such as EC or PC.[60] To confirm this result we prepared the PC contained electrolytes $[Li(PC)_x][TFSA]$ (x = 2~4) to operate the Li-S cell. **Figure 4-13** presents the cell performance. It was interesting to find that reversible charge-discharge could be obtained and the cell with $[Li(PC)_2][TFSA]$ electrolyte held ~400 mAh g^{-1} discharge capacity even after 40 cycles, which implies in the extreme concentrated $[Li(PC)_x][TFSA]$ electrolytes the decomposition of the PC could be suppressed to some extent. However, side reaction was found that in the discharge curves the first discharge plateau around 2.2V disappeared and the second plateau degraded to 1.8 V, which may owe to the reaction between Li_2S_m ($4<m\leq8$) and uncoordinated PC solvent. Even in extreme concentrated

$[Li(PC)_x][TFSA]$ electrolytes, free solvent would be exist due to the unstable $[Li(PC)]^+$ solvate.[61] Other high permittivity solvent such as DMSO was demonstrated unsuitable as the electrolyte for Li-S battery because it would stabilize the polysulfides, which could lead to a poor rate capability.[62] From what has been discussed above, the kinds of solvent and the stability of the solvate cation play an important role in the electrolyte of Li-S batteries.

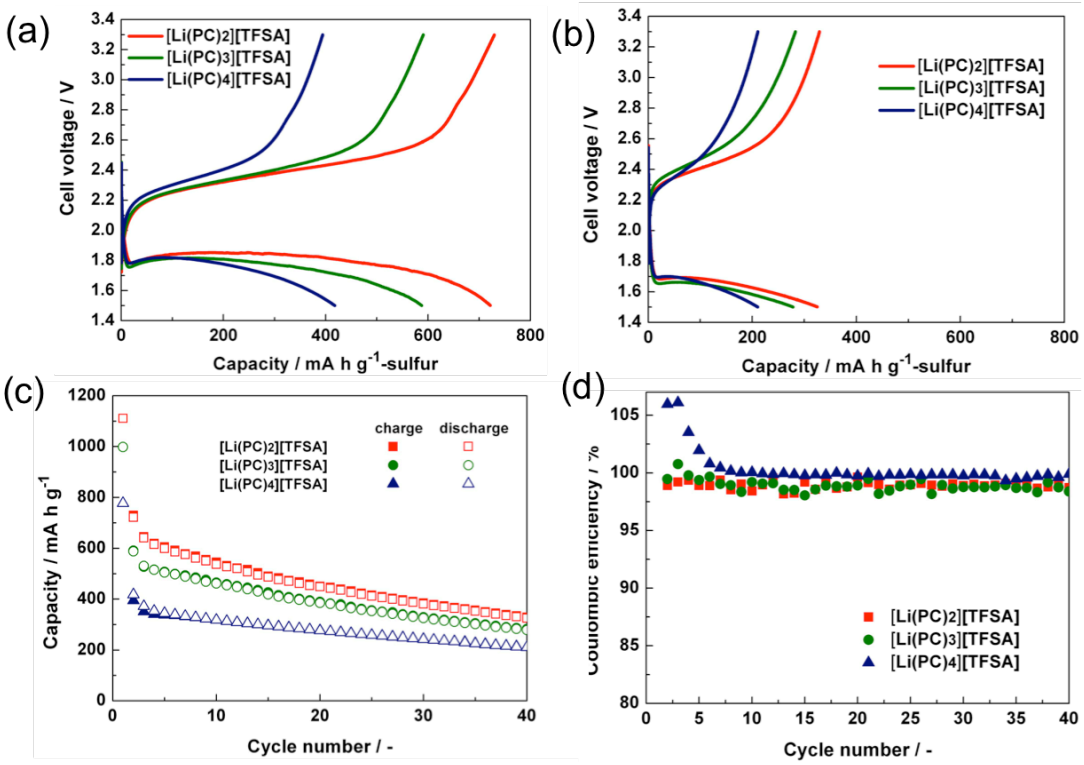

Figure 4-13. Galvanostatic charge-discharge curves of Li-S cells with $[Li(PC)_x][TFSA]$ (x = 2, 3 and 4) measured at a current density of 139 mA g^{-1} -sulfur at 30 °C; (a) 2nd charge-discharge curves, (b) 40th charge-discharge curves, (c) Capacity, (d) Coulombic efficiency. Closed and open plots represent charge and discharge capacity, respectively.

4.4. Concluding Remarks

A series of mixtures of glyme- or THF-Li[TFSA] were investigated as electrolytes for Li-ion and Li-S batteries. The oxidative stability of molten solvates of $[Li(glyme\ or\ THF)_x][TFSA]$ ([O]/[Li] = 4) changes depending on the structural stability of $[Li(glyme\ or\ THF)_x]^+$; for instance, a complex cation, $[Li(G3)_1]^+$, with tetradentate ligands is rather stable compared to $[Li(G1)_2]^+$ and $[Li(THF)_x]^+$ owing to the chelate effect. The performance of the Li-$LiCoO_2$ cell is affected significantly by the oxidative stability of electrolytes. The cell with the $[Li(G3)_1][TFSA]$ electrolyte had a good cycle stability with a high Coulombic efficiency, but degradation of performance due to the oxidative decomposition of the solvents was observed for cells with $[Li(THF)_4][TFSA]$ and $[Li(G1)_2][TFSA]$. In addition to the oxidative stability,

corrosion of the Al current collector was also affected by the structural stability of [Li(glyme or THF)$_x$][TFSA]. Although a detailed corrosion mechanism of Al in the electrolytes is not clear, the results of cyclic voltammetry and SEM observation of the Al electrode indicated that the electrochemical oxidation of the ether solvents on Al/Al_2O_3 (Al_2O_3: natural passivation film of Al) and solubility of Al (III) compounds in the electrolyte are involved in the corrosion processes. The rate of the corrosion reaction in [Li(THF)$_4$][TFSA] and [Li(G1)$_2$][TFSA] is much faster than that in [Li(G3)$_1$][TFSA], and consequently, the corrosion of the Al current collector in Li-$LiCoO_2$ cells causes a reduction in discharge capacity and the low Coulombic efficiency of charge-discharge in the [Li(THF)$_4$][TFSA] and [Li(G1)$_2$][TFSA] cells.

The charge-discharge properties of Li-S cells are strongly affected by the physicochemical properties of electrolytes. High ionic conductivity and low viscosity are favorable for achieving high rate capabilities, i.e., high power density in the Li-S cell. The electrolytes of the molten solvates with small ligands such as [Li(THF)$_4$][TFSA] and [Li(G1)$_2$][TFSA] possess high ionic conductivities and low viscosities and are favorable for high power Li-S cells. However, the solubility of Li_2S_m, which is a reaction intermediate of the sulfur cathode in the Li-S battery, is high in these electrolytes. The high solubility causes a redox shuttle mechanism during operation of the Li-S cell, leading to poor cycle stability and low Coulombic efficiency. This is problematic for practical applications. In contrast, molten solvates with long ligands such as [Li(G2)$_{4/3}$][TFSA] and [Li(G3)$_1$][TFSA] possess low solubility for Li_2S_m and are effective electrolytes to suppress the redox shuttle mechanism. Using this kind of electrolyte, good cycle stability and high Coulombic efficiency of the Li-S cell can be achieved. However, the low ionic conductivity and high viscosity of [Li(G2)$_{4/3}$][TFSA] and [Li(G3)$_1$][TFSA] cause a high resistance, resulting in a poor rate capability of the Li-S cell. This drawback can be solved by the addition of another solvent to [Li(G2)$_{4/3}$][TFSA] and [Li(G3)$_1$][TFSA]. Previously, we reported that the addition of a low polar solvent is effective in increasing the ionic conductivity and decreasing the viscosity of the electrolytes.[24] The added low polar solvent, hydrofluoroether (HFE), does not participate in the solvation of the Li^+ ion, and the coordination structure of [Li(glyme)$_1$]$^+$ is kept in the electrolyte. By using [Li(glyme)$_1$][TFSA]/HFE electrolytes, a good cycle stability, high Coulombic efficiency, and high rate capability of Li-S cell can be achieved.

4.5. Reference

1 Xu, K. *Chem. Rev.* **2004**, *104*, 4303.
2 Scheers, J.; Fantini, S.; Johansson, P. *J. Power Sources* **2014**, *255*, 204.
3 Balaish, M.; Kraytsberg, A.; Ein-Eli, Y. *Phys. Chem. Chem. Phys.* **2014**, *16*, 2801.
4 Rhodes, C. P.; Frech, R. *Macromolecules* **2001**, *34*, 2660.

5 Sutjianto, A.; Curtiss, L. A. *J. Phys. Chem. A* **1998**, *102*, 968.
6 Brouillette, D.; Perron, G.; Desnoyers, J. E. *J. Solut. Chem.* **1998**, *27*, 151.
7 Henderson, W. A.; McKenna, F.; Khan, M. A.; Brooks, N. R.; Young, V. G.; Frech, R. *Chem. Mater.* **2005**, *17*, 2284.
8 Henderson, W. A.; Brooks, N. R.; Young, V. G. *Chem. Mater.* **2003**, *15*, 4685.
9 Henderson, W. A.; Brooks, N. R.; Brennessel, W. W.; Young, V. G. *Chem. Mater.* **2003**, *15*, 4679.
10 Andreev, Y. G.; Seneviratne, V.; Khan, M.; Henderson, W. A.; Frech, R. E.; Bruce, P. G. *Chem. Mater.* **2005**, *17*, 767.
11 Henderson, W. A. *J. Phys. Chem. B* **2006**, *110*, 13177.
12 Tamura, T.; Yoshida, K.; Hachida, T.; Tsuchiya, M.; Nakamura, M.; Kazue, Y.; Tachikawa, N.; Dokko, K.; Watanabe, M. *Chem. Lett.* **2010**, *39*, 753.
13 Yoshida, K.; Nakamura, M.; Kazue, Y.; Tachikawa, N.; Tsuzuki, S.; Seki, S.; Dokko, K.; Watanabe, M. *J. Am. Chem. Soc.* **2011**, *133*, 13121.
14 Mandai, T.; Nozawa, R.; Tsuzuki, S.; Yoshida, K.; Ueno, K.; Dokko, K.; Watanabe, M. *J. Phys. Chem. B* **2013**, *117*, 15072.
15 Abouimrane, A.; Alarco, P.-J.; Abu-Lebdeh, Y.; Davidson, I.; Armand, M. *J. Power Sources* **2007**, *174*, 1193.
16 Dillon, R. E. A.; Shriver, D. F. *Chem. Mater.* **1999**, *11*, 3296.
17 Dillon, R. E. A.; Stern, C. L.; Shriver, D. F. *Chem. Mater.* **2001**, *13*, 2516.
18 Yoshida, K.; Tsuchiya, M.; Tachikawa, N.; Dokko, K.; Watanabe, M. *J. Electrochem. Soc.* **2012**, *159*, A1005.
19 Yoshida, K.; Tsuchiya, M.; Tachikawa, N.; Dokko, K.; Watanabe, M. *J Phys Chem C* **2011**, *115*, 18384.
20 Angell, C. A.; Ansari, Y.; Zhao, Z. F. *Faraday Discuss* **2012**, *154*, 9.
21 Orita, A.; Kamijima, K.; Yoshida, M.; Dokko, K.; Watanabe, M. *J. Power Sources* **2011**, *196*, 3874.
22 Seki, S.; Takei, K.; Miyashiro, H.; Watanabe, M. *J. Electrochem. Soc.* **2011**, *158*, A769.
23 Tachikawa, N.; Yamauchi, K.; Takashima, E.; Park, J. W.; Dokko, K.; Watanabe, M. *Chem. Commun.* **2011**, *47*, 8157.
24 Dokko, K.; Tachikawa, N.; Yamauchi, K.; Tsuchiya, M.; Yamazaki, A.; Takashima, E.; Park, J. W.; Ueno, K.; Seki, S.; Serizawa, N.; Watanabe, M. *J. Electrochem. Soc.* **2013**, *160*, A1304.
25 Tatara, R.; Tachikawa, N.; Kwon, H.-M.; Ueno, K.; Dokko, K.; Watanabe, M. *Chem. Lett.* **2013**, *42*, 1053.
26 Ueno, K.; Yoshida, K.; Tsuchiya, M.; Tachikawa, N.; Dokko, K.; Watanabe, M. *J. Phys. Chem. B* **2012**, *116*, 11323.
27 Zhang, C.; Ueno, K.; Yamazaki, A.; Yoshida, K.; Mandai, T.; Umebayashi, Y.; Dokko, K.; Watanabe, M. *J. Phys. Chem. B* **2014**, *118*, 5144.
28 Park, J. W.; Yamauchi, K.; Takashima, E.; Tachikawa, N.; Ueno, K.; Dokko, K.; Watanabe, M. *J Phys Chem C* **2013**, *117*, 4431.
29 Park, J. -W.; Ueno, K.; Tachikawa, N.; Dokko, K.; Watanabe, M. *J Phys Chem C* **2013**, *117*, 20531.
30 Rauh, R. D.; Shuker, F. S.; Marston, J. M.; Brummer, S. B. *J. Inorg. Nucl. Chem.* **1977**, *39*, 1761.
31 Kondo, K.; Sano, M.; Hiwara, A.; Omi, T.; Fujita, M.; Kuwae, A.; Iida, M.; Mogi, K.; Yokoyama, H. *J. Phys. Chem. B* **2000**, *104*, 5040.

32 Kameda, Y.; Umebayashi, Y.; Takeuchi, M.; Wahab, M. A.; Fukuda, S.; Ishiguro, S.-i.; Sasaki, M.; Amo, Y.; Usuki, T. *J. Phys. Chem. B* **2007**, *111*, 6104.
33 MacNeil, D. D.; Dahn, J. R. *J Electrochem Soc* **2001**, *148*, A1205.
34 Yang, H.; Kwon, K.; Devine, T. M.; Evans, J. W. *J. Electrochem. Soc.* **2000**, *147*, 4399.
35 Krause, L. J.; Lamanna, W.; Summerfield, J.; Engle, M.; Korba, G.; Loch, R.; Atanasoski, R. *J. Power Sources* **1997**, *68*, 320.
36 Morita, M.; Shibata, T.; Yoshimoto, N.; Ishikawa, M. *J. Power Sources* **2003**, *119–121*, 784.
37 Wang, X.; Yasukawa, E.; Mori, S. *Electrochim. Acta* **2000**, *45*, 2677.
38 Kühnel, R.-S.; Lübke, M.; Winter, M.; Passerini, S.; Balducci, A. *J. Power Sources* **2012**, *214*, 178.
39 Matsumoto, K.; Inoue, K.; Nakahara, K.; Yuge, R.; Noguchi, T.; Utsugi, K. *J. Power Sources* **2013**, *231*, 234.
40 McOwen, D. W.; Seo, D. M.; Borodin, O.; Vatamanu, J.; Boyle, P. D.; Henderson, W. A. *Energy Environ. Sci.* **2014**, *7*, 416.
41 Ellis, B. L.; Lee, K. T.; Nazar, L. F. *Chem. Mater.* **2010**, *22*, 691.
42 Bruce, P. G.; Freunberger, S. A.; Hardwick, L. J.; Tarascon, J. M. *Nature Mater.* **2012**, *11*, 19.
43 Ryu, H. S.; Guo, Z. P.; Ahn, H. J.; Cho, G. B.; Liu, H. K. *J. Power Sources* **2009**, *189*, 1179.
44 Mikhaylik, Y. V.; Akridge, J. R. *J. Electrochem. Soc.* **2004**, *151*, A1969.
45 Cheon, S. E.; Ko, K. S.; Cho, J. H.; Kim, S. W.; Chin, E. Y.; Kim, H. T. *J. Electrochem. Soc.* **2003**, *150*, A800.
46 Ueno, K.; Park, J.-W.; Yamazaki, A.; Mandai, T.; Tachikawa, N.; Dokko, K.; Watanabe, M. *J Phys Chem C* **2013**, *117*, 20509.
47 Tobishima, S. -I.; Yamamoto, H.; Matsuda, M. *Electrochim. Acta* **1997**, *42*, 1019.
48 Manan, N. S. A.; Aldous, L.; Alias, Y.; Murray, P.; Yellowlees, L. J.; Lagunas, M. C.; Hardacre, C. *J. Phys. Chem. B* **2011**, *115*, 13873.
49 Barchasz, C.; Molton, F.; Duboc, C.; Leprêtre, J. -C.; Patoux, S.; Alloin, F. *Anal. Chem.* **2012**, *84*, 3973.
50 Kamyshny, A.; Gun, J.; Rizkov, D.; Voitsekovski, T.; Lev, O. *Environ. Sci. Technol.* **2007**, *41*, 2395.
51 Martin, R. P.; Doub, W. H.; Roberts, J. L.; Sawyer, D. T. *Inorg. Chem.* **1973**, *12*, 1921.
52 Gaillard, F.; Levillain, E. *J. Electroanal. Chem.* **1995**, *398*, 77.
53 Nelson, J.; Misra, S.; Yang, Y.; Jackson, A.; Liu, Y. J.; Wang, H. L.; Dai, H. J.; Andrews, J. C.; Cui, Y.; Toney, M. F. *J. Am. Chem. Soc.* **2012**, *134*, 6337.
54 Jeong, S. S.; Lim, Y.; Choi, Y. J.; Cho, G. B.; Kim, K. W.; Ahn, H. J.; Cho, K. K. *J. Power Sources* **2007**, *174*, 745.
55 Yamin, H.; Penciner, J.; Gorenshtain, A.; Elam, M.; Peled, E. *J. Power Sources* **1985**, *14*, 129.
56 Yamin, H.; Gorenshtein, A.; Penciner, J.; Sternberg, Y.; Peled, E. *J. Electrochem. Soc.* **1988**, *135*, 1045.
57 Peled, E.; Sternberg, Y.; Gorenshtein, A.; Lavi, Y. *J. Electrochem. Soc.* **1989**, *136*, 1621.
58 Shin, E. S.; Kim, K.; Oh, S. H.; Il Cho, W. *Chem Commun* **2013**, *49*, 2004.
59 Suo, L.; Hu, Y. -S.; Li, H.; Armand, M.; Chen, L. *Nat Commun* **2013**, *4*, 1481.
60 Gao, J.; Lowe, M. A.; Kiya, Y.; Abruña, H. D. *J. Phys. Chem. C* **2011**, *115*, 25132.

61 Mandai, T.; Yoshida, K.; Ueno, K.; Dokko, K.; Watanabe, M. *Phys. Chem. Chem. Phys.* **2014**, *16*, 8761.
62 Lu, Y. -C.; He, Q.; Gasteiger, H. A. *J. Phys. Chem. C* **2014**, *118*, 5733.

Chapter Five

Concluding Remarks and Future Directions

5.1. General Conclusions

5.1.1. Chapter One

The background and aim of this work have been described in the light of the previous studies and current trend in the fundamental and application perspectives. Enormous interest in the recent days has been attracted on the preparation and characterization of novel series of electrolytes with tunable physicochemical properties for their use in electrochemical devices such as next generation lithium batteries. However, some substantial issues had to be solved for designing next generation electrolytes with desirable chemistry such as high thermal stability compared to the conventional organic solutions, high ionic conductivity at room temperature and high ionicity and high lithium transference number. This study was undertaken with a view to getting a fundamental understanding of the lithium solvate ILs based on coordination chemistry and solution chemistry.

5.1.2. Chapter Two

In this chapter To develop a basic understanding of a new class of ionic liquids (ILs), "solvate" ILs, the transport properties of binary mixtures of lithium bis(trifluoromethanesulfonyl)amide (Li[TFSA]) and oligoethers (tetraglyme (G4), triglyme (G3), diglyme (G2), and monoglyme (G1)) or tetrahydrofuran (THF) were studied. The self-diffusion coefficient ratio of the solvents and Li^+ ions (D_{sol}/D_{Li}) was a good metric for evaluating the stability of the complex cations consisting of Li^+ and the solvents. The maximum ionicity ($\Lambda_{imp}/\Lambda_{NMR}$) of [Li(glyme or THF)$_x$][TFSA] mixtures was found at a concentration range of [O]/[Li^+] ~4 or 5, and the ionicity decreased both in the higher and lower concentration range. To understand this ionicity behavior, two solvent effects were considered: the solvating effect of the ligands (the solvent and/or the anion) in the first coordination shell for the concentrated regime, and the dipolar effect of the solvent in the dilute regime. This study revealed the importance of ion-dipole (ion-induced dipole)

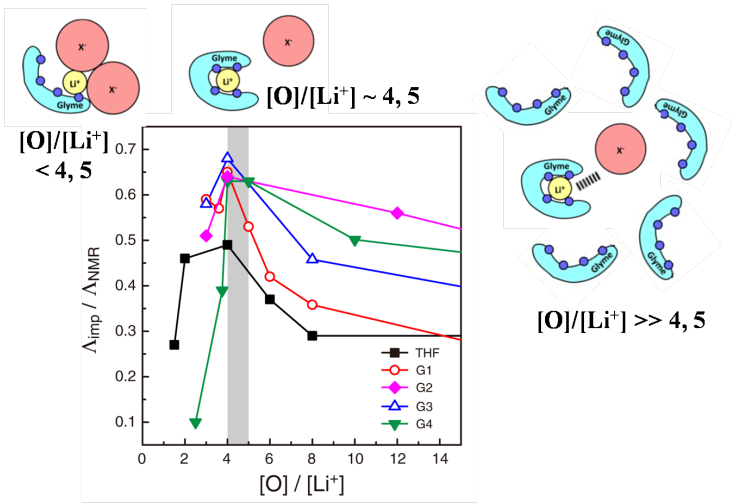

Figure 5-1. Ionicity ($\Lambda_{imp}/\Lambda_{NMR}$) at 30 °C for [Li(glyme or THF)$_x$][TFSA] mixtures as a function of [O]/[Li^+] ratio. Lines in the figure are a guide to the eye.

interactions and the chelate effect in the behavior of solvate ILs as distinguished from concentrated electrolyte solutions.

5.1.3. Chapter Three

A detail investigation was conducted for a series of binary mixtures of lithium bis(trifluoromethanesulfonyl)amide (Li[TFSA]) and oligoethers (tetraglyme (G4), triglyme (G3), diglyme (G2), and monoglyme (G1)) or tetrahydrofuran (THF) such as thermal properties, density, ionic conductivity, viscosity, self-diffusion coefficient, ionicity and ligand exchange lifetime. When the molar ratio of Li^+ ions and solvent oxygen atoms ([O]/[Li^+]) was adjusted to 4 or 5, D_{sol}/D_{Li} always exceeded unity for THF and G1-based mixtures even at the high concentrations, indicating the presence of uncoordinating or highly exchangeable solvents. In contrast, long-lived complex cations were evidenced by a D_{sol}/D_{Li} ~1 for the longer G3 and G4. The binary mixtures studied were categorized into two different classes of liquids: concentrated solutions and solvate ILs, based on D_{sol}/D_{Li}. Mixtures with G2 exhibited intermediate behavior, and is likely the borderline dividing the two categories. The effect of chelation on the formation of solvate ILs also strongly correlated with electrolyte properties; the solvate ILs showed improved thermal and electrochemical stability.

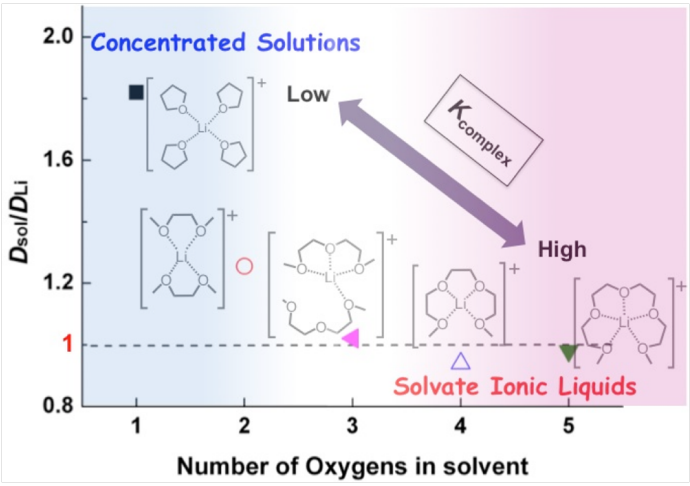

Figure 5-2. Number of oxygens in solvent dependencies of ratio of diffusion coefficient in the [Li(glyme or THF)$_x$][TFSA] mixtures.

5.1.4. Chapter Four

Highly concentrated, molten mixtures of lithium bis(trifluoromethanesulfonyl)amide (Li[TFSA]) and ether solvents (tetrahydrofuran (THF), monoglyme (G1), diglyme (G2), and triglyme (G3)) were investigatedas electrolytes for Li batteries. To compare the electrochemical reactions in the electrolytes with different solvents, the ratio of ether-oxygen atoms and Li^+

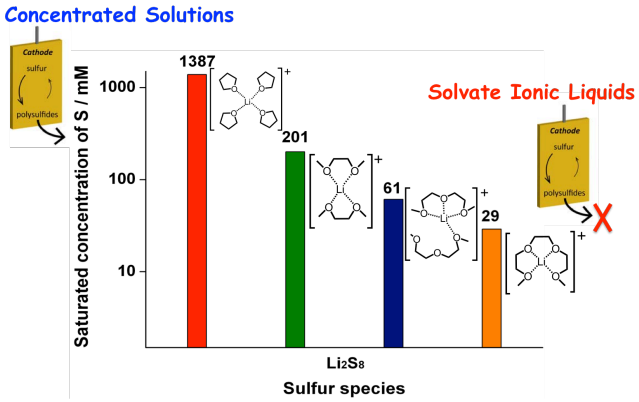

Figure 5-3. Saturated concentration of Li_2S_m in the [Li(glyme or THF)$_x$][TFSA] mixtures.

([O]/[Li]) in the electrolytes was fixed at four. The capacity of a Li-$LiCoO_2$ cell with $[Li(THF)_4][TFSA]$ dramatically decreased upon charge/discharge cycling, whereas $[Li(G3)_1][TFSA]$ allowed the cell to have a stable charge-discharge cycles and a Coulombic efficiency of greater than 99% over 100 cycles. Corrosion of the Al current collector of the cathode was also affected by the composition of the electrolytes. Persistent Al corrosion took place in $[Li(THF)_4][TFSA]$ and $[Li(G1)_2][TFSA]$, which contain shorter ethers, but the corrosion was effectively suppressed in $[Li(G3)_1][TFSA]$. Furthermore, lithium polysulfides, which are formed as discharge intermediates at the sulfur cathode of Li-S cell, were much less soluble in electrolytes with longer ethers. Therefore, a higher Coulombic efficiency and more stable cycle ability were achieved in Li-S cells with $[Li(G3)_1][TFSA]$. All the electrochemical properties in the batteries were dominated by the presence or absence of un-coordinating solvents in the concentrated electrolytes. This study demonstrates that the structural stability of $[Li(glyme\ or\ THF)_x]^+$ cations in electrolytes plays an important role in the performance of Li batteries.

5.2. Future Directions

Solvate ILs, as a sub-class of ILs is promising for widespread use in future. The physicochemical properties and correlations studied herein have the potential to optimize the future solvate ILs. It is anticipated that there will be strong growth in the field of solvate ILs as they become more widely known, which will lead to their use in many more applications due to its simple synthetic procedure and unique properties. However, there is still extensive research required before solvate ILs as electrolyte materials substituting the conventional organic electrolytes. The parameter provided the most attention in current research is the ionic conductivity, and indeed further improvements are still required to realize this phenomenon. This will be aided by a better understanding of the transport properties especially in extremely concentrated region. Thus, solvate ILs have an immense prospect from the standing point of both fundamental and diverse applications in multi-disciplinary areas and the door of ILs field is open for multiple directions for designing these next generation electrolytes with desirable properties.

List of Publications:

1. **Zhang**, **C.**; Ueno, K.; Yamazaki, A.; Yoshida, K.; Moon, H.; Mandai, T.; Umebayashi, Y.; Dokko, K.; Watanabe, M. Chelate Effects in Glyme/Lithium Bis(trifluoromethanesulfonyl)amide Solvate Ionic Liquids. I. Stability of Solvate Cations and Correlation with Electrolyte Properties, *J. Phys. Chem. B* **2014**, *118*, 5144-5153.
2. **Zhang**, **C.**; Yamazaki, A.; Murai, J.; Park, J. –W.; Mandai, T.; Ueno, K.; Dokko, K.; Watanabe, M. Chelate Effects in Glyme/Lithium Bis(trifluoromethanesulfonyl)amide Solvate Ionic Liquids, Part 2: Importance of Solvate-Structure Stability for Electrolytes of Lithium Batteries, *J. Phys. Chem. C* **2014**, *118*, 17362-17373.